UNIVERSITÀ DI PARMA

UNIVERSITA' DEGLI STUDI DI PARMA

DOTTORATO DI RICERCA IN

MEDICINA MOLECOLARE

XXXI CICLO

An experimental 3D model of the rat, thyroid gland stromal scaffold: implications for bioengineering of a bioartificial thyroid gland

Coordinatore: Chiar.ma Prof.ssa Stefania Conti

Tutor: Chiar.mo Prof. Roberto Toni

Co-tutor: Chiar.mi Proff. Lisa Elviri e Stephen R. Pennington

Dottorando: Marco Alfieri

Anni 2015 / 2018

INDEX

SUMMARY ..... 6.

INTRODUCTION ..... 8.

1. Organ matrix like a scaffold in the bioartificial organ engeneering ..... 8.
2. The topobiological theory ..... 11.
3. Decellularizzazion methods to obtain extracellular matrix scaffolds applicable to the rat thyroid gland ..... 14.
4. Distribution of the extracellular matrix and basement membrane proteins in the rodent thyroid gland ..... 18.
5. ECM and basement membrane proteins in the decellularized rat thyroid gland: preliminary studies ..... 22.
6. Bioprinting of natural and biocompatible hydrogels as an alternative substrate for growing of thyroid cells ..... 27.
7. Emergence of mass spectrometry-based proteomics useful to analysis of the rat thyroid gland matrix and cells ..... 29.
8. Current data on proteomic characterization of mammalian thyroid cells ..... 34.

AIM OF THE STUDY ..... 36.

MATERIALS AND METHODS ..... 38.

1. Decellularized rat thyroid gland ..... 38.
   - 1.1 Animals ..... 38.
   - 1.2 Decellularization of the rat thyroid gland ..... 38.
   - 1.3 Molecular analysis of the residual DNA with CyQuant® ..... 40.
   - 1.4 Mass spectrometry analysis ..... 41.
2. 3D biopriting of collagen from rat tail tendons ..... 46.

2.1 Extraction and solubilisation of collagen from rat tail tendons .....46.
2.2 Solubilisation of chitosan .....47.
2.3 Preparation of 2D film of collagen and chitosan .....47.
2.4 Mass spectrometry analysis of collagen from rat tail tendons.....47.
2.5 3D printing of scaffolds of collagen and chitosan with specific geometry.....48.
2.6 Attenuated total reflectance-fourier transform infrared spectroscopy (ATR-FT-IR) of collagen from rat tail tendons.....49.
2.7 Morphometric analysis on the microporosity of the 3D printed collagen from rat tail tendons.....49.
2.8 Functionalization of Poly-L-lactic acid (PLLA) microporous scaffolds with collagen and chitosan.....50.
2.9 Scanning electron microscopy (SEM) .....51.
2.10 Evaluation of cell morphology after growth on bioprinted collagen and chitosan scaffolds, and microporous plla disks coated with either collagen or chitosan.....51.
3. Proteomics signature of adult, male rat thyroid stem cell / progenitors .....53.
3.1 Growth and exphansion of rat thyrocytes and thyroid stem cell / progenitors.....53.
3.2 Filter aided sample preparation (FASP) .....53.
3.3 Mass spectrometry analysis .....56.
3.4 Data processing and statistic analysis.....56.

RESULTS.....57.
1. Decellularized rat thyroid gland .....57.
1.1 CyQUANT® analysis.....57.
1.2 Mass spectrometry analysis .....60.

2. 3D bioprinting of collagen from rat tail tendons ..... 73.
2.1 Mass spectrometry analysis ..... 73.
2.2 3D bioprinting ..... 76.
2.3 ATR-FT-IR of collagen from rat tail tendons ..... 78.
2.4 SEM morphological analysis ..... 80.
2.5 Morphometric analysis on the microporosity of the 3D printed collagen from rat tail tendons ..... 83.
2.6 Evaluation of cell morphology after growth on bioprinted collagen and chitosan scaffolds, and microporous plla disks coated with either collagen or chitosan ..... 85.
3. Proteomics signature of adult, male rat thyroid stem cell / progenitors ..... 91.
3.1 Chromatograms and proteins identification ..... 91.
3.2 Statistical analysis and biological interpretation of the data ..... 97.
3.3 Plasma membrane molecular signature of rat thyroid stem cell / progenitors ..... 102.

DISCUSSION ..... 110.
1. Decellularized rat thyroid gland ..... 110.
2. 3D bioprinting of collagen from rat tail tendons ..... 115.
3. Proteomics signature of adult, male rat thyroid stem cell / progenitors ..... 119.

CONCLUSIONS ..... 122.
REFERENCES ..... 124.
ACKNOWLEDGMENTS ..... 146.

SUMMARY

My PhD project aims at characterizing an *ex situ* model of adult male rat thyroid gland, recently designed and experimentally developed at the University of Parma, Parma, Italy by the research group headed by Prof. Roberto Toni MD PhD, and chosen as a key experimental tool for the activity of the recently funded, five-years Horizon 2020 SCREENED research project (Coordinator, Prof. Lorenzo Moroni, PhD, University of Maastricht, NL). According to the principles of regenerative medicine and tissue engineering, we have selected a combination of biocompatible / bioerodible materials to be used as 3D scaffold substrates, and adult rat thyroid stem cells induced to differentiation to give rise to a 3D thyroid organoid, grown in either static or dynamic bioreactor-like cell culture.

In the first year of my PhD program, I have characterized the stromal composition of the decellularized adult male rat thyroid lobe (i.e. its matrix) using two different mass spectrometry approaches coupled to appropriate bioinformatics software.

In the second year of my PhD program, I have investigated the use of collagen from rat tail tendons and polysaccharide substances like chitosan as chemical substrates suitable for bioprinting technology. Under the supervision of Prof. Lisa Elviri PhD at the Department of Food Science and Pharmacology of the University of Parma, Parma, Italy I have *in vitro* engineered 3D reticular structures, geometrically and chemically consistent with parts of the stromal matrix of the rat thyroid lobe, to be used as scaffolds for thyroid stem cell homing.

In the third year of my PhD program, in collaboration with the Proteomic Group of the University College of Dublin (Ireland) leaded by Prof. Stephen R. Pennington PhD, I have conducted a study leading to the proteomic signature of adult male rat thyroid stem cell /

progenitors. These results will be exploited to identify molecular makers for selective sorting by cytometric technology of adult male rat thyroid stem cells directly from their native tissue, and to enlighten still uncovered biological properties of these cell precursors.

INTRODUCTION

1. ORGAN MATRIX AS A SCAFFOLD IN BIOARTIFICIAL ORGAN ENGINEERING

Over the past decade, research has shown that the extracellular matrix (ECM) plays a fundamental role in the welfare of cells, tissues, and organs. This role extends far beyond mechanical support and architecture influencing molecular composition, cell adhesion, intracellular signalling, and binding of growth factors. In addition, the mechanical stiffness and deformability of the ECM significantly contributes to the commitment, differentiation, proliferation, survival, polarity, migration, and behaviour of cells[1].

The ECM is a collection of molecules, and provides a unique and tissue-specific three-dimensional (3D) environment[2,3]. Its structural and functional molecules are secreted by the resident cells, and provide structural and functional support to the surrounding cells[2,3]. ECM specific proteins include ligands for cell-surface receptors serving to initiate cell adhesion, and provide a 3D mechanical framework that dynamically interacts with cells[4].

All these functions make the ECM an excellent model of biocompatible scaffold for 3D organ reconstruction. This approach is currently assuming considerable clinical relevance due to the paucity of organ donors, allowing for organ replacement in a number of pathological settings[5,6]. It is based on the concept of dynamic reciprocity between the ECM and the resident cell population, suggesting that the ECM materials may offer a substantial advantage over the synthetic ones, and emphasizing the importance to maintain as much as possible the composition and 3D geometry of the native matrix during the preparation of 3D scaffolds[7].

In design biomaterial scaffolds to be eventually colonized by cells, a strategy has been to use single ECM components (e.g. collagens, stromal proteins, proteoglycans) or their mixtures[5]. Indeed, ECM proteins exhibit minimal immunogenicity. In addition, these natural product may keep intact biochemical and biophysical signals adequate to drive cell colonization, while having high degradation rates that may favour their replacement by the growing cells.

Finally, there is growing acceptance of the concept that to adequately induce seeded cells to reconstruct *on the laboratory bench* (i.e. *ex situ*) a functional 3D organ, a 3D substrate mimicking the original 3D geometry of the natural organ is required. This 3D substrate can be either physical (acellular organomorphic matrix, scaffold of biocompatible material) or virtual (machine-driven deposition of cells or biopriting with bioink). This requirement is the reflection of a general biological property of the embryonic development. In fact, during the *in vivo* organogenesis stem cells and precursor elements (i.e. transient amplifying cells and progenitors) acquire different phenotypes (immune-tolerance included) depending upon the 3D geometry of their host environment or niche, a phenomenon proved to occur also in bioengineered contexts[8], and predicted by the Theory of Topobiology (see below)[9,10].

In particular, elasticity and stiffness of the 3D substrate (properties inherent to the ECM in vivo) strongly contribute to address cell fate. Therefore, the 3D architecture of cell assembly and its inherent physical-chemical properties (primarily represented by the organ's stromal matrix) are fundamental to regulate expansion and functional differentiation of the resident cells[8].

To engineer a 3D bioartificial scaffold, it is important to provide a thin layer of ECM between the scaffold and the cells, mimicking the basement membrane (BM). BM, in fact, is implicated in the function of the stem cells niche[11,12], regulates cell polarity, cell

adhesion, spreading, and migration via effects on the cytoskeleton[13], and interacts with a number of molecules in the fibrous matrix stroma[13].

2. THE TOPOBIOLOGICAL THEORY

The idea that the 3D geometry of the stromal matrix is a key factor for the function of the mature organ stands on the morphoregulatory principles at the base of the Theory of Topobiology proposed by the Nobel Laureate for Medicine and Physiology, Gerald M. Edelman[10,14]. His theory aims at answering to two major questions related to the morphogenetic process:

1. The developmental genetic question. How does the one dimensional genetic code specify a 3D animal?
2. The evolutionary question. How is any proposed answer to the developmental genetic question reconciled with relatively large changes in form occurring in relatively short periods of evolutionary time?

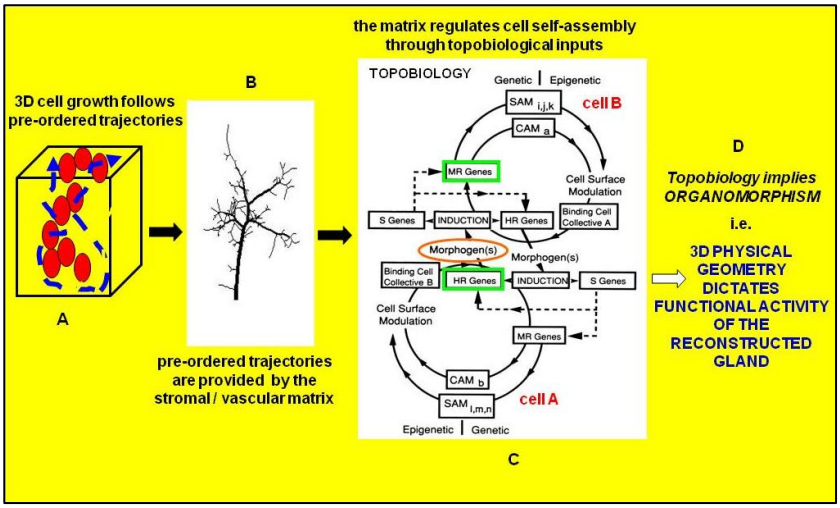

Figure 1. Edelman topobiological theory as exemplified for a pre-established 3D environment as proposed by Toni R, et al. [14]

According to the morphoregulator hypothesis, a general answer to the questions above is provided by evidence of coordinated expression of three families of morphoregulatory molecules during development: cell adhesion molecules (CAMs), substrate adhesion molecules (SAMs), and cell junctional molecules (CJMs)[15,16]. All these molecules are transcribed under the control of three specific classes of genes including 1) morphoregulatory (MR) genes for CAMs, SAMs, and CJMs. These genes are necessary for pattern but not for maintenance of the cell life; 2) historegulatory (HR) genes for cytodifferentiation. Their products are essential to all *housekeeping* functions, and are necessary for the life of the cell; 3) selector (S) genes, like the homeotic genes (so called HOX family), aimed at restricting the expression of both MR and HR genes to certain developmental places and times.

The hypothesis assumes that MR genes act in strict interdependence with HR genes. This assumption is essential if the cell differentiation, i.e. the expression of cell- and tissue-specific properties, proceeds *pari passu* with mechanochemical regulation of shape, and is supposed to be driven by relatively small number of genes. The fact that the promoter regions of CAM and SAM structural genes contains elements responding to homeobox gene products is one of the most striking predictions of this theory. As mentioned above, the key issue upon which the MR hypothesis is focused is how gene expression can be linked to the control in time and space of the mechanics of cell motion, division, and death. Protein mediating cell adhesion to other cells or substrates are the obvious candidates for carrying out this linkage. Here lies the key challenge of topobiology: what governs the place-dependent sequence of expression of MR and HR genes in such a way as to link cell number, cell signalling, and cell position to yield a higher order structure or a tissue? And how does this sequence form the basis for further inductive events in development?[17] While the structural gene for any MR molecule does not contain information for cell position or place, the production of homeodomain transcription factors may reflect the

place-dependent responses and signals of particular cell collectives modulated by adhesion.

As a result, the physical topology of a natural scaffold coincides, at least in large part, with the signal topology of the cells growing on it[17]. Therefore, any successful *ex situ* organ reconstruction should rely on the comprehension of this regulatory cascade, expected to be operative also in *ex situ* contexts[18].

3. DECELLULARIZZAZION METHODS TO OBTAIN EXTRACELLULAR MATRIX SCAFFOLDS APPLICABLE TO THE RAT THYROID GLAND

Solid organ transplantation is a victim of its own success. As results have dramatically improved, the demand for transplantable grafts has increased but the offer has not kept pace. Therefore, the gap between the number of patients who have received a transplant and those who are in the waiting list has become wider than ever; also, the mortality while on the waiting list is increasing[19,20].

For this reason, alternative sources of transplantable grafts have been investigated. Among these, *ex situ* organ engineering has come into the spotlight due to expectations to overcome possible xenotransplantation complications. One of the most popular methods in *ex situ* organ engineering is the recellularization of decellularized matrices, acting as natural scaffolds. In this manner, the decellularized matrix would be free of potentially immunogenic cells, would have a native ECM with several bioactive molecules, and would keep a vascular structure, essential for oxygen and nutrients to reach the seeded cells[21].

Numerous clinical products composed by mammalian ECM are already available. Clinical products such as surgical mesh materials composed of ECM are harvested from a variety of allogeneic or xenogeneic tissue sources, including dermis, urinary bladder, small intestine, mesothelium, pericardium, and heart valves, and from several different species. The potential advantage of tissue specificity for maintaining selected cell functions and phenotype has been suggested by studies of cells and ECM isolated from tissues and organs such as the liver, respiratory tract, nerve, adipose, and mammary gland[22].

A biological scaffold from ECM can be produced by variety of decellularization methods, whose caveat consists in efficiently eliminating cells from the treated tissue while maintaining the native 3D matrix architecture[23]. However, the response to acellular

xenogeneic or allogeneic biologic scaffold materials is less well understood[24]. Studies demonstrated the importance of macrophages in tissue repair and regeneration, particularly in applications involving biologic scaffolds[25,26]. Macrophages are responsible, in part, for the degradation of ECM scaffolds[24]. Depletion of circulating macrophages severely attenuates scaffold degradation and the associated constructive remodelling response[26]. The preservation of the ECM ultrastructure is highly desirable because of its unique architecture, its growth factors (GFs) content and decreased immunological response. All of these properties provide attachment sites and adequate environment for cells that colonize the scaffold, reconstituting the decellularized organ[24]. Based on these premises, successful decellularization and organ reconstruction have been achieved for the rodent and human heart, liver, and lungs[27].

The preparation of a matrix from a large, intact mammalian organ requires several sophisticated processing steps. The selection of decellularization reagents is critically important because these agents can damage the structure and composition of the resultant matrix[28]. Factors that may affect organ decellularization include:

1. The cellular density of a particular tissue or organ (e.g. liver vs. tendon)
2. The specific density of the tissue/organ (e.g. dermis vs. adipose tissue)
3. Lipid content (e.g. brain vs. urinary bladder)
4. Thickness of the tissue/organ (e.g. dermis vs. pericardium)
5. Properties of the selected decellularization agents (e.g. chemical, enzymatic, and physical)[22]

Every cell removal agent and method will alter ECM composition and cause some degree of ultrastructure disruption. The goal of decellularization is to minimize these side effects[22]. To achieve this purpose, several different groups of decellularization agents have been explored, including:

1. Non-ionic (Triton-X), ionic (sodium dodecyl sulfate: SDS) and zwitterionic detergents
2. Enzymatic agents
3. Physical agents
4. Direct application of force or mechanical breakingh[22-29]

Acids and bases cause or catalyse hydrolytic degradation of biomolecules. In particular, peracetic acid removes the residual nucleic acids with minimal effect on the ECM composition and structure[30,31].

Bases likes calcium hydroxide, sodium sulphide, and sodium hydroxide are used to remove hair from dermis samples during the early stages of decellularization[32]. However, bases (e.g. NaOH) can completely eliminate GFs from the matrix and decrease ECM mechanical properties more significantly than chemical and enzymatic agents through the cleavage of collagen fibrils and disruption of collagen crosslinks[33,34].

Hypertonic saline dissociates DNA from proteins. Hypotonic solutions can readily cause cell lysis by simple osmotic effects with minimal changes in matrix molecules and architecture[35].

Between the non-ionic detergents, Triton X-100 can effectively remove cellular residues by membrane disruption, and its use does not produce an adverse immune response *in vivo*[36]. Alcohols, such as glycerol help in tissue decellularization by dehydrating and lysing cells; isopropanol, ethanol, and methanol are more effective than lipase in removing lipids from tissues, and are capable of rendering adipose tissue lipid-free in a relatively brief period[37,38].

Enzymes can provide high specificity for removal of cell residues and those reported in tissue decellularization protocols include nucleases, trypsin, collagenase, lipase, dispase, thermolysin, and galactosidase. However, complete cell removal by enzymatic treatment alone is difficult, and enzyme residues may impair recellularization or evoke an adverse

immune response. Nucleases (e.g. DNases and RNases) can help in removal of nucleotides after cell lysis in tissues[39,40].

Trypsin is a serine protease that cleaves peptide chains mainly at the carboxyl side of the amino acids lysine or arginine, except when is followed by proline[41]. Trypsin is commonly used as an enzymatic decellularization agent. However, ECM proteins such as collagens have limited resistance to trypsin cleavage[42]. In comparison to detergents, trypsin is more disruptive to elastin and collagen, and removes less efficiently cells but better preserves glycosaminoglycans (GAGs)[43,44]. Exposure to trypsin in the initial steps of a tissue decellularization protocol may be desirable or even necessary for a complete removal of cell from dense tissues[39].

Freeze-thaw processing effectively lyses cells within tissues and organs, but the resulting membranous and intracellular contents remain un-removed by subsequent processing. A single freeze-thaw cycle can reduce adverse immune responses such as leukocyte infiltration in vascular ECM scaffolds and have no influence on the loss of ECM proteins from tissue[45].

Collectively, variable combinations of two or more of the above mentioned agents can be successfully used to yield satisfactory cleaning of native matrices by resident cells, and be adapted to different kinds of tissues with different types of cells, and their attachment to the surround fibrous stroma.

4. DISTRIBUTION OF THE EXTRACELLULAR MATRIX AND BASEMENT MEMBRANE PROTEINS IN THE RODENT THYROID GLAND

In the rodent thyroid gland, the principal epithelial cells are the thyrocytes: they are polarized, presenting an apical and a basal surface, and organized in a single cell layer with their apical pole surrounding a thyroglobulin-containing cavity (follicle). A thin of BM faces the basal surface of these cells, and that of the endothelial cells providing a support and a contact medium with the interstitial connective tissue. The BM of the follicular epithelium has a sheet-like structure of 50-100 nm in thickness, with an amorphous appearance[46]. It is composed of various proteins originally thought to be unique to the BM, and include type IV collagen, laminin, heparan sulphate proteoglycans like perlecan, entactin, and several other glycoproteins[47-49]. Each of these molecules exhibit a precise and unique distribution within the ECM stroma or the BM.

- <u>Proteins of the stroma</u>

1. Fibronectin

Fibronectin (FN) usually is a dimer composed of two nearly identical ~250 kDa subunits linked covalently near their C - terminal by a pair of disulfide bonds. Each monomer consists of three types of repeating units[50]. The structure of FN depends on whether it is secreted in plasma or synthesized by resident cells[51]. It binds to a number of biologically important molecules including integrins, heparin, collagen/gelatin, and fibrin through distinct structural and functional domains[52]. FN interactions with collagens is believed to depend on its binding to unfolded regions of the collagen triple helix.

FN is the predominant non collagenous protein of the stroma. In the thyroid gland, its most intensive immunocytochemical reaction is in the central zone of the lobes, specifically between the thyroid follicles. As a rule, this reaction decreases sharply closer to the capsule. Intensive staining for FN can be found around the blood vessels[53]. In contrast, staining of follicular and vascular BM is very weak or completely absent[54].

FN mediates a wide variety of cellular interactions with the ECM, and plays important roles in cell adhesion, migration, growth and differentiation. It has been suggested that FN-collagens interactions is related to the unfolded regions of the collagen triple helix and influence more the clearance of denatured collagenous materials from blood and tissue than mediating cell adhesion to collagen[50]. In the adult male rat thyroid gland FN is present in the interfollicular stroma, as evidenced by immunocytochemistry on decellularized thyroid matrix during my master degree experimental thesis.

2. Fibrillar collagen

Of all collagens types, the fibril-forming types (i.e. the types I, II III, V and XI) are the most abundant and the most extensively studied and, among these, collagen type I is the most represented. It is organized as thick fiber bundles in the stroma and capsule. In the rodent thyroid, the stromal collagen is believed to regulate the formation of the BM layer, allowing for correct cellular polarization during follicular formation[9].

- <u>Proteins of the Basement Membrane</u>

1. Laminin

Laminin (800 kDa) is a large and complex molecule that was first isolated from the murine Engelbreth-Holm-Swarm (EHS) sarcoma, which is rich in BM proteins. In mammals different isoforms of laminins are present depending on the tissues, each of them variably

composed as an heterotrimer. In particular, a laminin heterotrimer has one molecule variably composed by one of five different types of α chain, another molecule variably composed by one of three different types of β chains, and a third molecule variably composed by one of three different types of γ chain[55-57]. The table below summarizes all possible chain combinations found in mammalian laminins.

Laminin isoforms.

Isoform	Chain composition	Mediates cell adhesion	Nidogen binding
Laminin-1	α1β1γ1	+	+
Laminin-2	α2β1γ1	+	+
Laminin-3	α1β2γ1	nt	nt
Laminin-4	α2β2γ1	+	+
Laminin-5	α3β3γ2	+	–
Laminin-6	α3β1γ1	nt	nt
Laminin-7	α3β2γ1	nt	+
Laminin-8*	α4β1γ1	nt	nt
Laminin-9*	α4β2γ1	nt	nt
Laminin-10*	α5β1γ1	nt	nt
Laminin-11*	α5β2γ1	nt	nt

Figure 2. Laminin isoform present in BM of different cells types [57]

Laminins appear as cross-shaped molecules[58] whose long arm (~80 nm in length) is an α-helical coil formed by three chains, whereas the three short arms (35–50 nm) are composed each of a single chain including one α, one β, and one γ chains[56,59]. The heterotrimeric laminins are a component of all BMs, and self-assemble to favour association of cells in a ordered network. Specifically, the three short arms of the cross-shaped laminin molecule are directed towards the external stroma, where they form a network of nodes, each node being the point of contact between three adjacent short arms, and each arm belonging to a different laminin molecule. In contrast, the globular domain situated at the bottom of the long molecular arm is directed towards the cells, and

binds to either cellular receptors or other molecules present in the BM including integrins α-dystroglycan, heparan sulfates, and sulfated glycolipids[56].

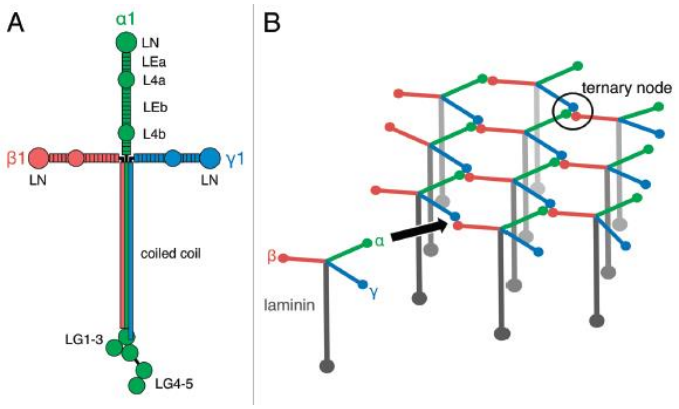

Figure 3. Laminin structure (A) and network (B)[56]

In the rat thyroid gland, α1β1γ1 laminin isoform is present in the BM around individual follicles, thus surrounding the basal surface of each follicular cells and the endothelium of capillary blood vessels that tightly envelop each follicle[48,54].

2. Collagen IV

Heterotrimers (α1α1α2 chains) of collagen type IV constitute one of the most abundant components of nearly all BMs, and are an excellent marker of the BM itself. Collagen type IV is considered responsible for the mechanical stability of the BM[49,60, 61].

Figure 4 shows the 30nm long triple-helical segment (α1α1α2) that forms tetrameric arrangements by parallel and anti-parallel alignment at the N terminus (7s domain, indicated by the number 1). In contrast, the C-terminal NC1 domain forms dimers which become covalently connected by disulfide rearrangement (represented by numbers 2). The final collagen IV networks are stabilized by superhelical twisting between two heterotrimers (indicated by the number 3 in figure 4) and disulfide or lysine aldehyde-derived cross-links between their interacting NC1 and 7s domains[49]. Similar to laminin,

collagen IV appears as a single thin membrane in the rat thyroid, continuously surrounding the basal surface of follicular epithelium and endothelium of capillary blood vessels[48,54].

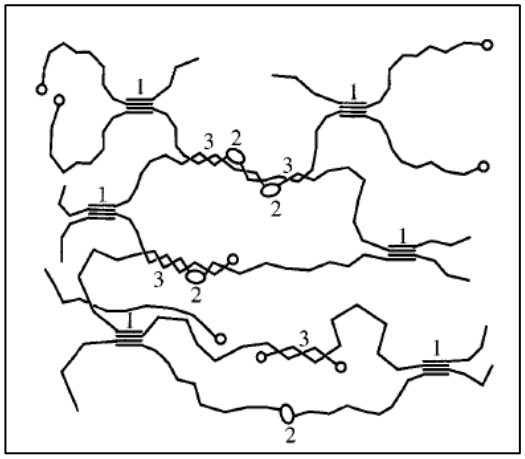

Figure 4. Illustration of the reticular structure of collagen type IV[49].

3. Perlecan

Proteoglycans are remarkably complex molecules with functions associated not only with their protein cores but also with their constituent carbohydrate chains. These functions range from structural roles in the extracellular matrix to control of growth factor gradients, cell migration and behavior. Proteoglycans are classified based on the types of carbohydrate chains they contain. In this regard, the signature carbohydrate chains are large, linear, highly negatively charged polymers called glycosaminoglycans. Glycosaminoglycans are further classified based on their characteristic disaccharide repeating structures. Heparan sulfate (HS) is one class of glycosaminoglycans initially assembled as a polymer of N-acetylglucosamine and glucuronic acid and subsequently modified in several ways to generate more complex, biologically active structures[62].

Perlecan, also called heparan sulfate proteoglycan 2 (HSPG2), is an ancient, structurally conserved HS bearing a proteoglycan. This molecular complex is secreted into the extracellular space, where it is incorporated into the BMs separating epithelial and stromal

compartments[62-64]. It is composed of five domains, having the ability to self-assemble into oligomers, and interacts with growth factors, receptors and diverse ECM/BM molecules likes laminin and collagen IV[56].

Immunofluorescence staining of unfixed cryosections of rat thyroid gland reveals that perlecan is one of the major BM component, being strongly expressed in the follicular and vascular BM[54, 65].

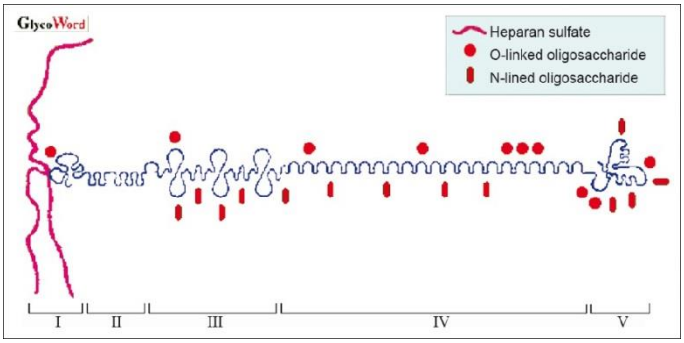

Figure 5. Perlecan structure[62].

5. ECM AND BASEMENT MEMBRANE PROTEINS IN THE DECELLULARIZED RAT THYROID GLAND: PRELIMINARY STUDIES

In preliminary studies carried out in the Laboratory of Regenerative Morphology and Bioartificial Structures (Re.Mo.Bio.S. lab, Director Roberto Toni MD, PhD) at the University of Parma, Parma, Italy during my Master Degree in Medical, Veterinary, and Pharmaceutical Biotechnologies, some of the main ECM proteins in the adult male rat thyroid gland were identified. In a first step, the presence of collagen, elastic and reticular fibers in both the native (not decellularized) and decellularized thyroid was evaluated with histological staining (figure 6).

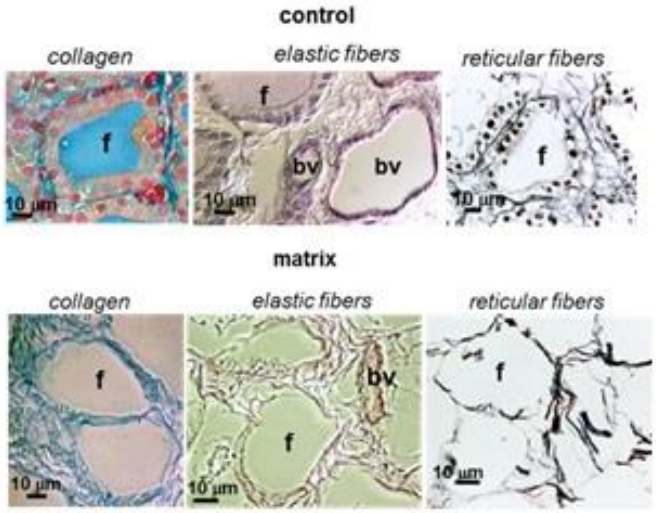

Figure 6. Native and decellularized rat thyroid lobes stained with Mallory trichrome (collagen), Weigert (elastic fibers) and silver salts (reticular fibers). Mallory's trichromy stain nuclei and fibrin in red, collagen fibers in blue. Weigert stain elastic fibers in violet. Silver salts stain the reticular fibers in black. f = follicle. bv = blood vessels. Scale bar = 10 µm

In a second step, using transmission and scanning electron microscopy (TEM and SEM) an ultrastructural analysis was conducted on the the decellularized thyroid matrix. TEM analysis revealed that collagen fibers had a very specific geometry at the level of the follicular cavities, with fibers intersecting perpendicular each other, and forming a regular network around each follicle. SEM analysis confirm that both the macro- and micro-structure (i.e. the follicular cavities) of the rat thyroid lobe matrix were maintained after the decellularization process (figure 7). Details on the latter have been reported in the Master Degree Thesis, and are described again the Materials and Methods of the present PhD Thesis (see below).

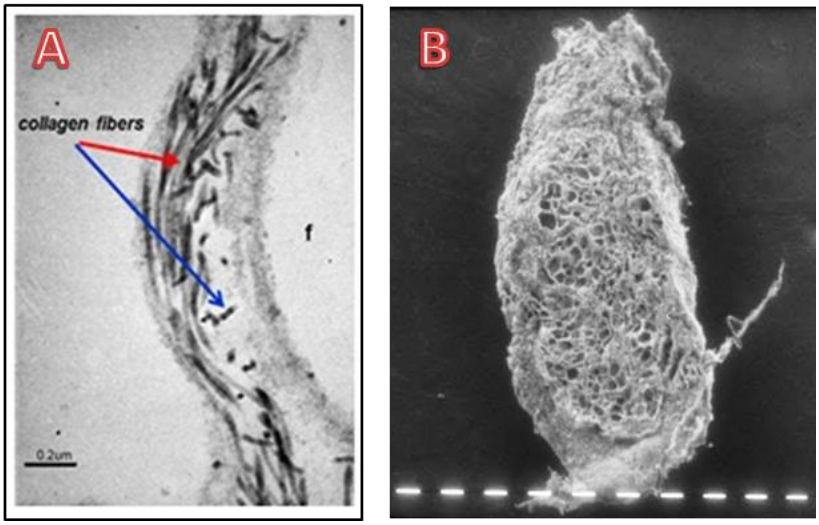

Figure 7. A: TEM image of collagen fibers near the follicular lumen. f = follicle. Scale bar = 0.2 µm B: SEM image of decellularized male rat thyroid lobe. Scale bar = 100 µm

Finally, immunocytochemical analysis showed that the applied decellularization protocol allowed for the preservation of 3 different stromal and basement membrane proteins: fibronectin, laminin and perlecan.

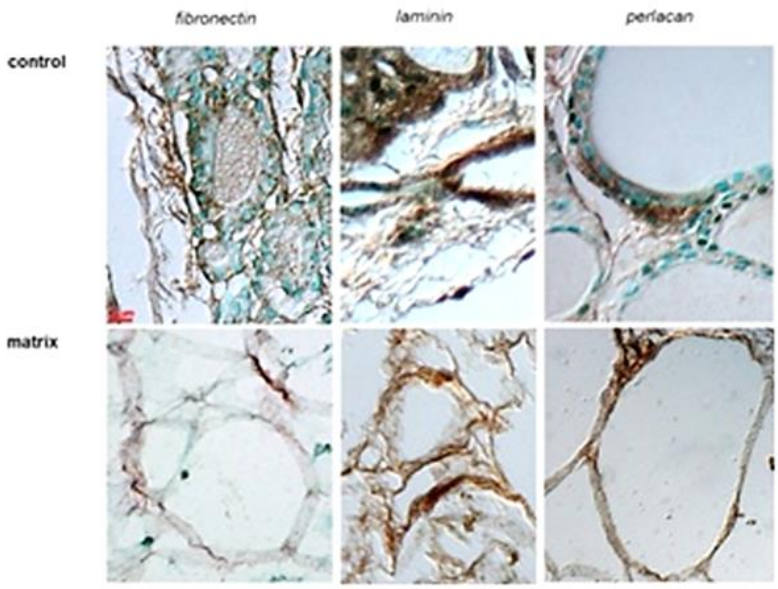

Figure 8. Immunocytochemistry of ECM and BM proteins in the rat thyroid native (control) and decellularized lobes. The stromal protein fibronectin and basal proteins laminin and perlecan are stained in brown, cells in blue.

6. BIOPRINTING OF NATURAL AND BIOCOMPATIBLE HYDROGELS AS AN ALTERNATIVE SUBSTRATE FOR GROWING OF THYROID CELLS

In parallel to the decellularization methododolgy, an innovative perspective for Tissue Engineering is represented by the 3D reconstruction of visceral matrices using the additive layer manufacturing (ALM or rapid prototyping), also known as 3D bioprinting, including most recent developments with direct 3D deposition of cells even in the absence of a 3D scaffolding. In particular, a relevant advantage of 3D printing is the use of ECM proteins-based solution (variably mixed with other bioerodible materials) mimicking the ECM composition of the organ to be reconstructed[66]. Among the rapid prototyping techniques, the Fused Deposition Modelling (FDM) is one of the most widely used as it allows for reconstruction of 3D structures with controlled and reproducible geometry and porosity[67]. A reliable technology to drive FDM printing is Computer-Aided-Design (CAD). This is based on:

- Digital models
- Scans of the original viscera in computed tomography (CT) and its reproduction with 3D rendering techniques
- Scans of the original viscera in magnetic resonance imaging (MRI) and its reproduction with 3D rendering techniques[67]

By combining CAD with FDM, 3D structures can be obtained based on layer-by-layer deposition of the chosen biomaterial.

Among the various biomaterials available, versatile products for the FDM printing process are natural (alginates, chitosan) and synthetic polymers (polylactic acids)[68]. The ECM itself can be considered a natural hydrogel due to the presence of ECM proteins and glycoproteins. Of all these, the most representative proteins belong to the collagens family,

with collagen type I being the most abundant ECM protein. Typical sources of collagen type I are the rat tail tendons, and the bovine or pig skin[69].

Collagen is considered an optimal biomaterial due to its low immunogenicity, and high biodegradability, biocompatibility, and sensitivity to the temperature. In fact, after one hours of incubation at 37^{o}C and neutral pH, collagen acquires rheological characteristics of a typical hydrogel[70]. However, due to its low mechanical strength and viscosity, collagen is rarely used in the FDM printing method, and is typically cast in preformed molds or printed together with other biomaterials as a functionalization compound[71].

The fact that collagens are the main ECM proteins in the rat thyroid gland led us to investigate collagen as a biomaterial for FDM. In particular, the use of a native solution of collagens obtainable from the rat tail tendons, which is rich in elastin and proteoglycans[72], exhibit strong similarities to the composition of the native rat thyroid matrix.

7. EMERGENCE OF MASS SPECTROMETRY-BASED PROTEOMICS USEFUL TO ANALYSIS OF THE RAT THYROID GLAND MATRIX AND CELLS

The understanding of when and where the proteins were expressed became the major challenge after the completion of the Human Genome project in 2003[73]. In order to reach this objective, a new branch of study called proteomics was developed, aimed at the complete detection of the protein expression (i.e. the proteome) of a cell, tissue, organ or organism[73,74]. Founded in 2001, the main goals of the Human Proteome Organization (HUPO) are to promote the field of proteomics, and its applications through international cooperation and collaborations, including a continuous development of new technologies leading to a rapid expansion and comprehension of this field[75] (figure 9).

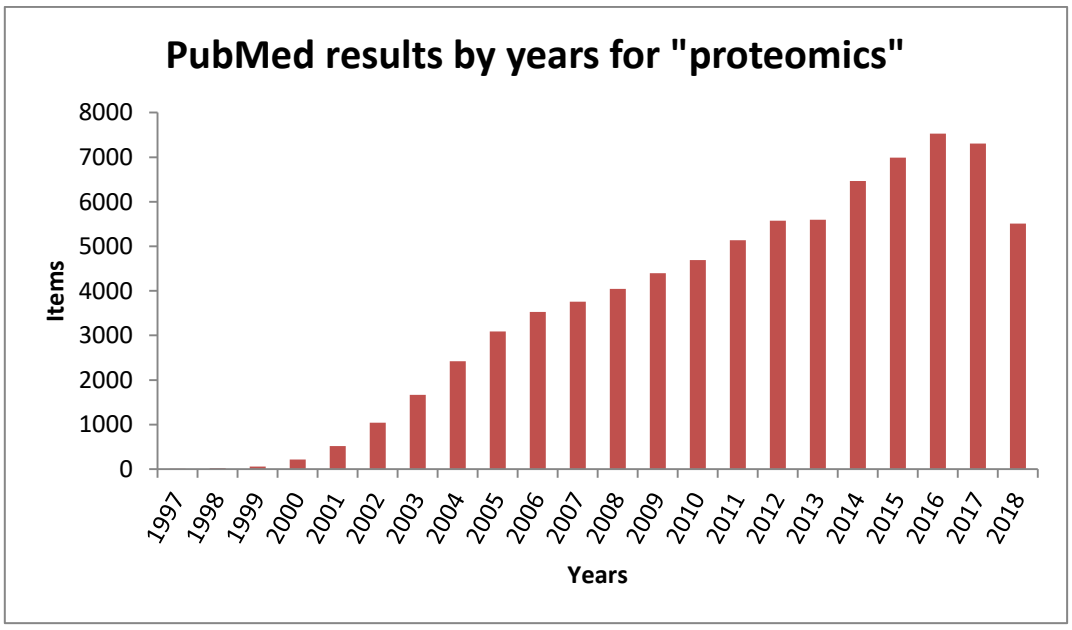

Figure 9. The number of items for "proteomics" in PubMed during years update to September 2018

The importance of studying protein expression lay on the fact that proteins essentially catalyse and control all cellular process and the proteome define the cell's functional state

(i.e. the functional phenotype). Remarkably, proteomics stands at a different level with respect to genomics because the true size of a proteome cannot be derived from the number of cell genes and, conversely the same genome can express proteome profiles very different in relation to the overall functional state of the cell (table 1).

The main way to investigate the proteome is the use of mass spectrometry (MS). A mass spectrometer consists of an ion source (common ion source are the electrospray source ionization (ESI) and matrix-assisted laser desorption/ionization (MALDI)), a mass analyser that measures the mass-to-charge ratio (m/z) of the ionized analytes, and a detector that registers the number of ions at each m/z value[76].

Table 1. Differences between the genome and proteome[73].

	Genome	Proteome
Size	Exactly defined	Unknown
Building blocks	4 + some modified units	20 + numerous modified units
Abundance range	1 or several gene copies	9 orders between protein abundances
Repair system	Highly effective	No repair, processing, variable turnover
Biological dynamics	Mainly stable	Moderately to highly dynamic
Localization	Nucleus	Everywhere
Safety Shell	Nucleus, histones	None
Synthesis	Linked to mitosis, tightly controlled	Both continuous and stimulated gene expression

As shown in figure 10, the main approach used in proteomics is the “bottom-up” method, i.e. the identification of a protein starting from its proteolyzed peptides[77]. Specifically, proteins are digested by sequence-specific enzymes such as trypsin, and ensuing peptides are separated by reverse-phase chromatography, following by their ionization, and channeling to a mass spectrometer for analysis.

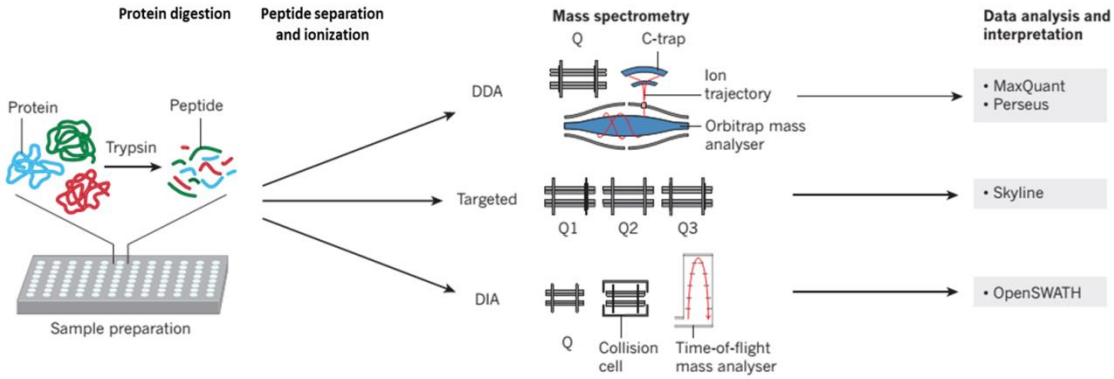

Figure 10. The three typical proteomics workflows. DDA methods is commonly used for bottom-up proteomics analysis. Targeted MS usually rely on triple quadruple MS for accurate quantification of a small set of proteins. DIA method represent the last frontier in high resolution MS-based proteomics[78].

The typical "bottom-up" experiment for a proteome discovery is called data-dependent acquisition (DDA) and its made using a high resolution mass spectrometer (such as Time of Flight or Orbitrap technology)[78]. Although this instrument has a high cost, this technique has the advantage that the researcher does not need to know the identity of the expected proteins in advance. DDA mode, in fact, is based on the acquisition of all ions forming the protein spectra of the analyte, eluted in a specific time (MS1), whose the instrument select ions with the most intense signal (MS2). This process lasts for the time needed to evaluate the ion composition of the analyte, and provides a label free quantification (LFQ) of the entire set of proteins into the sample[79]. Then, peptides identification is achieved by the use of appropriate softwares such as MaxQuant[80] that compares the mass spectra derived from peptide fragmentation with theoretical mass spectra generated from *in silico* digestion in a protein database like Uniprot (www.uniprot.org)[78]. Because peptides identified in this manner can be either uniquely assigned to a single protein or shared by more than one protein, the proteins putatively identified with this procedure may be further scored, and a valid false discovery rate is provided by the instrument software (e.g. MaxQuant). Then, biological interpretation of the identified proteins can be made with bioinformatics tools such as Perseus[81] .

The following step is proteins quantification. A common way to reach this goal is MS targeted approach that can be made using a triple quadrupole mass spectrometer (figure 10). In this MS technique, a peptide of known m/z is selected in the first quadrupole, fragmented in the second quadrupole, and monitored over time in the third quadrupole in a method called single reaction monitoring (SRM) or multiple reaction monitoring (MRM)[82,83]. These m/z transition are then analysed with appropriate software such as Skyline[84]. The main advantages of targeted proteomic approaches over DDA method is the lower cost of the instrument, and its capability for consistently quantify multiple proteins.

The recently developed data-independent acquisition (DIA) technique represent the last frontier in proteins discovery, and quantification with MS. In DIA, the researcher defaults a specific m/z range, and the instrument generates all the ions (called MS2 spectra) within the previously selected m/z range[85], and not only those with the most intense signal (as in the DDA methodology, see above). An example of this application is the sequential window acquisition of all theoretical mass spectra (SWATH-MS) mode, which attempts to analyse the spectra of all ions. Using this method, Rosenberger and his group have identified more than 10,000 proteins from a large range of human cell and tissue types[86]. However, the main limitation of DIA-based method is the storage and the complexity of the large amount of data generated during the analysis, requiring large informatics resources. For this reason, the DDA method continues to be the election method in the proteomic field.

All the previous MS methods have found recent application in the analysis of cells proteomes. Indeed, with respect to genomics, proteomics may provide hints to the main functional units driving cellular processes[87,78] including identification of low-abundance proteins in high-complex samples[88]. The comprehension of cell proteomes supported by accurate bioinformatic tools has allowed for protein localization and protein-protein interactions[89]. Mass spectrometry-based proteomics has been applied to a wide range of

studies in the field of stem cells, including embryonic stem cells (ESC), induced pluripotent stem cells (iPSC), hematopoietic stem cells (HSC) or adipose derived stem cells (ADSC)[90-92]. In the near future the analysis of complete proteomes could be feasible with low cost and in a high-throughput manner, and intensive study of biomarkers expression will drive in the era of precision medicine[93].

8. CURRENT DATA ON PROTEOMIC CHARACTERIZATION OF MAMMALIAN THYROID CELLS

Although its low cell turnover, experimental evidence has shown that the mammalian adult thyroid gland may self-renew[94-97], and evidence for thyroid stem cell / progenitors (TSC/P) in the mouse, rat, and human thyroid has been confirmed[98-102]. In humans, these cells exhibit co-expression of the pluripotent marker *Oct-4*, the endodermal markers *Gata-4* and *HNF4α*[100], and the expression of cluster of differentiation CD34+CD45-[98]. Mouse TSC/P seems to be represented by two populations: CD45-/c-kit-/Sca1+ and CD45-/c-kit-/Sca1- cells[99]. The expression of the multipotency marker ATP-binding cassette subfamily G member 2 (*ABCG2)* has been proven in mouse TSC/P[99], and the research group leaded by Roberto Toni MD PhD has recently confirmed this evidence in the adult male rat, demonstrating that long-term expansion of primary rat thyrocytes results in substantial increase in immunoreactive (IR)- *ABCG2* cells, as opposed to less than 1% IR-*ABCG2* elements in standard monolayer culture[101]. These cells resulted *Oct-4*, GATA-4 and SCA1 positive, with a 1-2% of CFU-like cultures expressing ABCG2, thus suggesting existence of a double stem cell / progenitor population of endodermal and mesodermal origin. Confirmation of this possibility was provided by showing differentiation to thyrogenic, adipogenic and hepatocyte-like lineages[101,103,104]. Overall, it is believed that thyroid stem cells / progenitors could represent a therapeutic aid for the regeneration of the adult thyroid gland, and for the treatment of diseases such as primary hypothyroidism due to autoimmune glandular degeneration[105].

Currently, only few study have analysed the normal thyroid gland proteome in the whole thyroid tissue[106-108] and thyroid cell cultures[109]. However, proteomic analysis of TSC/P in

either human or rodent models are lacking, thus requiring upgrade of this information that we have decided to tackle in the present PhD Thesis.

AIM OF THE STUDY

My experimental work has been carried out in the frame of the PhD program in Molecular Medicine at the University of Parma, Parma, Italy and developed at:

- the Laboratory of Regenerative Morphology and Bioartificial Structures (Re.Mo.Bio.S. lab) of the Section of Human Anatomy, Unit of Biomedical, Biotechnological and Translational Sciences of the Department of Medicine and Surgery of the University of Parma, Parma, Italy under the supervision of Prof. Roberto Toni MD PhD;
- the Department of Food Science and Pharmacology of the same University, under the supervision of Prof. Lisa Elviri PhD;
- the Conway Institute of Biomolecular and Biomedical Research, University College of Dublin (UCD), Ireland under the supervision of Prof. Stephen R. Pennington PhD.

The first part of my project has been focused on obtaining and characterizing the decellularized, adult male rat thyroid gland matrix as a model of natural thyroid ECM. I have developed three different decellularization protocols consisting in a combination of mechanical, enzymatic and chemical treatments, and investigated the residual DNA using the CyQUANT® Cell Proliferation Assay Kit. Then, the qualitative and quantitative characterization of the rat thyroid matrix has been achieved with two different MS-based methods, using the linear trap quadrupole (LTQ) Orbitrap XL and the triple quadrupole–tandem mass spectrometry under SRM mode (HPLC-MS/MS-SRM).

The second part of my project has been focused on the production of a 3D collagen scaffold mimiking some of the basic geometrical features of the rat thyroid matrix. To this aim, I have used a bioprinting technology based on the FDM method. Initially, efforts have been focused on the chemical-physical characterization of different collagen solutions obtained from the rat tail tendons, and solutions of the polysaccharide chitosan, to verify

which one was the most suitable and reproducible for the printing process. In a second step, the protein composition of the collagen solution from rat tail tendons was analyzed using LTQ-Orbitrap XL, and its *in vitro* biocompatibility for growth and survival of rat thyroid stem cells / progenitors and mouse Swiss 3T3 cells evaluated using scanning electron microscopy.

The third and last part of my project has been focused at identifying a specific proteomic signature of adult male rat, thyroid stem cells / progenitors recently identified and characterized by the research group of Prof. Toni at Parma University.

MATERIALS AND METHODS

1. DECELLULARIZED RAT THYROID GLAND

1.1 ANIMALS

Thirteen adult male Sprague Dawley® rat weighing 225 to 250 g. (7-8 weeks old) have been purchased from Charles River Laboratories (Calco, Lecco), and housed in temperature-controlled rooms (22°C) with a humidity of 50% and a 12:12 hour light–dark cycle, according to the stabulary rules. All animal experimentation have been conducted in accordance with the European Communities Council Directive of 24 November 1986 (86/EEC) and approved by Ethical committees of the University of Parma (approval code n. 165 18/2016-PR released on 12/01/2016).

1.2 DECELLULARIZATION OF THE RAT THYROID GLAND

Twenty-two thyroid lobes (coming from eleven rats) were used for the decellularization processes. Animals were deeply anesthetized with intraperitoneal tiletamine-zolazepam (40 mg kg−1), and sacrificed by cervical dislocation. The thyroids were surgically removed and cleaned from the capsule and adjacent parathyroid glands, the two lobes of each gland separated at the level of the isthmus, the lobes putted into vials containing PBS 0.1 M, frozen in liquid nitrogen, and stored at -80^{o}C until use. To initiate decellularization, lobes were brought to 4^{o}C for either 24 or 5 hours in the first and second or third protocols, respectively. This passage allows for cells lysis using thermic shock. Then, the thyroid lobes were processed using three different protocols.

1.2.1 First decellularization protocol

- Add trypsin 0.02% EDTA 0.25% (Sigma Aldrich n^{o} T4049) in PBS 0.1M (Sigma Aldrich n^{o} P4417) for 1 hour at 37^{o}C;
- Rinse with sterile distilled H_2O (dH_2O) for 1 hour at room temperature (RT);
- Add triton X-100 3% (Sigma Aldrich n^{o} T8532) in PBS 0.1M for 48 hrs at 4^{o}C;
- Rinse twice with dH_2O for 30 minutes;
- Add sodium deoxycholate (Sigma Aldrich n^{o} 30970) 0.03% in PBS 0.1M for 24 hrs at 4^{o}C;
- Rinse twice with PBS 0.1M for 30 minutes, then rinse with dH_2O sterile;
- Store the decellularized thyroid lobe in PBS 0.1M at 4^{o}C until sterilization (see below).

1.2.2 Second decellularization protocol

- Add trypsin 0.01% EDTA 0.25% in PBS 0.1M for 1 hour at 37^{o}C;
- Rinse with dH_2O for 2 hrs at RT;
- Add triton X-100 3% in PBS 0.1M overnight (ON) at 4^{o}C;
- Rinse twice with dH_2O for 30 minutes;
- Add sodium deoxycholate 0.3% in PBS 0.1M ON at 4^{o}C;
- Rinse twice with PBS 0.1M for 30 minutes at RT, then rinse with dH_2O sterile;
- Store the decellularized thyroid lobe in PBS 0.1M at 4^{o}C until sterilization (see below).

1.2.3 Third decelularization protocol

- Add triton X-100 0.1% in PBS 0.1M for 24 hrs at 4^{o}C;
- Rinse twice with dH_2O for 1 hour at RT;
- Add sodium deoxycholate 2% in PBS 0.1M for 24 hours at 4^{o}C;
- Rinse twice with dH_2O for 1 hour at RT;

- Add sodium chloride (NaCl) 1M in PBS 0.1M for 1 hour at RT;
- Rinse twice with dH_2O for 1 hour at RT;
- Add DNAase (Sigma Aldrich n^o D4263) 30 µg/ml + 1,3 mM $MgSO_4$ + 2mM $CaCl_2$ in dH_2O for 1 hour at RT;
- Rinse with PBS 0.1M ON at RT;
- Rinse twice with dH_2O for 30 minutes at RT, then rinse with dH_2O sterile;
- Store the decellularized thyroid lobe in PBS 0.1M at 4°C until sterilization (see below).

- Sterilization of the decellularized thyroid matrices

  This passage was made in sterile conditions, under a laminar flow hood;

- Add peracetic acid 0.1% in PBS 0.1M for 3 hrs at RT;
- Rinse twice with sterile dH_2O for 10 minutes;
- Store the matrix in PBS 0.1M + Gentamicin 0.01 mg/ml (Sigma Aldrich n^o G1397) at 4°C.

1.3 MOLECULAR ANALYSIS OF THE RESIDUAL DNA WITH CyQUANT® Cell Proliferation Assay Kit

Prior to the DNA molecular analysis, all decellularized (4 lobes in total) and native (3 lobes in total) thyroid lobes were weighed with an analytical balance to get their wet weight. Then, each lobe was digested in 1 ml of Lysis Solution (LS) at 56°C ON. The LS was composed by 1 mg/ml proteinase K (Sigma Aldrich n^o P2308) in 50 mM Tris (Sigma Aldrich n^o A5456-3) pH 7.6, and a protease inhibitor cocktail made with 1 mM EDTA + 1 mM iodoacetamide + 10 µg/ml Pepstatin A (Sigma Aldrich n^o P5318) diluted in DMSO (FLUKA n^o 41640).

Preparation of the CyQUANT dye solution was made by mixing the Working Buffer with the CyQUANT® GR dye 400X, both supplied by the kit. For DNA measurements, a calibration curve was prepared in a 96 multiwell plate using 200 µl serial dilutions (0, 50, 200, 600, 1000 ng/ml) of the bacteriophage λ DNA in CyQUANT dye solution.

For analysis, 5 µl of each digested samples (decellularized and native thyroid lobes) were dissolved in 195 µl of CyQUANT dye solution in a 96 well plate. Three replicates for each sample were made. Finally, the results were averaged, and standard deviation calculated.

The analysis of the calibration curve and samples multiwell plates were performed using a Victor 3V Multilabel Plate Readers (Perkin Elmer), with the fluorescein protocol at λ 485/535. Resultant readings provide an optical density number (OD) that increases with the increase of the DNA quantity. For each sample, the amount of DNA was normalized to the dilution factor and wet weight of the native tissue (intact thyroid and decellularized matrix), and expressed as ng DNA/mg wet tissue.

1.4 MASS SPECTROMETRY ANALYSIS

1.4.1. Sample preparation

For mass spectrometry analysis, 18 thyroid lobes were used whose 6 for each decellularization protocol. First, thyroid matrices were disrupted by immersion in liquid nitrogen, and mechanical breaking using a pestle, then samples were suspended in Trizma HCl 0.1M + NaCl 0.1M at pH 7.8 and processed as follow:

- Sonication of samples at 42 kHz in an ultrasonic bath (Bransonic ultrasonic cleaner 2510E) at 60^{o}C for 24 hrs,
- Reduction of the bi-sulfur bound with dithiotreitol (DTT) (Sigma Aldrich D0632) 5mM at 37^{o}C for 55 minutes;

- Alkylation with iodoacetamide (IAA) (Sigma Aldrich I1149) 10mM at RT for 30 minutes in the dark;
- Reduction with DTT 5mM at 37^{o}C for 15 minutes;
- Digestion of proteins with trypsin 5 µg/µl (Sigma Aldrich T4799) for a final 1:50 enzyme/substrate ratio at 37^{o}C for 24 hrs;
- Stop trypsin digestion with 3 µl of acetic acid 98%.

Subsequently, all samples were dried in a stream of nitrogen, and the pellet resuspended in 100 µl of a water/acetonitrile (AcN) (Fisher 75058) mixture (50/50, v/v).

1.4.2. LTQ Orbitrap XL shotgun proteomics

In order to obtain a qualitative proteomic screening of the thyroid matrix, a single decellularized lobe for each protocol was digested (see point 1.4.1 of this section), and subjected to MS analysis. LC analysis was made with a capillary column Jupiter® 5 µm C18 300 Å, 150 x 0.3 mm (Phenomenex) at a flow-rate of 5 µL min-1. Eluting mixtures included solvent A (0.1% aqueous formic acid (FA), v/v) and B (0.05% FA in AcN, v/v). Gradients were set as follows: 5 minutes with the 2% solution B, then a graded increase of 2% solution B/min for 15 minutes, cleaning for 3 minutes with 85% solution B, and column re-conditioning for 11 minutes with 2% solution B. The mobile phase was delivered by a Dionex Ultimate 3000 chromatographic system (Dionex Corporation, San Josè, CA, USA) with a 200-vial capacity. Volume of the injected sample was 5 µL. Mass spectrometer was an LTQ Orbitrap XL instrument (ThermoScientific Corporation, San Josè, CA, USA) equipped with ESI interface and controlled by Xcalibur software.

Conditions of the interface were as follows: ESI voltage 3.5 kV, capillary voltage 13 V, capillary temperature 275°C, tube lens 85 V. In the first scan event (full scan) the m/z window was 200-1800 with a resolution of 60.000. The four highest mass-to-charge ratios

over a threshold of 100.000 counts were selected for collision-induced dissociation (CID) in the ion trap, with normalized collision energy of 35% and collision gas pressure of 2.3x10-3 mbar in the collision cell. The obtained raw data were imputed into Proteome Discoverer software (version 1.4) with SEQUEST as search algorithm. Cysteine carbamidomethylation was selected as fixed modification. Confident identification was obtained using stringent filter criteria: DeltaCN was set at 0.1, XCorr vs. charge state was set at 1.5 (for 1+ charge) and 2 (for 2+ charge). Peptide probability was set at 0.05 (5%). Proteins identification was made processing data for the *Rattus Norvegicus proteins* database (Uniprot). As a further parameter to assess the reliability of the result, only the proteins with Proteome Discoverer protein score value ≥ 2.5 has been selected in this analysis.

1.4.3. HPLC-MS/MS-SRM

The standard of collagen type I (Bovine), II (Bovine tracheae), III (Human), IV (Human) and V (Human placentae) were all purchased from Sigma Aldrich (St. Louis, MO, USA). These collagen standards have been used to set up the HPLC-MS/MS-SRM protocol: for each collagen type, one specific target peptide for each collagen types (I to V) has been previously selected by high resolution MS analysis. Subsequently, BLAST (Basic Local Alignment Search Tool; www.ncbi.nml.nih.gov link NCBI BLAST) search (algorithm: blastp; MATRIX PAM 30; GAP COASTS: existence 10, extension 1; DATABASE: non redundant protein sequences) analysis was performed to further confirm targeted peptides uniqueness. The chosen peptides from Bovine (Bos Taurus, Uniprot id: 9913) and Human (Homo Sapiens, Uniprot id: 9606) collagen standards share 100% identity at the aminoacidic level with Rattus Norvegicus (Uniprot id:10116).

For the quantification of collagen I to V have been used five thyroid lobes for each decellularization protocols (15 lobes in total). Samples preparation for both collagen standard and samples was set as previously described (see 1.4.1 paragraph in this section).

LC separation has been carried out on a Agilent Poroshell 120 C18 column (75x2.1 mm, 2.7 µm), thermostated at 25^{o}C using a gradient solvent elution system [(A) aqueous FA 0.1% solution (v/v)/(B) 0.08% (v/v) FA in AcN] delivered at 0.2 ml/min under gradient elution. The mobile phase was delivered by the Agilent HP 1260 chromatographic system (Agilent Technologies, USA) equipped with a 200-vial capacity sample tray. Injection volume was 5 µl and the concentration of each collagen standard was 1 µg/µl. A QTRAP 4000 triple quadrupole instrument (ASCIEX) equipped with a pneumatically assisted ESI interface has been used. The system was controlled by the Analyst v 1.4 software. The sheath gas (nitrogen, 99.999% purity) and the auxiliary gas (nitrogen, 99.998% purity) were delivered at flow-rates of 45 and 5 arbitrary unit, respectively. ESI conditions were set as follows: voltage 4.5 kV, capillary voltage 50 V, capillary temperature 350^{o}C. MS/MS experiments were performed under SRM conditions with a collision gas (N_2) pressure of 2.1×10^{-3} mbar in the collision cell. The amino acid composition of the signal peptide and the respective m/z transitions were reported in table 2.

Table 2. Peptides selected for each collagen type for targeted SRM analysis.

Collagen type	Peptide sequence	SRM transition (m/z) / (m/z)
Iα1	GSEGPQGVR	443/613
IIα1	TGPAGAAGAR	414/335
IIIα1	GNDGAR	498/377
IVα1	GPPGGVGFPGSR	558/962
Vα1	AGSDGAR	504/853

Quantitation of collagen types I-V in the matrix samples was achieved through proportion, by comparing the ionic intensity corresponding to a known concentration of the selected tryptic peptide of each collagen standard with that of the corresponding peptide in the volume of solubilized matrix with unknown concentration.

For the SRM analysis, every ionized peptide had to meet the following criteria:

a. detected in all standard samples of given collagen type;

b. be a tryptic peptide, i.e. a peptide obtained by cleavage with trypsin at the specific sites;

c. be unique to a given collagen type;

d. be common to mouse, rat, and humans.

2. 3D BIOPRINTING OF COLLAGEN FROM RAT TAIL TENDONS

2.1 EXTRACTION AND SOLUBILISATION OF COLLAGEN FROM RAT TAIL TENDONS

To obtain a collagen solution starting from rat tail tendons, we used tails derived from adult male Sprague-Dawley rats weighing 225-250g, sacrificed for the general experimentation. Tendon bundles were surgically extracted and placed in PBS 0.1M, then washed with dH_2O and lyophilized (Christ Alpha 2-4 LSC plus) (table 3).

Table 3. Lyophilisation process.

	Loading	Freezing	Principal drying						Final drying		
Time (h:m)	-	0:02	0:15	2:00	2:00	2:00	2:00	2:00	2:00	2:00	10:00
Temp. (^oC)	-40.0	-40.0	-20.0	-20.0	-10.0	0.0	10.0	20.0	30.0	40.0	40.0
Vacuum (Mbar)	-	-	0.1	0.1	0.1	0.1	0.1	0.1	01	0.02	0.02

The lyophilisation process is necessary for obtain a correctly weight of the tendons. Subsequently, tendon bundles were solubilized at 4°C in dH_2O and acetic acid for 48 hrs in slow stirring. Different molarities of acetic acid (0.5M, 1M and 2M) were tested.

Finally, solutions were purified with two cycles of ultracentrifugation at 4^oC including 14.636 G for 1 hour and 39.191 G for 1.30 hrs (Beckman Coulter Avanti J-20 XP).

2.2 SOLUBILISATION OF CHITOSAN

Chitosan powder (PRIMEX Ehf, Siglufjordur, Iceland; degree of deacetylation 95%) was solubilized at a concentration of 6% w/v at RT in dH_2O with 0.5M acetic acid (pH 3). The solution was kept in slow stirring for 48-72 hrs until the powder was completely dissolved.

2.3 PREPARATION OF 2D FILM OF COLLAGEN AND CHITOSAN

2D films of solutions of collagen (2% w/v of rat tail tendons solubilized in acetic acid 0.5M) and chitosan (6% w/v solubilized in acetic acid 0.5M) were obtained by layering each solution on glass slides for optical microscopy, and making them of the same thickness (600 μm) using a mechanical pressure device. Finally, each biomaterial film was subjected to lyophilization (table 3).

2.4 MASS SPECTROMETRY ANALYSIS OF COLLAGEN FROM RAT TAIL TENDONS

2.4.1 Sample preparation

The protein composition of the rat tail tendon solution was analyzed by digesting the sample with pepsin (Sigma Aldrich n^o P7012) 0.1 g/ml in a 1:50 enzyme to proteins ratio at 37^{o}C for 72 hrs. Digestion was stopped with the addition of sodium hydroxide (NaOH) 2% in dH_2O (v/v). Then, the sample was dried-out under a nitrogen flow, and resuspended in a HPLC water-AcN 1:1 ratio for MS analysis.

2.4.2 LTQ-Orbitrap XL

Proteomic analysis to characterize the collagen composition of the rat tail tendons was performed using the same MS system and data analysis applied to analyze the composition of the decellularized thyroid matrix (see section 1.4.2). Protein identification was made using data from the *Rattus Norvegicus proteins* database. As a further parameter to assess the reliability of the result, only proteins with Proteome Discoverer protein score value ≥ 2.5 were selected.

2.5 3D PRINTING OF SCAFFOLDS OF COLLAGEN AND CHITOSAN WITH SPECIFIC GEOMETRY

For the bioprinting process, a 3D printer prototype developed by Rubens Forensi PhD of the Department of Mechanical Engineering at the University of Parma (Parma, Italy), was used. The bioprinter was generously made available by the Department of Pharmacy of the University of Parma. Before extrusion, the viscosity of the collagen solution from the rat tail tendons was measured at RT using a Brookfield viscometer (Fungilab), to ensure a viscosity compatible with the bioprinting equipment (acceptable range: 8,000-25,000 centiPoise). The extrusion was performed on a cooled surface (Peltier plates at -18^{o}C), and the solution deposited in three alternate layers reciprocally orthogonal, each layer stacked on top of the other, to give rise to a sort of gauze with congruent rectangular openings. The final result was porous collagen filaments with a filament thickness of 200 µm, spaced by 200-250 µm rectangular openings, with a maximum height of 600 µm. The obtained 3D scaffolds were lyophilized (see above Table 3) and sterilized in PBS 0.1M with 2% penicillin / streptomycin (Aurogene AU-L0022), and 40 µl/100ml of gentamicin (Sigma Aldrich G1397).

2.6 ATTENUATED TOTAL REFLECTANCE-FOURIER TRANSFORM INFRARED SPECTROSCOPY (ATR-FT-IR) OF COLLAGEN FROM RAT TAIL TENDONS

Infrared spectroscopy is a spectroscopic absorption technique used for the characterization of materials. It is based on recording changes in the vibrational state of a molecule when it absorbs photons. Specifically, such absorption determines a passage from the fundamental vibrational state to an excited vibrational state. This produces a spectrum characterized by peaks in which the frequency scale (expressed as wave number, cm-1) is placed on the x-axis while the percentage of transmittance (fraction of incident light that passes through the sample at a given wavelength) is placed on the y-axis. This technique has been used to verify possible modifications in the chemical bonds of the collagen from the rat tail tendons caused by the use of different molarities of acetic acid for collagen solubilization, or by the bioprinting process. A Thermo Nicolet 5700 spectrometer equipped with Thermo Smart Orbit ATR diamond was used for the analysis of a 2% w/v (tendon in water) collagen scaffold, solubilized with different molarities of acetic acid (0.5, 1 and 2 M). Analysis was performed with a spectrum in the range of 4000-400 cm-1 wavelength.

2.7 MORPHOMETRIC ANALYSIS ON THE MICROPOROSITY OF THE 3D PRINTED COLLAGEN FROM RAT TAIL TENDONS

In order to verify the reproducibility of the bioprinting process of collagen from the rat tail tendons, the surface area of filament microporosities was analyzed using the AxioVision 4.8 image analysis software (Zeiss). The morphometric calculations were performed on SEM images of four different 3D collagen scaffolds, acquired at the same magnification (160X), and in the same area (the intersection of the extruded filaments). All the examined

scaffolds were printed using a 2% w/v collagen from a rat tail tendons solution, solubilized with acetic acid 1M. For each sample, 20 different pores were randomly selected.

Starting from the scale bar size of each SEM image (scale bar = 100 μm), the edges of each pore were manually traced with the cursor. At the end of the trace, the software returned the surface area measurement (μm^2). Differences in the mean size of the filaments porosities for each collagen scaffold were determined with a multiple-way ANOVA. Differences were considered statistically significant for $p<0.05$.

2.8 FUNCTIONALIZATION OF POLY-L-LACTIC ACID (PLLA) MICROPOROUS SCAFFOLDS WITH COLLAGEN AND CHITOSAN

Different concentrations of collagen from rat tail tendons (0.1%, 0.5%, 2.5% and 5%) and chitosan (0.2%, 0.5%, 1% and 2.5%) were used to cover microporous disks of PLLA 4% in dichloromethane w/v (Sigma Aldrich $n^0$270997). These PLLA disks engineered by the research group of Prof. Toni have a surface of 0.785 cm^2, and details on their biomaterial synthesis, structural characteristics, and biocompatibility have been recently published[110].

Coating of the PLLA disks with the lowest biomaterial concentrations (0.1% and 0.5%) was obtained by direct immersion of PLLA scaffold in the collagen and chitosan solutions, to obtain an homogeneous and very thin coating, stable for capillarity. In contrast, coating of the PLLA disks with the highest biomaterial concentrations (2.5 % and 5% for collagen, 1% and 2.5% for chitosan) was obtained by dropping the biomaterial onto the disk, followed by mechanical stretching of the viscous solution, to obtain an homogeneous and very thin biomaterial thickness. Immediately after coating, all samples were subjected to lyophilization (see Table 3) to favor the stabilization of weak intermolecular bonds such as dipole-dipole interactions, between the polymerized PLLA and the positively charged amino groups of collagen and chitosan.

2.9 SCANNING ELECTRON MICROSCOPY (SEM)

SEM was used to investigate the geometry of the 3D bioprinted collagen or chitosan scaffolds, microporous PLLA scaffolds coated with either collagen or chitosan, and the morphology of cells grown on these supports. Initially, samples were fixed with glutaraldehyde 2.5% in cacodylate sodium buffer 0.1M ON at 4°C, and subsequently dehydrated in graded ethanols (50% to 100%). Then, samples were subjected to Critical Point Drying (Balzers) with ethanol/liquid CO_2 system, without substantial deformation of their 3D structure. Finally, dried samples were mounted on aluminium stubs, and metallized for 90s using gold sputtering to cover scaffolds with a 60 nm gold film. This coating increases the ability of samples to conduct electricity, and emit secondary electrons. All samples were observed with a Philips SEM501.

2.10 EVALUATION OF CELL MORPHOLOGY AFTER GROWTH ON BIOPRINTED COLLAGEN AND CHITOSAN SCAFFOLDS, AND MICROPOROUS PLLA DISKS COATED WITH EITHER COLLAGEN OR CHITOSAN

To study the effect on cell morphology of scaffolds bioprinted with different concentrations of either rat tail collagen or chitosan, and that of coating microporous PLLA disks with either collagen or chitosan, two different cell types were used:

1. Swiss 3T3 (courtesy of Prof. Lucio Cocco, University of Bologna) murine fibroblast cell line, growing in DMEM high glucose (Euroclone ECB7501L) with 10% FBS (Fetal Bovine Serum) (Aurogene AU-S1810), 1% essential amino acids (Aurogene AU-X0557), 1%

glutamine (Aurogene AU-X0550), 1% of penicillin / streptomycin (P/S) (Aurogene AU-L0022) and 20 µl/100ml of gentamicin (Sigma Aldrich G1397);

2. Rat TSC/P recently isolated and characterized by the group of Prof. Toni[100,102,103]. Cells were cultured in DMEM low glucose (Aurogene AU-L0064) with 10% FBS and 5% FHS (Fetal Horse Serum) (AU-5090H), 1% of essential amino acids, 1% glutamine, 1% P/S and 20µl/100ml of gentamicin.

Initially, both 3D bioprinted and microporous scaffolds of PLLA coated with either collagen or chitosan were conditioned for 24 hrs in culture medium. For 3D bioprinted scaffolds, Swiss 3T3 cells were seeded at 10,000 cell/cm^2 , and grown for 24, 48 and 72 hrs at 37°C. In contrast, TSC/P were seeded and grown in the same condition but only for 24 hrs. For microporous PLLA scaffolds coated with collagen, TSC/P were seeded at 10,000 cells/cm^2 for 24 hrs, while for microporous PLLA scaffolds coated with chitosan TSC/P were seeded either at 12,500 cells/cm^2 for 24 hrs, or at 6,250 cells/cm^2 for 5 days.

3. PROTEOMICS SIGNATURE OF ADULT, MALE RAT THYROID STEM CELL / PROGENITORS

3.1 GROWTH AND EXPANSION OF RAT THYROCYTES AND THYROID STEM CELLS / PROGENITORS

Primary adult male rat thyrocytes (THY) at passage 5 (P5), and adult male rat TSC/P at passage 22 (P22) were isolated from the thyroids of 50-75 gr. (3-4 weeks old), Sprague Dawley® (SD®) male rats, as previously described[101,103,104]. For the proteomics experiment, cells were grown up to 80% of confluence, harvested using a cell scraper, and centrifuged at 272 G for 10min (ThermoScientific SL-8 centrifuge). Cell pellets were washed twice with PBS 0.1M, and stored at -80^{o}C until the day of analysis.

3.2 FILTER AIDED SAMPLE PREPARATION (FASP)

- Cells pellet were lysed by sonication (Elmasonic S40) in Sodium Dodecyl Sulphate (SDS) (Fisher BP166) lysis buffer (1% (w/v) SDS in 0.1M Tris/HCl, pH 7;6) and incubated at 95°C for 5 minutes. Working volume was 130 µl;
- Cell lysates were centrifuged at 16,000 G for 5 minutes (Eppendorf centrifuge 5417r) and the supernatants were recovered;
- The protein content was measured using Pierce® BCA Protein Assay Kit (Thermo Scientific), at λ of 562nm (BMG LABTECH CLARIOstar spettrophotometer);
- 100 µg of proteins for each sample were mixed with UA buffer (8 M urea in 0.1M Tris/HCl, pH 8.5) in a new 1.5 ml Eppendorf vial;

- Samples were reduced with DTT 0.1M (Apollo BIMB1015) in UA buffer, and incubated at 37^{o}C for 5 minutes;
- Samples were loaded onto 30,000 MWCO Vivacon 500 spin membranes (Sartorius), and centrifuged at 14,000 G for 40 minutes (4^{o}C);
- 200 µl of UA solution were added to each sample, gently mixed, and centrifuged at 14,000 G for 40 minutes (4^{o}C);
- Samples were alkylated with IAA 0.05M (Sigma Aldrich 16125) in UA buffer (pH 8.0), and incubated without mixing for 5 minutes at RT in the dark;
- The filter unit of the 30,000 MWCO Vivacon 500 spin membranes was centrifuged at 14,000 G for 30 minutes (20^{o}C);
- 100 µl of UB buffer (8M urea in 0.1M Tris/HCl, pH 8.0) were added to the filter unit, and centrifuged at 14,000 G for 40 minutes (4^{o}C). This step was repeated twice;
- Samples were digested ON at RT with 40 µl of UB buffer with Lys-C 0.66 µg/µl (Wako 125-05061) at 1:50 enzyme to protein ratio. Then, the filter unit was transferred into a new 1.5 ml Eppendorf vial;
- Peptides were digested again with trypsin 0.2 µg/µl (Promega V5111) in ABC buffer (0.05 M NH_4HCO_3 in MilliQ dH_2O), 1:100 enzyme to protein ratio, for 3 hrs at 37^{o}C;
- Filters with digested peptides were centrifuged at 14,000 G for 40 minutes at 4^{o}C;
- NaCl 0.5M was added, and samples were centrifuged at 14,000 G for 20 minutes at 4^{o}C;
- Peptide concentration was estimated using a ND-1000 NanoDrop spectrophotometer at λ of 280 nm;
- To stop the digestion, trifluoroacetic acid (TFA) 1% was added to the samples;
- Peptides were desalted and purified with in house prepared StageTip using solid phase extraction disk (Empore™ SPE Disks C8, diam. 47 mm). StageTips were activated by

washing with 50% AcN 0.1% TFA prior to addition of peptides in aqueous 1% TFA (5 µg of peptides for each samples);

- StageTip were washed twice with 1% TFA, and peptides were eluted with 50% AcN 0.1% TFA, then the peptides were dried by evaporation (Eppendorf concentrator plus).

3.3 MASS SPECTROMETRY ANALYSIS

Samples were analysed by nano- flow reverse phase UltiMate™ 3000 RSLCnano system (ThermoScientific, USA) connected to a Orbitrap Fusion Tribrid system (ThermoScientific, USA). Dried peptides (10 µg) were reconstituted in 20 µl of 2% AcN with 0.1% FA and 2 µg of peptides were used for the analysis. Tryptic peptides were separated using a PepMap RSLC C18, 2 µm, 100 Å, 75 µm internal diameter × 25 cm of length, using 146 minutes linear gradient from 2% to 90% AcN with a flow rate of 0.300 µl/min. The resolution of the Orbitrap at full scan MS was 120,000 and MS/MS spectra was obtained using high collision induced (HCD) fragmentation.

3.4 DATA PROCESSING AND STATISTIC ANALYSIS

The raw data from the Orbitrap Fusion were first visually analysed with Xcalibur™ software, then MaxQuant computational proteomics platform (version 1.4.1.2) was used for process the data. Proteins identification was made by Andromeda search engine against the *Rattus Norvegicus* database (Uniprot proteome ID: UP000002494), containing 29,966 proteins. Trypsin was chosen as a specific digestion mode with up to two missed cleavages. Proteins N-terminal acetylation and oxidation of methionine was set as variable modifications and carbamidomethylation of cysteine as a fixed modification. Minimum

peptide length was fixed at 7, mass tolerances and false discovery rate (FDR) for both peptides and proteins was set at 1%.

Analysis of the biological relevance of data from MaxQuant was made with Perseus (version 1.6.1.1). In order to facilitate the calculation of the proteins expression fold change, rat TSC/P and THY samples were grouped in two group and values were transformed to a log2 scale. This transformation generate a pool of “NaN” (Non Assigned Number) values that were sorted choosing 3 as a minimum number of valid values in at least one group (which means that a protein must be present in at least one group to be consider a valid values). Overlap and variability between biological replicates was reported as Venn diagrams and Pearson correlations. Different proteins expression between rat TSC/P and THY was highlighted with Student’s t-tests with a p-value threshold of 0.05. Hierarchical clustering with Euclidean distances was performed after z-score normalisation. GO analysis for cellular components, biological processes, networks and KEGG (Kyoto Encyclopedia of Genes and Genomes) annotations was performed with Perseus and STRING (Search Tool for the Retrieval of Interacting Genes/Proteins) version 10.5.

RESULTS

1. DECELLULARIZED RAT THYROID GLAND

1.1 MOLECULAR ANALYSIS OF THE RESIDUAL DNA WITH CyQUANT® Cell Proliferation Assay Kit

The calibration curve resulting from the OD vs λ bacteriophage DNA concentration plotting gave an optimal interpolation with an $R^2 = 0.994$. The resulting straight line's equation was y = 2241.3x + 130942 (figure 11).

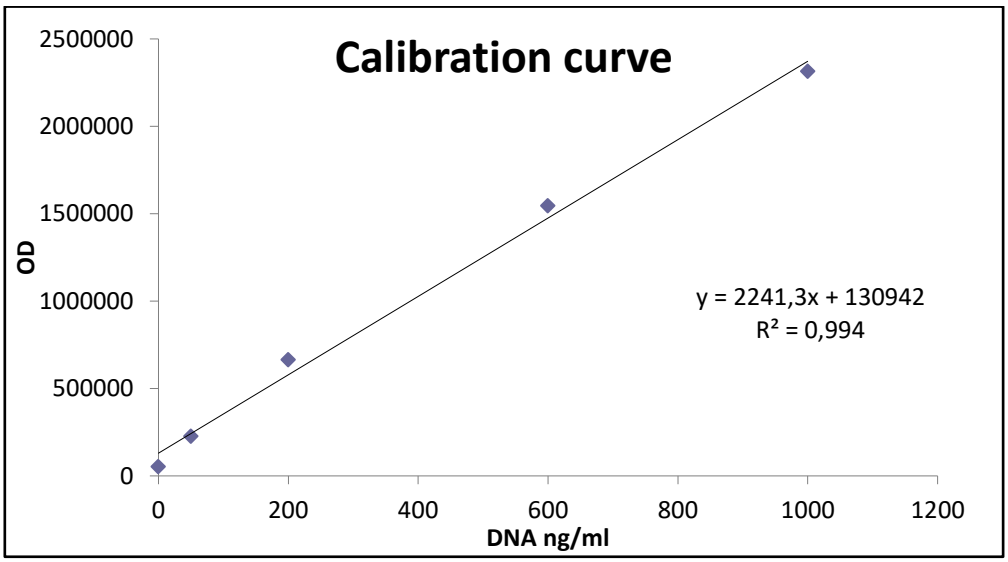

Figure 11. Calibration curve of λ DNA

Table 4 shows the mean of results obtained from the DNA quantification of 3 adult male rat native thyroid lobes (Ctrl1, Ctrl2 and Ctrl3), 2 rat thyroid matrices decellularized with the first protocol, and one thyroid matrix for the second and

third protocol, respectively. Native rat thyroid lobes showed a DNA amount ranging from 723 to 1791 ng/mg of tissue, conversely decellularized matrices resulted not contaminated with residual DNA, confirming that all decellularization method was efficient and reliable.

Table 4. Results of the DNA quantification in control and decellularized rat thyroids lobes by CyQUANT® analysis. n.d.= not detected.

Sample (wet weight)	DNA concentration on interpolation (ng/ml)	DNA concentration after dilution factor correction (ng/ml)	DNA concentration in the thyroid tissue (ng / mg wet tissue)
ctrl 1 (3 mg)	114.84 ± 8.28	4593.49 ± 331.26	1531.16 ± 110.42
ctrl 2 (5 mg)	90.43 ± 13.06	3617.03 ± 522.57	723.40 ± 104.51
ctrl 3 (2 mg)	89.56 ± 10.85	3582.38 ± 434.18	1791.19 ± 217.09
protocol 1 matrix 1 (5 mg)	n.d.	n.d.	n.d.
protocol 1 matrix 2 (3 mg)	n.d.	n.d.	n.d.
protocol 2 matrix (4.5mg)	n.d.	n.d.	n.d.
protocol 3 matrix (3.9mg)	n.d.	n.d.	n.d.

1.2 MASS SPECTROMETRY ANALYSIS

1.2.1 LTQ Orbitrap XL

Tables 5 shows the main ECM proteins, receptors, enzymes and GFs detected in each thyroid matrix after different decellularization protocols. Proteins are classified with their respective Uniprot IDs, names, Proteome Discoverer score value and the percentage of the protein sequence covered by identified peptides (coverage):

Table 5. Proteins identified in rat thyroid matrix after each decellularization protocol

First protocol

Uniprot ID	Protein name	Score	Coverage (%)
P02454	Collagen alpha-1(I) chain	196.04	32.69
A0A0G2KAN1	Collagen alpha-2(I) chain	119.32	30.32
P13941	Collagen alpha-1(III) chain	32.39	10.25
F1LNH3	Procollagen. type VI, alpha 2, isoform CRA_a	31.52	15.48
P05539	Collagen alpha-1(II) chain	25.34	8.17
A0A0G2K601	Protein Col4a6	20.12	2.20
D3ZUL3	Protein Col6a1	15.79	8.39
Q5EB88	Col6a2 protein (Fragment)	14.73	24.44
Q80ZF0	Collagen alpha-1(XXVII) chain	8.33	3.67
M0RDG5	Protein Col25a1	6.16	2.52
F1M897	Protein Col22a1	5.58	5.58
F1M6Q3	Protein Col4a2	5.09	4.62
Q9ERB4-3	Isoform Vint of Versican core protein	4.33	1.81
A0A0G2K944	Versican core protein	4.33	1.86
F1LQ00	Protein Col5a2	4.30	5.42
F1LUN5	Protein Col4a5	4.14	4.55
Q01129	Decorin	3.78	5.65
G3V9M6	Fibrillin 1	3.55	1.01
Q31261	Rat MHC class I truncated cell surface antigen	3.55	6.60
P51886	Lumican	3.47	6.51
F1MA59	Protein Col4a1	3.12	5.33
G3V830	Interleukin 10 receptor, alpha	2.90	6.68
P70505	Disintegrin and metalloproteinase domain-containing protein 1	2.52	7.35
Q9R1E9	Connective tissue growth factor	2.50	11.24

Second protocol

Uniprot ID	Protein name	Score	Coverage (%)
P02454	Collagen alpha-1(I) chain	157.36	26.22
A0A0G2KAN1	Collagen alpha-2(I) chain	119.39	30.39
D3ZUL3	Protein Col6a1	29.26	10.24
Q5EB88	Col6a2 protein (Fragment)	23.28	30.67
P05539	Collagen alpha-1(II) chain	16.31	7.75
A0A0G2K601	Protein Col4a6	14.81	4.46
P13941	Collagen alpha-1(III) chain	12.60	4.65
F1LND0	Protein Col16a1	7.63	3.96
D3ZE04	Procollagen, type VII, alpha 1 (Predicted)	7.53	5.06
Q01129	Decorin	6.90	6.78
Q9Z1Y3	Cadherin-2	5.06	7.17
A0A0G2K742	Protein Col4a4	4.74	5.29
Q80ZF0	Collagen alpha-1(XXVII) chain	4.49	5.71
D3ZCQ0	Protein Col19a1	3.91	1.59
F1M6Q3	Protein Col4a2	3.85	1.03
M0RDG5	Protein Col25a1	3.85	2.52
G3V824	Insulin-like growth factor 2 receptor	3.85	1.13
Q9JI03	Collagen alpha-1(V) chain	3.54	3.86
Q9JI04	Alpha 4 type V collagen	3.13	3.74
F1MA59	Protein Col4a1	3.12	3.71
F1LQ00	Protein Col5a2	2.65	4.22
F1MA59	Protein Col4a1	3.12	3.71
Q10739	Matrix metalloproteinase-14	3.05	7.39
A0A0G2QC48	Thyroid hormone receptor beta	2.80	7.24
Q05030	Platelet-derived growth factor receptor beta	2.80	3.37
J9SG97	Epidermal growth factor	2.73	2.92
O35757	Vascular endothelial growth factor C	2.63	15.90
A0A0G2K210	Fibroblast growth factor receptor	2.62	3.62
D4A8I9	Interleukin 9	2.56	29.86

Third protocol

Uniprot ID	Protein name	Score	Coverage (%)
P02454	Collagen alpha-1(I) chain	252.25	34.96
A0A0G2KAN1	Collagen alpha-2(I) chain	200.35	31.92
P13941	Collagen alpha-1(III) chain	60.46	17.57
P05539	Collagen alpha-1(II) chain	26.10	6.91
D3ZUL3	Protein Col6a1	23.30	9.56
A0A0G2K601	Protein Col4a6	21.55	5.98
F1LNH3	Procollagen, type VI, alpha 2, isoform CRA_a	18.01	9.25
Q5EB88	Col6a2 protein (Fragment)	14.63	16.00
Q01129	Decorin	11.81	13.84
F1LQ00	Protein Col5a2	10.70	8.77
F1M897	Protein Col22a1	6.70	5.33
M0RDR9	Protein Col6a1	6.67	4.51
D4AC70	Protein Col8a1	6.14	10.48
Q9JI03	Collagen alpha-1(V) chain	5.69	3.80
Q80ZF0	Collagen alpha-1(XXVII) chain	5.63	3.45
D3ZX71	Protein Col9a3	5.13	16.03
Q5BJ95	Interleukin-17F	4.88	30.43
F1LZF4	Protein Col6a5	4.82	3.31
A0A0G2K742	Protein Col4a4	4.67	7.13
P15207	Androgen receptor	4.41	1.44
F1LND0	Protein Col16a1	3.82	5.75
Q31261	Rat MHC class I truncated cell surface antigen	3.66	6.60
O35800	Hypoxia-inducible factor 1-alpha	3.38	4.85
P26342	Transforming growth factor beta receptor type 3	3.34	5.28
Q1EHB3	A disintegrin and metalloproteinase with thrombospondin motifs 7	3.30	2.82
P06882	Thyroglobulin	3.16	2.35
P70570	Laminin-5 alpha 3 chain	3.11	2.38
P35859	Insulin-like growth factor-binding protein complex acid labile subunit	2.94	6.80
F1LPI5	Laminin, beta 3	2.88	3.24
P25961	Parathyroid hormone-related peptide receptor	2.62	5.08
P38438	TGF-beta receptor type-2	2.60	5.29

Figure 12 shows the collagens detected in the decellularized thyroid gland in relation to each of the decellularization protocols used, based on the Proteome Discoverer score value.

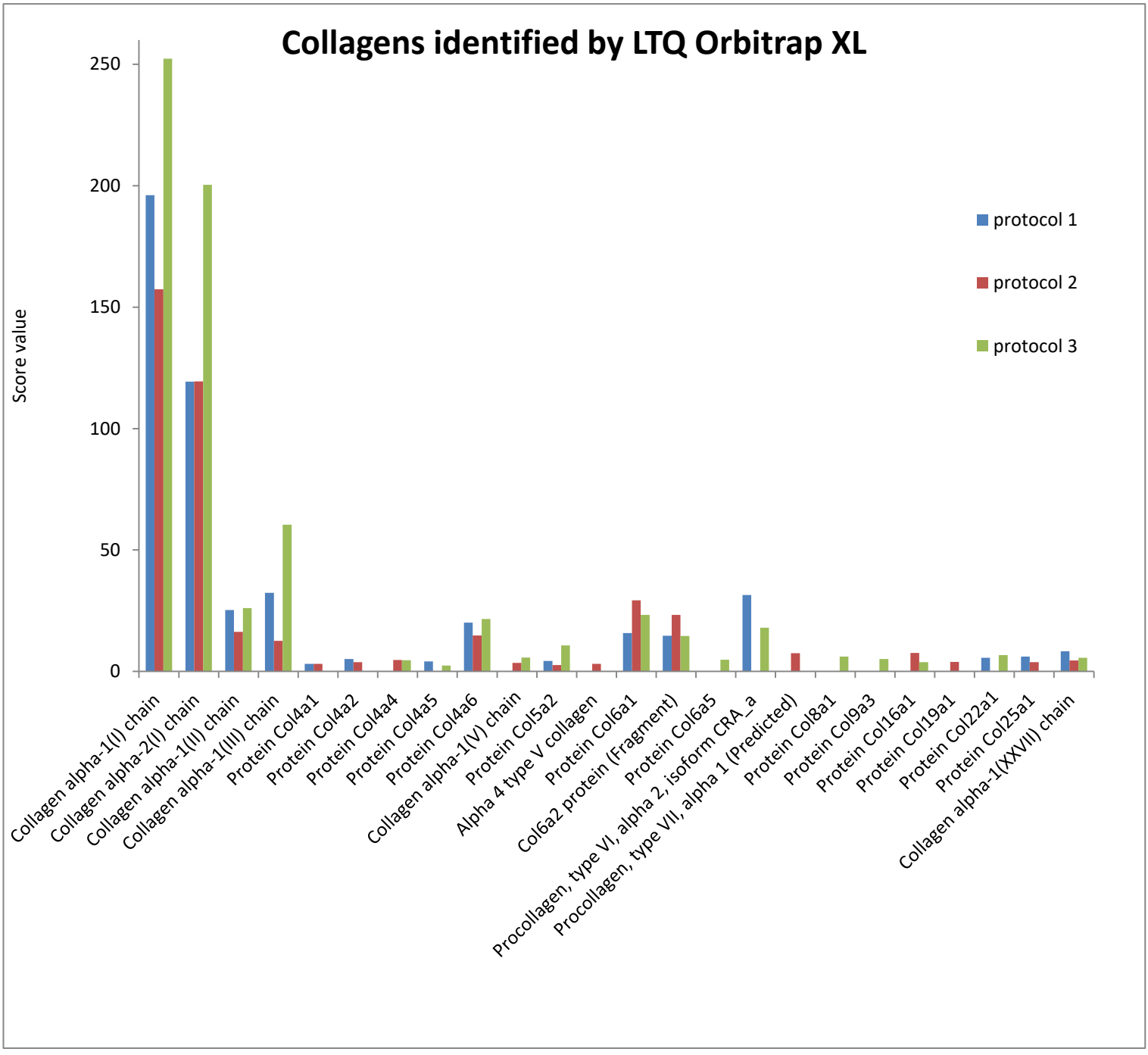

Figure 12. Collagens with score ≥ 2.5 identified by LTQ Orbitrap XL in rat thyroid matrices decellularized with three different protocols.

Figure 13 shows the presence of non-collagenous ECM proteins in each decellularization process.

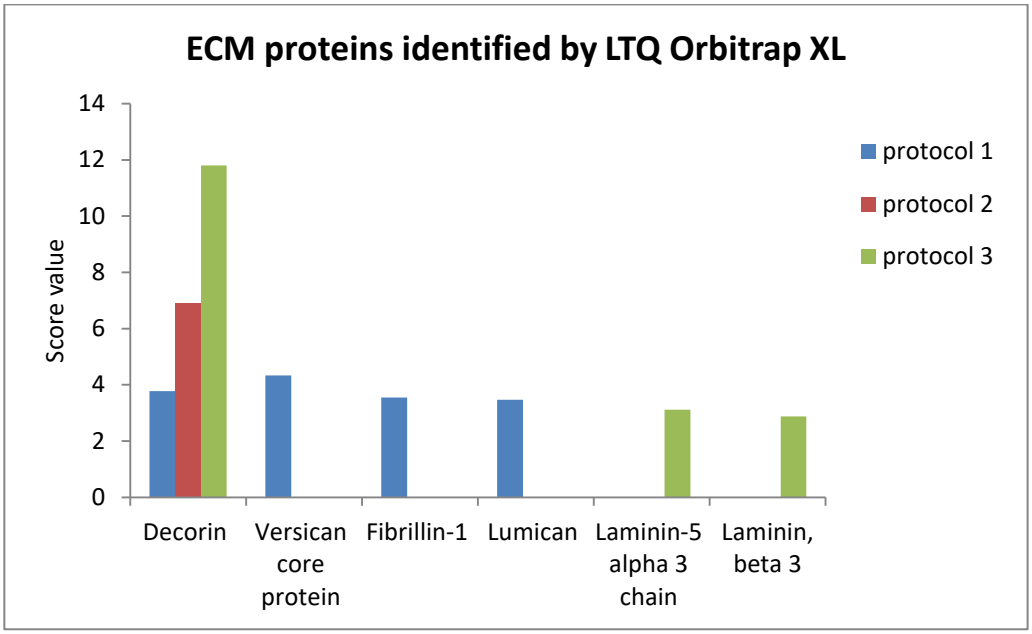

Figure 13. ECM proteins with score ≥ 2.5 identified by LTQ Orbitrap XL in rat thyroid matrices decellularized with three different protocols.

Figure 14 shows that after the decellularization processes each thyroid matrix retains several molecules such as GFs, receptor and enzymes.

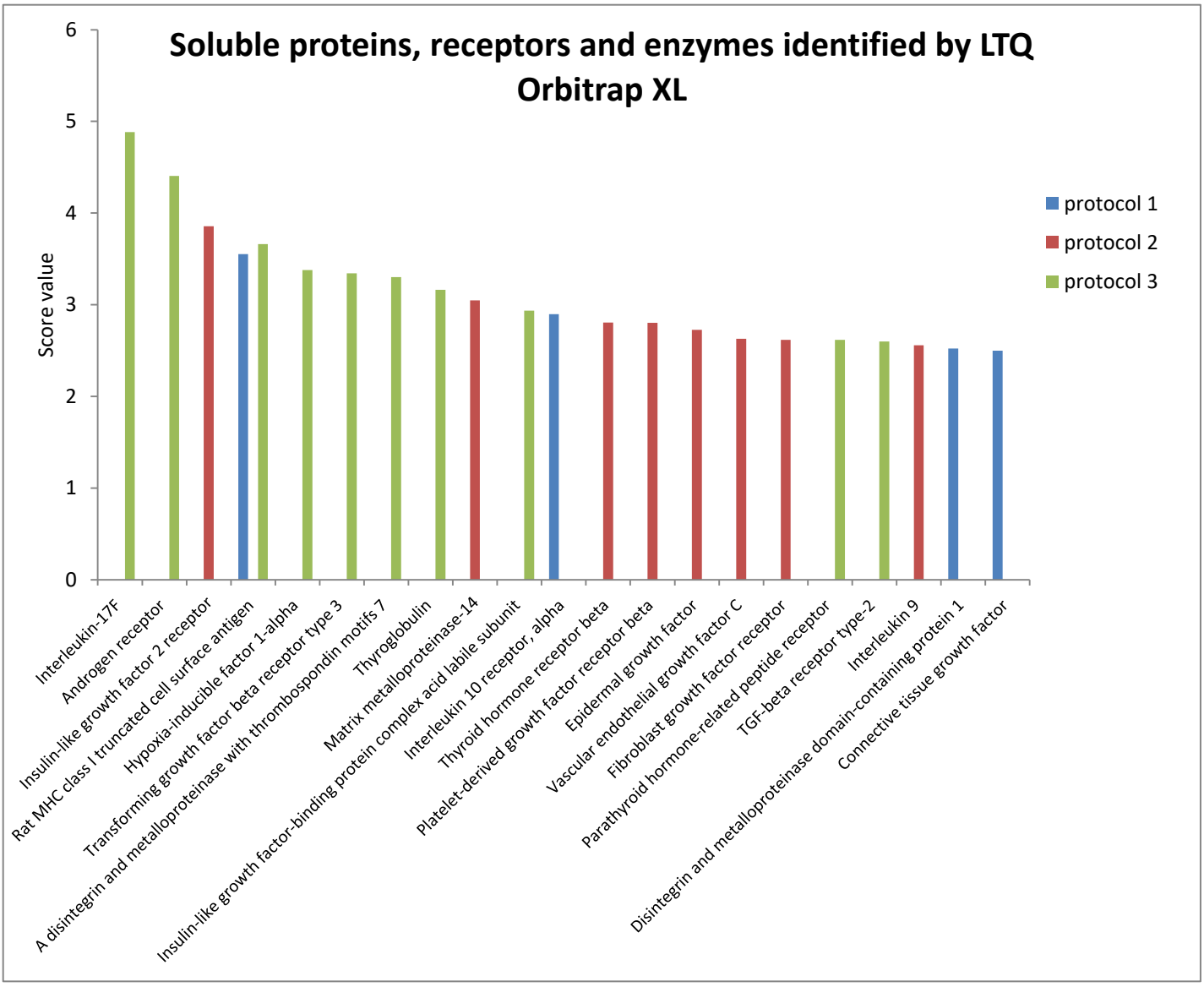

Figure 14. Receptors, GFs, major histocompatibility complex, and enzymes with score ≥ 2.5 detected in the thyroid lobes decellularized with three different decellularization protocols.

1.2.2 HPLC-MS/MS-SRM

Table 6 shows the weight of each collagen standard (I, II, III, IV and V) used for the HPLC-MS/MS-SRM collagen quantification in decellularized thyroid lobes.

Table 6. Total µg of collagen standards in the injection volume.

Standard collagen type	Collagen in 5 µl of injected sample
Collagen I	5.10 µg
Collagen II	5.65 µg
Collagen III	5.00 µg
Collagen IV	5.10 µg
Collagen V	5.05 µg

Table 7 shows the amounts of collagen I to V in the thyroid stromal matrix. Thyr-1 to Thyr-5 have been prepared with the first decellularization protocol, Thyr-6 to Thyr-10 with the second protocol and Thyr-11 to Thyr-15 with the third protocol.

Each collagen weight was then expressed as a percentage of the sum of the total collagens (I to V) for each thyroid lobes (table 8).

Table 7. Collagen type I-V and sum of five collagen weights for every thyroid lobes

First decellularization protocol

	COLL I (µg)	COLL II (µg)	COLL III (µg)	COLL IV (µg)	COLL V (µg)	Total COLL (µg)
Thyr 1	1.784	0.000	1.957	0.077	0.118	3.937
Thyr 2	10.254	0.000	1.858	0.052	0.562	12.725
Thyr 3	0.000	0.000	0.940	0.000	0.000	0.940
Thyr 4	4.350	0.000	1.610	0.027	0.000	5.987
Thyr 5	9.163	0.000	1.469	0.019	0.000	10.651
Mean	5.110	0.000	1.567	0.035	0.136	6.848
S.D.	4.490	0.000	1.502	0.030	0.244	4.825

Second decellularization protocol

	COLL I (µg)	COLL II (µg)	COLL III (µg)	COLL IV (µg)	COLL V (µg)	Total COLL (µg)
Thyr 6	6.250	0.000	2.376	0.013	0.000	8.639
Thyr 7	66.383	1.840	2.253	0.852	0.743	72.070
Thyr 8	32.980	0.000	2.341	0.498	0.881	36.700
Thyr 9	48.487	0.000	1.708	0.342	0.841	51.377
Thyr 10	21.993	0.000	1.405	0.035	0.000	23.433
Mean	35.219	0.368	2.017	0.348	0.493	38.444
S.D.	23.272	0.823	0.436	0.349	0.453	24.570

Third decellularization protocol

	COLL I (µg)	COLL II (µg)	COLL III (µg)	COLL IV (µg)	COLL V (µg)	Total COLL (µg)
Thyr 11	7.550	0.000	0.647	0.107	0.000	8.303
Thyr 12	5.166	0.000	0.922	0.061	0.000	6.149
Thyr 13	13.681	1.280	1.281	0.055	0.000	16.296
Thyr 14	231.536	0.000	4.532	2.471	1.722	240.260
Thyr 15	84.944	0.000	2.571	1.543	1.045	90.103
Mean	68.575	0.256	1.991	0.847	0.553	72.222
S.D.	96.931	0.572	1.600	1.109	0.795	100.169

Table 8. Percentage distribution of collagens I-V in each thyroid matrix

First decellularization protocol

	COLL I (%)	COLL II (%)	COLL III (%)	COLL IV (%)	COLL V (%)
Thyr 1	45.323	0.000	49.722	1.947	3.009
Thyr 2	80.578	0.000	14.597	0.408	4.417
Thyr 3	0.000	0.000	100.000	0.000	0.000
Thyr 4	72.662	0.000	26.888	0.449	0.000
Thyr 5	86.029	0.000	13.792	0.180	0.000
Mean	56.918	0.000	41.000	0.597	1.485
S.D.	35.458	0.000	36.033	0.776	2.094
Mean – thyr 3	71.148	0.000	26.250	0.746	1.856
S.D. – thyr 3	18.070	0.000	16.756	0.809	2.219

Second decellularization protocol

	COLL I (%)	COLL II (%)	COLL III (%)	COLL IV (%)	COLL V (%)
Thyr 6	72.351	0.000	27.502	0.148	0.000
Thyr 7	92.108	2.553	3.126	1.182	1.031
Thyr 8	89.864	0.000	6.379	1.356	2.400
Thyr 9	94.373	0.000	3.325	0.665	1.637
Thyr 10	93.856	0.000	5.996	0.148	0.000
Mean	88.510	0.511	9.266	0.700	1.014
S.D.	9.204	1.142	10.302	0.564	1.045

Third decellularization protocol

	COLL I (%)	COLL II (%)	COLL III (%)	COLL IV (%)	COLL V (%)
Thyr 11	90.926	0.000	7.790	1.284	0.000
Thyr 12	84.012	0.000	14.997	0.991	0.000
Thyr 13	83.951	7.855	7.860	0.335	0.000
Thyr 14	96.369	0.000	1.886	1.028	0.717
Thyr 15	94.274	0.000	2.854	1.713	1.160
Mean	89.906	1.571	7.077	1.070	0.375
S.D.	5.747	3.513	5.211	0.502	0.537

Figure 15 summarizes the results of the statistical analysis based on multiple-way ANOVA and Student-Newman-Keuls tests. Quantitative changes occurred only to collagens type I (ANOVA test, P = 0.015) and type III (ANOVA test, P = 0.012). Specifically, collagen type I was reduced in protocol 1 (71% of the total collagen analysed) with respect to protocols 2 and 3 (88-90% of the total collagen analysed). In contrast, collagen type III resulted more elevated after protocol 1 (26% of the total collagen analysed) as compared to protocols 2 and 3 (7-9% of the total collagen analysed). No statistically significant differences between the three decellularization protocols were apparent for collagen types II, IV and V representing from 0.4% to 1.6% of the total collagen analysed.

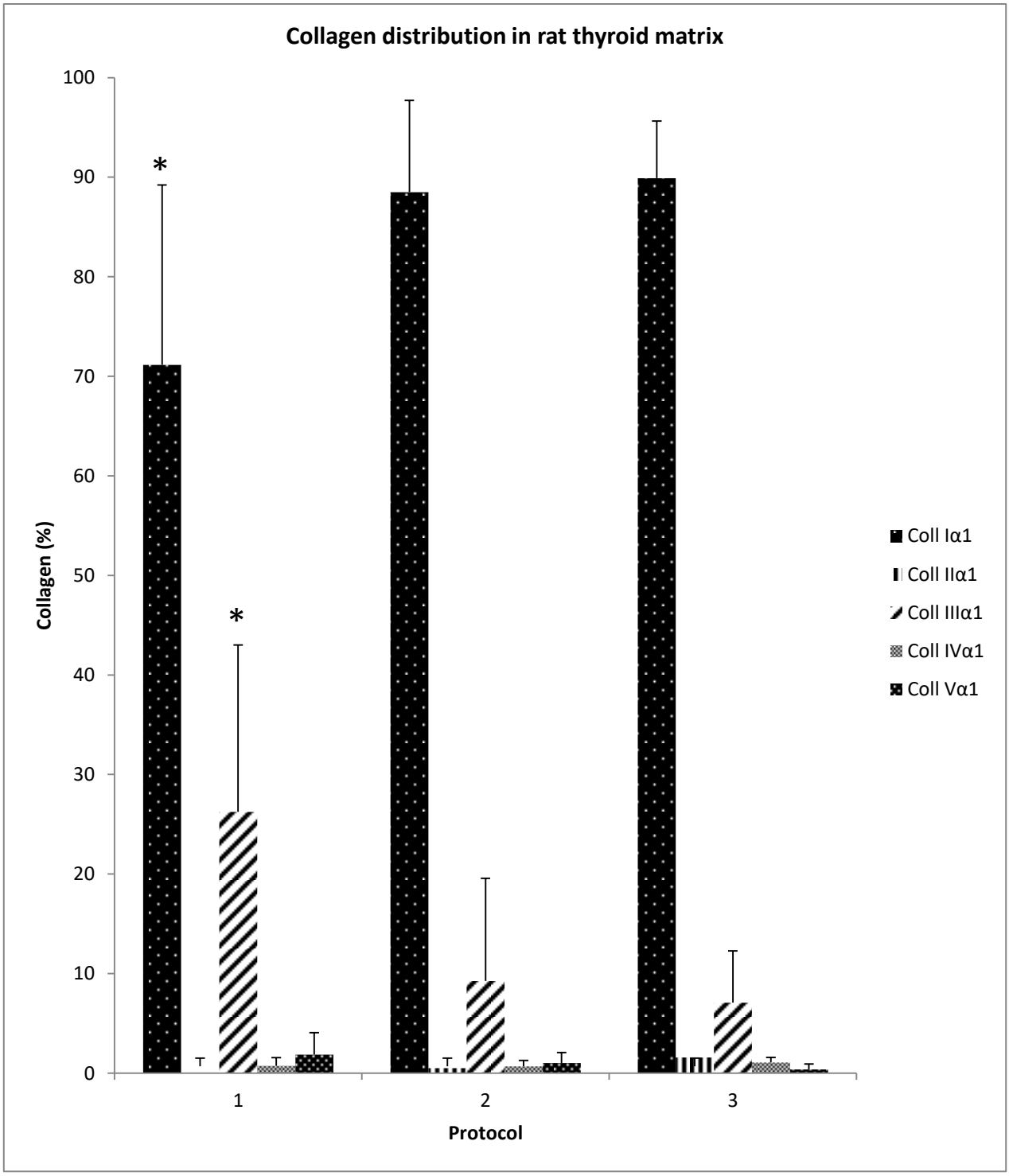

Figure 15. Percentage distribution of collagen I - V in the fibrous matrix of the decellularized rat thyroid. Results are shown for each decellularization protocol.

Table 9 shows the contribution (in percentage) of each of the five collagen types resulting from the three decellularization protocols used in relation to the dry weight of a single matrix (dry matrix weight = 269.30 µg). A summary value of collagen is also provided.

Table 9. Percentage contribute (% w/w) of each collagen type to the total weight of a decellularized rat thyroid.

	COLL I (%)	COLL II (%)	COLL III (%)	COLL IV (%)	COLL V (%)	Total COLL (%)
1st protocol	2.37	0.00	0.64	0.01	0.06	3.09
2nd protocol	13.09	0.13	0.75	0.12	0.18	14.29
3th protocol	25.49	0.09	0.74	0.31	0.20	26.84

2. 3D BIOPRINTING OF COLLAGEN FROM RAT TAIL TENDONS

2.1 MASS SPECTROMETRY ANALYSIS

Tables 10 shows the main ECM proteins detected in collagen from the rat tail tendon. Proteins are classified with their respective Uniprot IDs, names, Proteome Discoverer protein score value, and the percentage of the protein sequence covered by identified peptides (coverage). The cut-off of the result were set at protein score ≥ 2.5.

Table 10. ECM proteins of rat tails tendon detected by LTQ Orbitrap XL.

Uniprot ID	Protein name	Score	Coverage (%)
A0A0G2KAN1	Collagen alpha-2(I) chain	845.99	68.80
P02454	Collagen alpha-1(I) chain	674.30	62.28
P13941	Collagen alpha-1(III) chain	58.52	37.80
P05539	Collagen alpha-1(II) chain	43.88	43.55
Q80ZF0	Collagen alpha-1(XXVII) chain	38.22	24.37
F1LUN5	Protein Col4a5	32.72	40.09
Q99372	Elastin	30.33	21.26
P20909	Collagen alpha-1(XI) chain	28.91	28.94
Q9JI03	Collagen alpha-1(V) chain	26.26	30.65
A0A0G2K601	Protein Col4a6	22.74	20.21
A0A0G2K742	Protein Col4a4	21.77	36.62
F1LRJ1	Protein Col4a3	21.37	23.22
D3ZNT5	Procollagen, type IX, alpha 2	15.19	45.78
F1M748	Protein Col24a1	11.19	22.93
M0RDG5	Protein Col25a1	10.81	49.79
F1LQ00	Protein Col5a2	10.22	29.59
F1LQ93	Collagen alpha-1(IX) chain	9.39	38.44
F1MA59	Protein Col4a1	7.68	29.48
D3ZX71	Protein Col9a3	6.87	23.09

F1M897	Protein Col22a1	6.62	22.19
A0A0G2K2Q8	Protein Col13a1	6.44	21.38
A0A0G2K8N4	Protein Col26a1	6.06	31.13
F1LRP9	Collagen alpha-1(XXIII) chain	6.03	40.85
F1LND0	Protein Col16a1	5.29	28.99
F6T0B3	Procollagen, type XI, alpha 2	4.38	21.70
A0A0G2K7A5	Protein Col10a1	3.84	38.68
A0A0G2K449	Protein Col17a1	3.09	24.44

Figure 16 shows differences in the protein score of the collagen extracted from the solubilization of the rat tail tendons. The result shows that different types of collagen and elastin are the main proteins, with an high representation of the two chains of collagen type I.

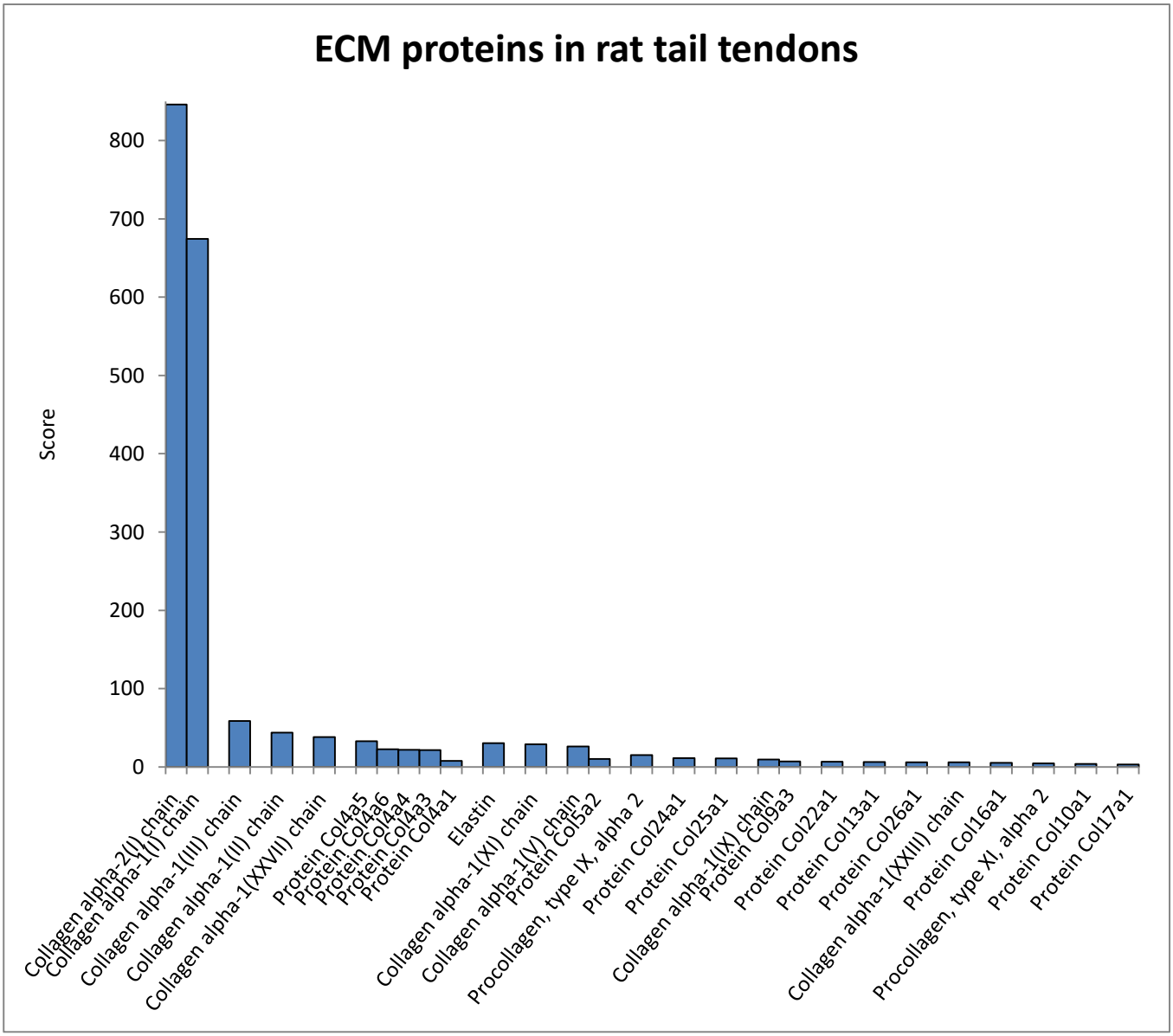

Figure 16. ECM proteins identified in rat tail tendons with LTQ Orbitrap XL. The parameters of validation of protein identity have been set at protein score ≥ 2.5

2.2 3D BIOPRINTING

Table 11 shows differences in the viscosity in relation to different molarity of acetic acid used to solubilize the collagen from rat tail tendons. The solution at 2% w/v of tendons, solubilized in water and 1M acetic acid has proved to be the most suitable for the printing process. The use of 1M acetic acid has allowed to obtain a viscosity value compatible with the range of the printer (acceptable range: 8,000-25,000 centiPoise).

Table 11. The viscosity values at 60 and 100 rpm of three different collagen solutions with the same w/v ratio of tendons in water, but different molarities of acetic acid.

w/v of tendon (%)	acetic acid (M)	viscosity at 60 rpm (cP)	viscosity at 100 rpm (cP)
2	0.5	34,200	20,000
2	1	25,000	15,600
2	2	9,060	6,500

Figure 17 shows the mechanics of the bioprinter of the Department of Pharmacy, University of Parma, Italy. Peltier cells are used to maintain the printing surface in a stable temperature of -18^{o}C degrees.

Figure 17. 3D printer used for obtain collagen and chitosan scaffolds

Figure 18A shows the structure of a 2D film of lyophilized rat tail tendon, collagen solution while figure 18B shows the structure of a 3D bioprinted collagen scaffold referred to the same scale bar (each line corresponds to 1 mm).

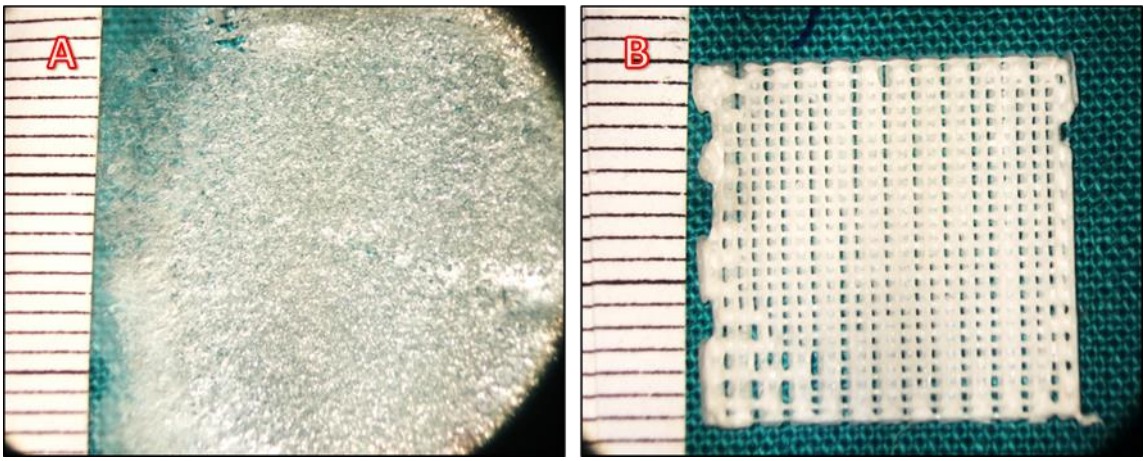

Figure 18. A: 2D film of lyophilized rat tail collagen solution. B: 3D printed collagen scaffold. Scale bar = 1 mm

2.3 ATR-FT-IR OF COLLAGEN FROM RAT TAIL TENDONS

Figure 19 compares the ATR-FT-IR spectra of rat tail collagen solutions (2% w/v) solubilized with three different molarity of acetic acid (0.5M, 1M, 2M).

Figure 20 shows the comparison between 2% w/v collagen solution solubilized with 1M of acetic acid before and after the printing process.

It should be noted that neither the molarity of acetic acid or the printing process affect the number and the types of chemical bonds in the biomaterial. The latter, according to the different zones of interest in the IR spectrum, are represented by:

- 4000-3000 cm-1 : hydrogen bonds (O-H, N-H, C-H ...)
- 3000-2000 cm-1 : triple bonds
- 2000-1500 cm-1 : double bonds (C=O, C=C)
- 1500-1000 cm-1 : single bonds (C-Cl, C-O...)
- 1000-400 cm-1 : finger-print region (specific for each materials)

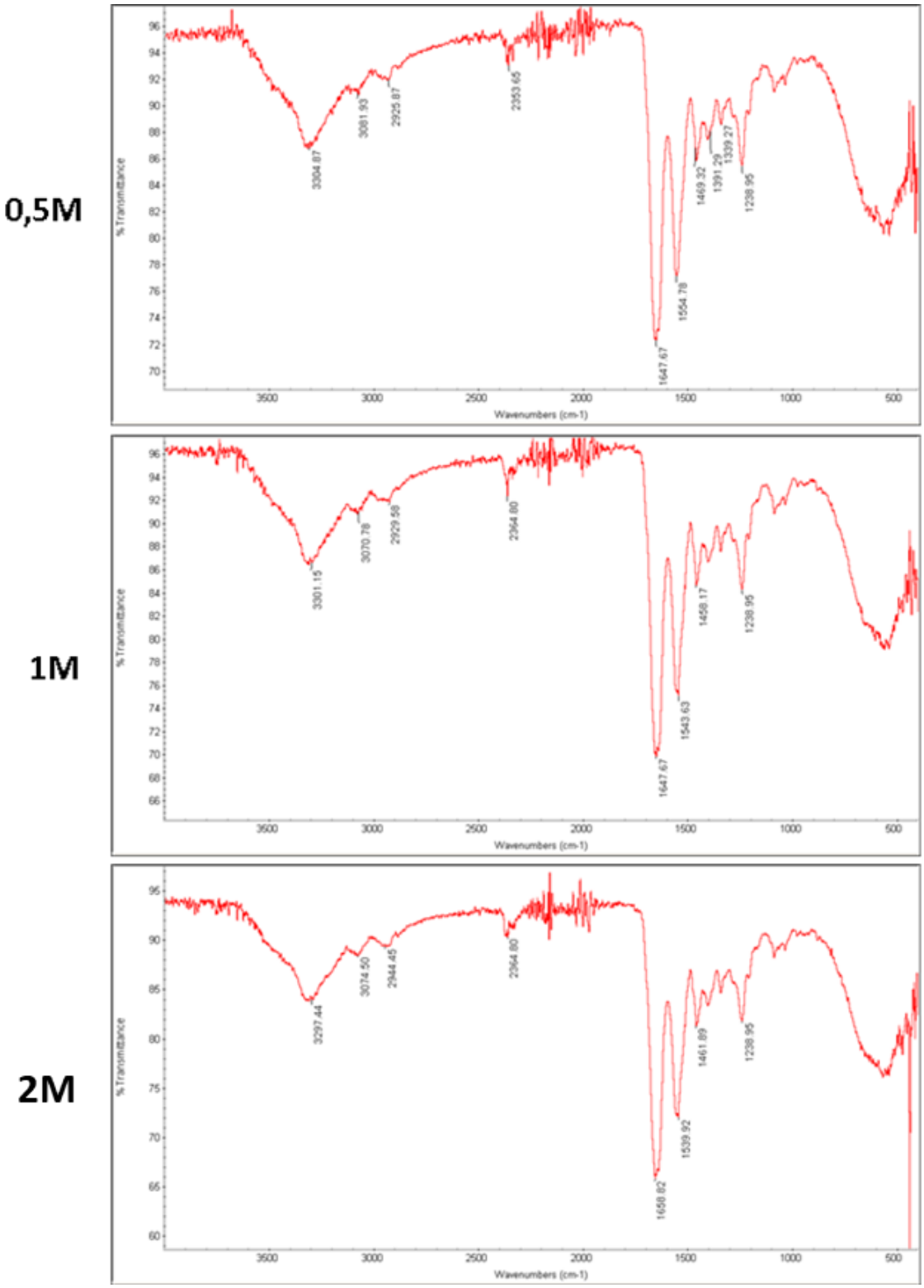

Figure 19. ATR-FT-IR spectrum of 2% w/v rat tail collagen solutions solubilized with three different molarities of acetic acid.

1M

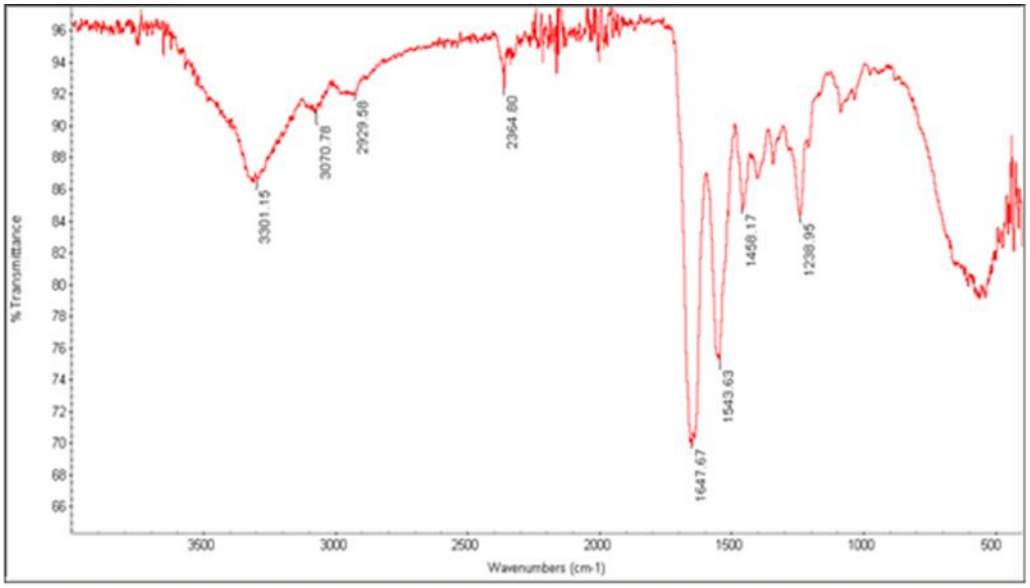

1M
3D printed

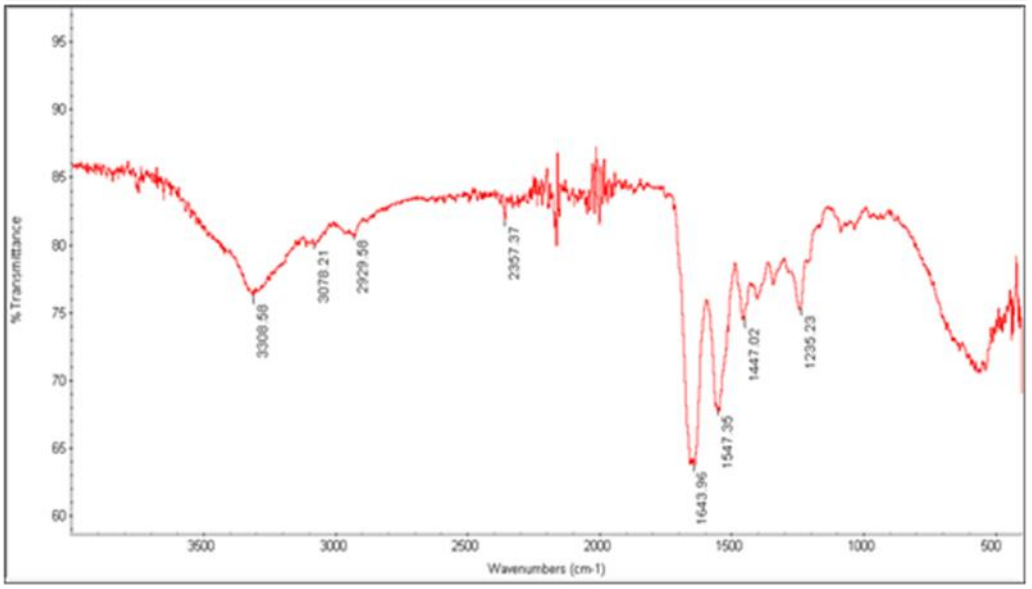

Figure 20. Spectrum comparison of 2% w/v 1M acetic collagen solution before and after the printing process.

2.4 SEM MORPHOLOGICAL ANALYSIS

Figure 21A shows the structure of a 2D film of lyophilized collagen from rat tail tendons. It results as an apparently random substrate, with fibers of different lengths and arranged at various depths, giving rise to poorly homogeneous and variably interconnected spaces. In contrast, figure 21B shows a detail of the bioprinted 3D scaffold at the intersection of the filament. In this case, a more ordered network of fibers with more homogeneous and less interconnected inter-fibrillary spaces is apparent.

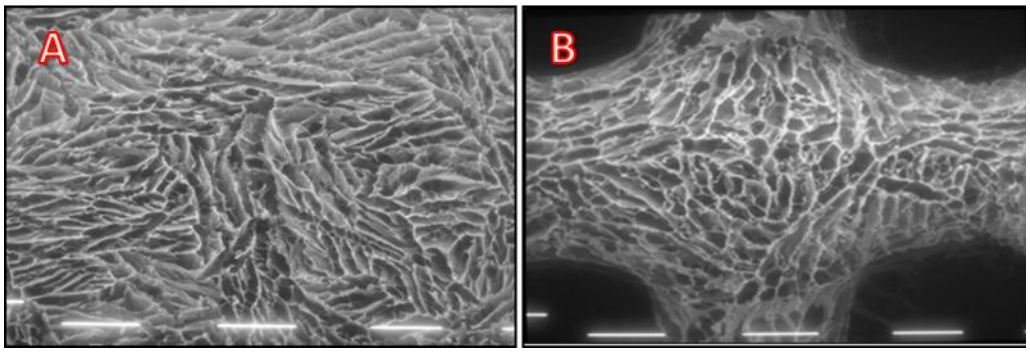

Figure 21. A: 2D collagen film. B: 3D printed collagen scaffold. Scale bar = 100 µm

Figure 22 shows an overview of the 3D printed collagen scaffold. It is a 3 layers microporous reticulated structure with regular openings of 250-300 µm of maximum diameter.

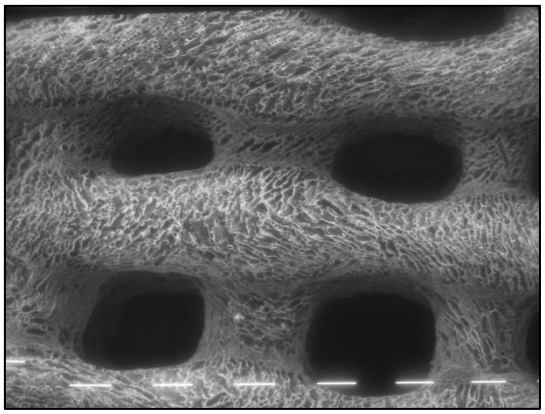

Figure 22. Macro structure of a 3D printed collagen scaffold. Scale bar = 100 µm

2.5 MORPHOMETRIC ANALYSIS ON THE MICROPOROSITY OF THE 3D PRINTED COLLAGEN FROM RAT TAIL TENDONS

Figure 23 shows SEM images of the 3D collagen scaffolds where an analysis of the surface area of the micropores has been performed.

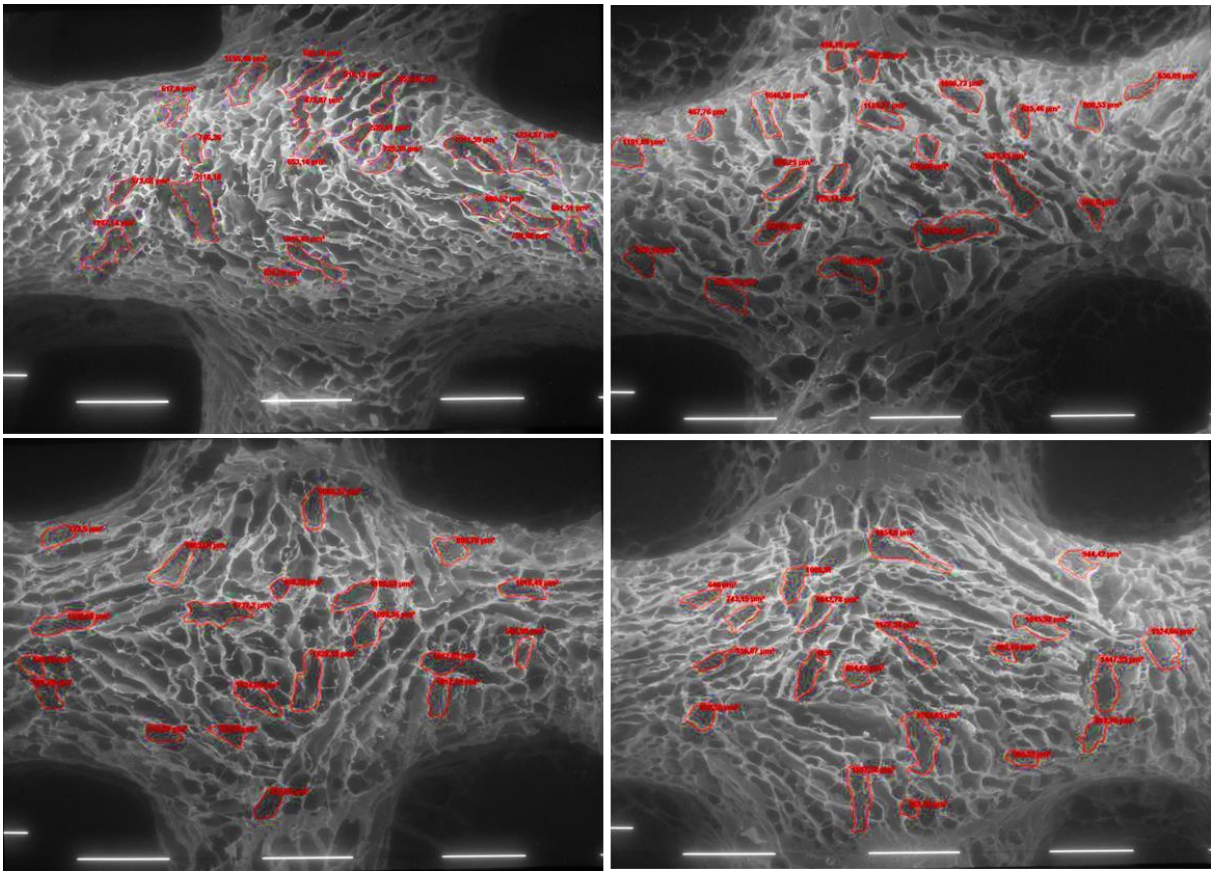

Figure 23. The four 3D scaffold of collagen 2% w/v solubilized in 1M of acetic acid. In red, the surface of the measured pores and their respective values. Scale bar = 100 µm

Table 12 shows the values of randomly selected pores present on each surface area of the four scaffolds considered in the analysis.

Table 12. Surface area of each porosity measured in four different collagen scaffolds.

First scaffold	Second scaffold	Third scaffold	Fourth scaffold
Area (μm2)	**Area (μm2)**	**Area (μm2)**	**Area (μm2)**
1,155.48	2,714.65	1,826.19	1,042.78
318.18	726.13	1,095.36	1,009.59
653.85	626.66	765.49	409.75
472.87	1,529.45	1,017.12	1,954.90
525.61	1,090.73	408.22	743.15
729.35	926.29	1,405.64	646.00
1,511.59	762.96	1,528.08	944.42
746.36	1,046.58	773.50	1,524.66
573.08	1,185.77	584.88	694.68
2,118.18	1,403.16	718.97	1,447.95
634.56	1,191.89	1,017.02	506.32
896.52	498.79	542.99	1,051.63
922.18	467.76	1,018.49	862.59
653.16	900.53	1,134.04	392.36
1,045.42	636.09	1,737.20	2103.95
1,287.14	635.46	822.02	1,597.58
681.51	518.60	993.78	516.07
750.68	643.20	1,199.53	819.76
1,224.87	1,501.48	1,003.27	1,045.57
616.60	848.16	781.88	1,176.34
mean	**mean**	**mean**	**mean**
875.86	992.72	1,018.68	1,024.50
S.D.	**S.D.**	**S.D.**	**S.D.**
± 420.01	± 522.29	± 378.80	± 487.95

Statistical analysis showed no statistically significant differences in the structure of 3D bioprinted collagen scaffolds, confirming the reproducibility of the printing process with this biomaterial (ANOVA test = 0.630).

2.6 EVALUATION OF CELL MORPHOLOGY AFTER GROWTH ON BIOPRINTED COLLAGEN AND CHITOSAN SCAFFOLDS, AND MICROPOROUS PLLA DISKS COATED WITH EITHER COLLAGEN OR CHITOSAN

2.6.1 Swiss 3T3

Figure 24 shows SEM images of the distribution of the Swiss 3T3 fibroblasts after 24, 48 and 72 hours of culture on 2D collagen film.

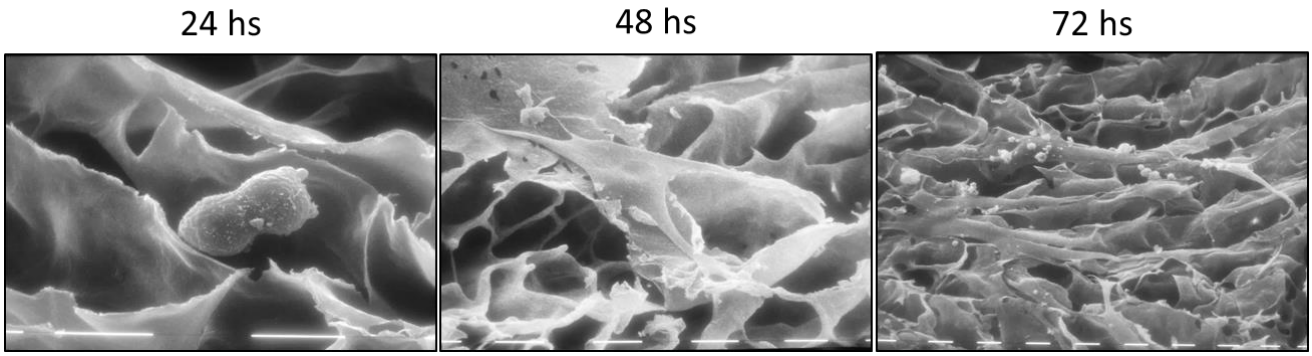

Figure 24. Swiss 3T3 cell line grown on 2D collagen film for 24, 48 and 72 hours. Scale bar = 10 µm

Figure 25 shows cells seeded on the 3D bioprinted collagen scaffolds. Cells homed and grew in substantial number during all the days of culture. Compared to the 2D film, cells on 3D bioprinted collagen scaffolds acquired a flat morphology, with marked adhesion to the substrate likely as a result of its porosities offering an optimal surface area for adhesion.

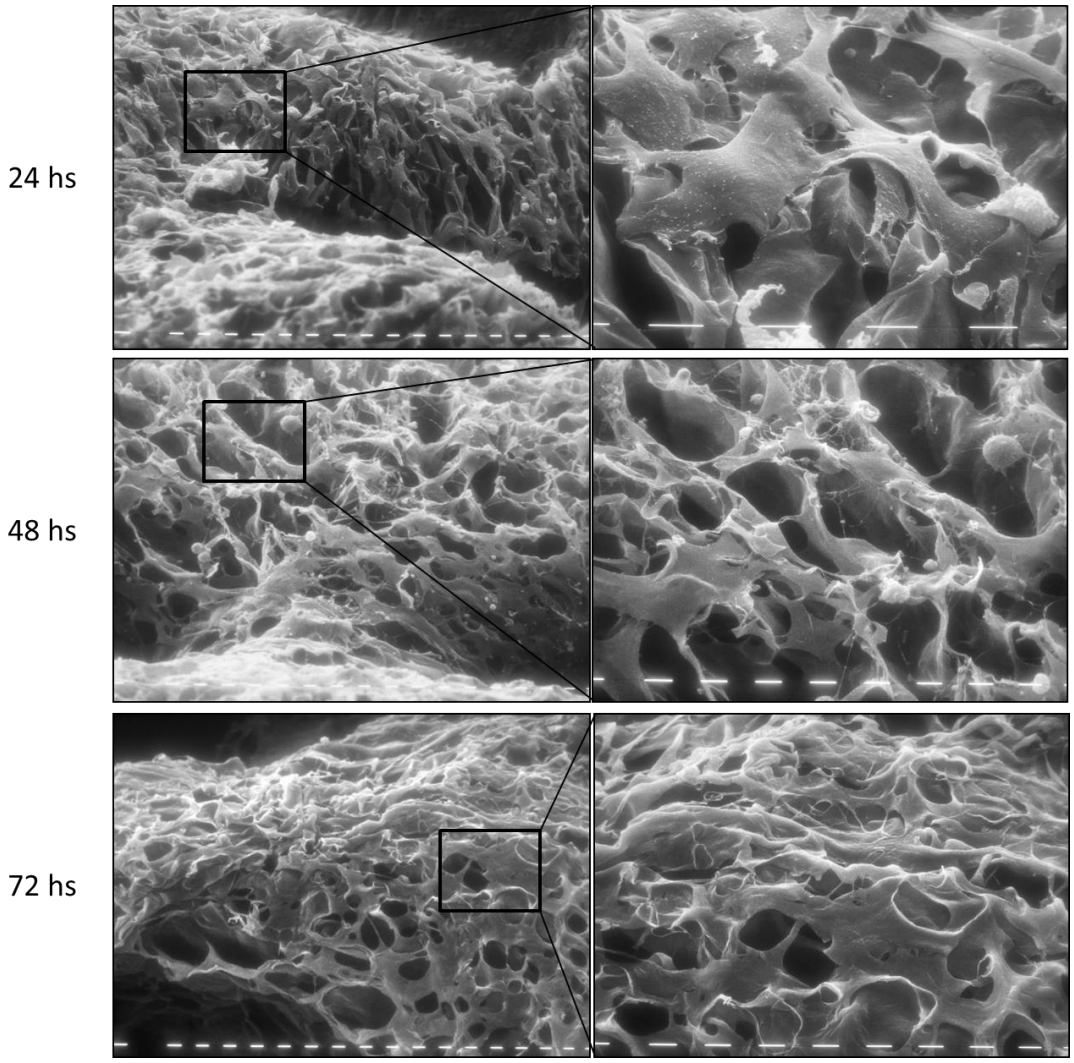

Figure 25. Swiss 3T3 cell line on 3D collagen scaffold at 24, 48 and 72 hours. Scale bar = 10 µm

Figure 26 shows SEM images of the Swiss 3T3 fibroblasts grown for 24, 48 and 72 hours on the 3D bioprinted chitosan. The cellular morphology appears fibroblastoid, but cells exhibited a lower adhesion to substrate, and grew in minor number with respect to those 3D collagen scaffolds.

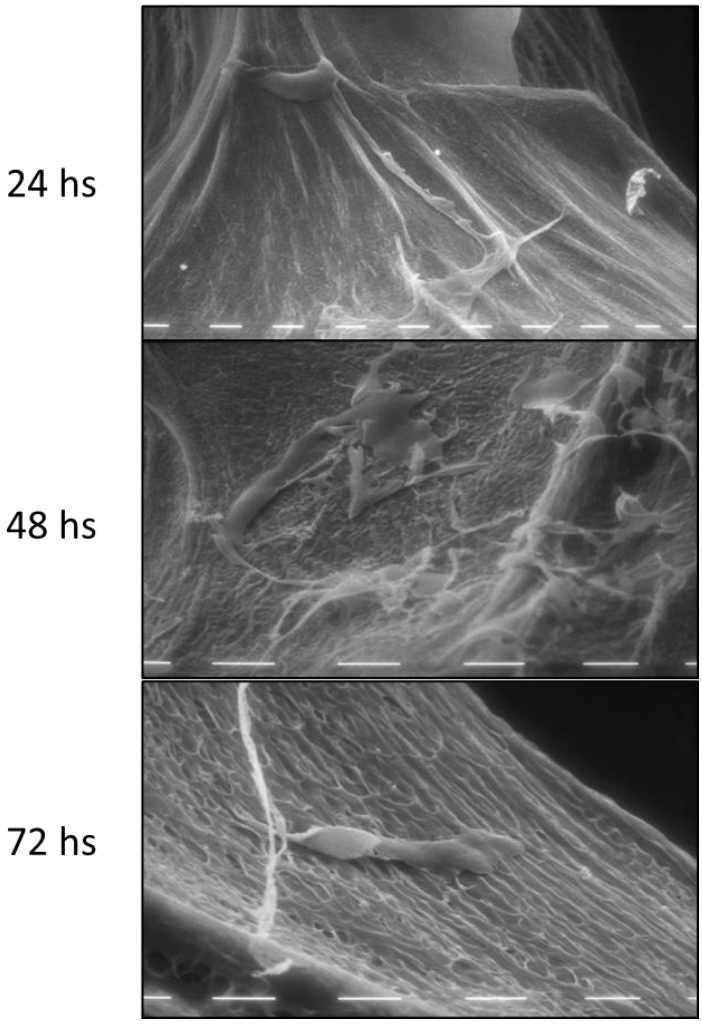

Figure 26. Swiss 3T3 cell line grown on 3D bioprinted chitosan surface for 24, 48 and 72 hours. Scale bar = 10 µm

2.6.2 Rat thyroid stem cell / progenitors

Figure 27 shows SEM images of adult rat, thyroid stem cells / progenitors seeded on 2D and 3D collagen or chitosan scaffolds. On both collagen structures, cells had a fibroblastoid and multipolar morphology, rich in pseudopodia and microvilli. On the other hand, cells grown on chitosan exhibited a spherical morphology gathering in pseudofollicular agglomerates.

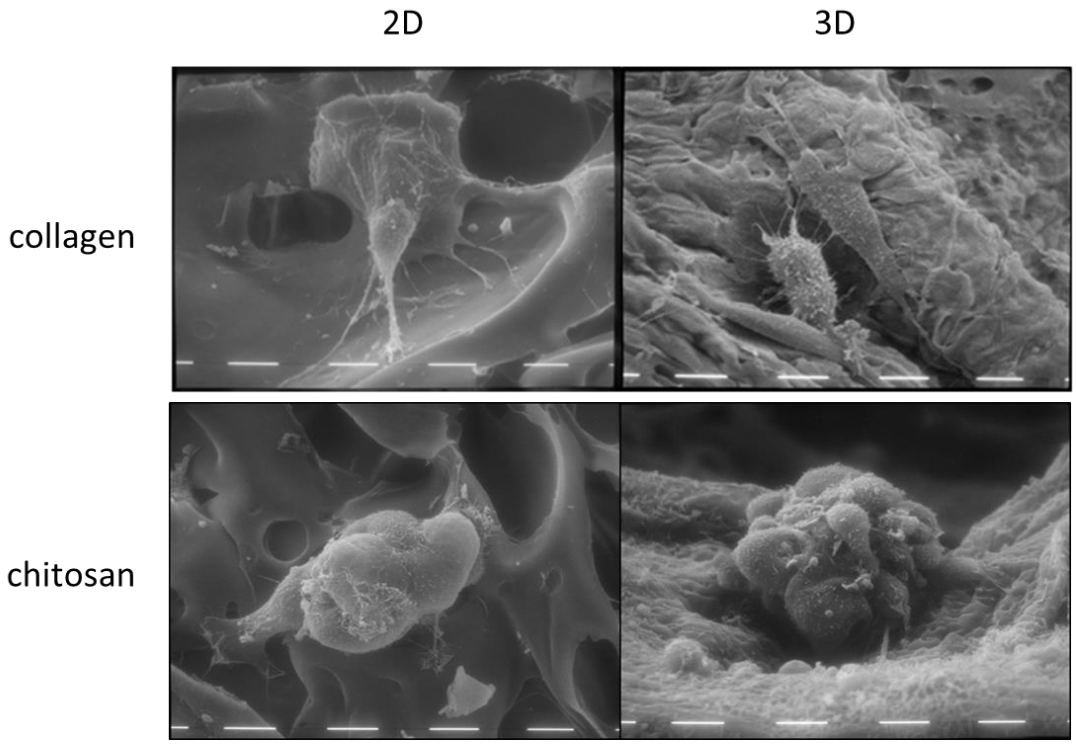

Figure 27. Rat thyroid stem cell / progenitors grown for 24 hours on 2D and 3D collagen and chitosan scaffolds. Scale bar = 10 μm

Figure 28 shows the same thyroid cells cultured for 24 hours on microporous PLLA films coated with 4 different concentrations of collagen (0.1%, 0.5%, 2.5%, 5%). At low concentrations of collagen, cells tend to strongly adhere to the substrate, showing a flat surface, enlarged morphology, and numerous pseudopodia. Differently, at higher collagen concentrations cells regain a fibroblastoid and polygonal morphology, maintaining morphological individuality. In the image of 5% collagen concentration it is possible to notice the boundary between the collagen coatings and the underlying PLLA film.

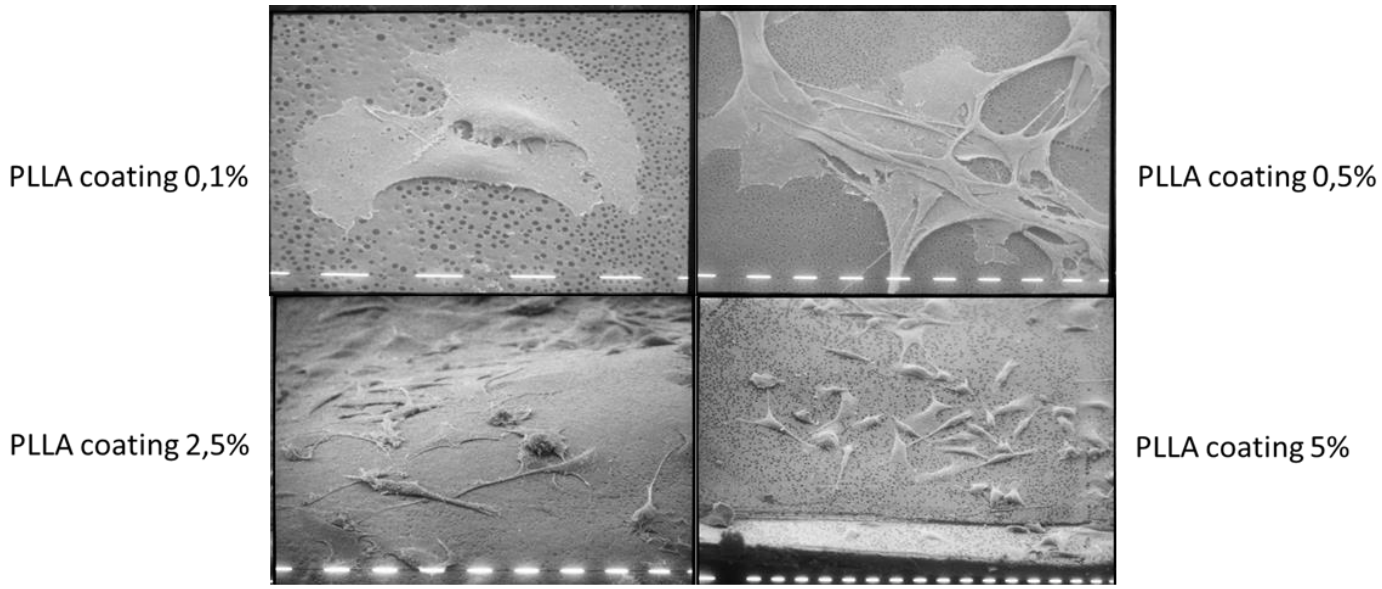

Figure 11. Rat thyroid stem cell / progenitors grown for 24 hours on PLLA film covered with different concentration of collagen. Scale bar = 10 µm

Figure 29 shows the same cells grown for 24 hours on a microporous PLLA film with a chitosan coating of 1%. Also in this case, the presence of chitosan leaded adult thyroid stem cells / progenitors to a spherical morphology, and to form pseudofollicular aggregates.

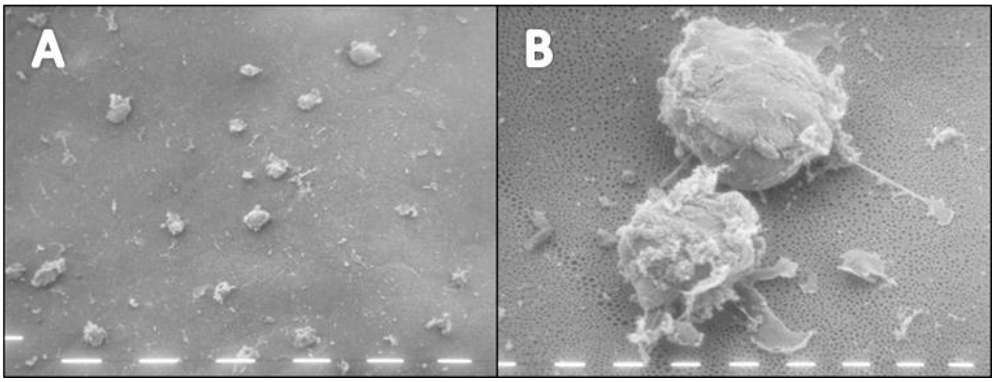

Figure 29. Rat thyroid stem cell / progenitors grown for 24 hours on PLLA film coated with 1% chitosan. Scale bar A = 100 µm, scale bar B = 10 µm.

Figure 30 shows that after 5 days of culture adult thyroid stem cells / progenitors on PLLA coated with different concentration of chitosan (0.2%, 1%, 2.5%) are able to maintain a spherical morphology. At the highest concentrations of chitosan, the number of cells that are organized in pseudofollicular aggregates is greater than those observable at the lowest concentrations.

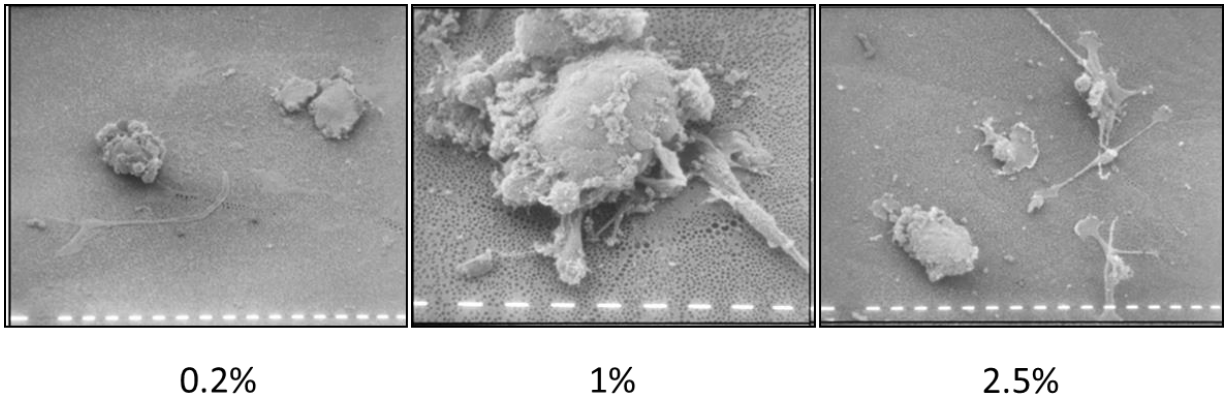

Figure 30. Rat thyroid stem cell / progenitors grown for 5 days on PLLA film coated with three different concentrations of chitosan. Scale bar = 10 µm.

3. PROTEOMICS SIGNATURE OF ADULT, MALE RAT THYROID STEM CELL / PROGENITORS

3.1 CHROMATOGRAMS AND PROTEINS IDENTIFICATION

Figure 31 shows the total ion chromatograms (TICs) of three rat THY biological replicates. Conservative distribution of the TICs and similar number of protein are shown in the figure.

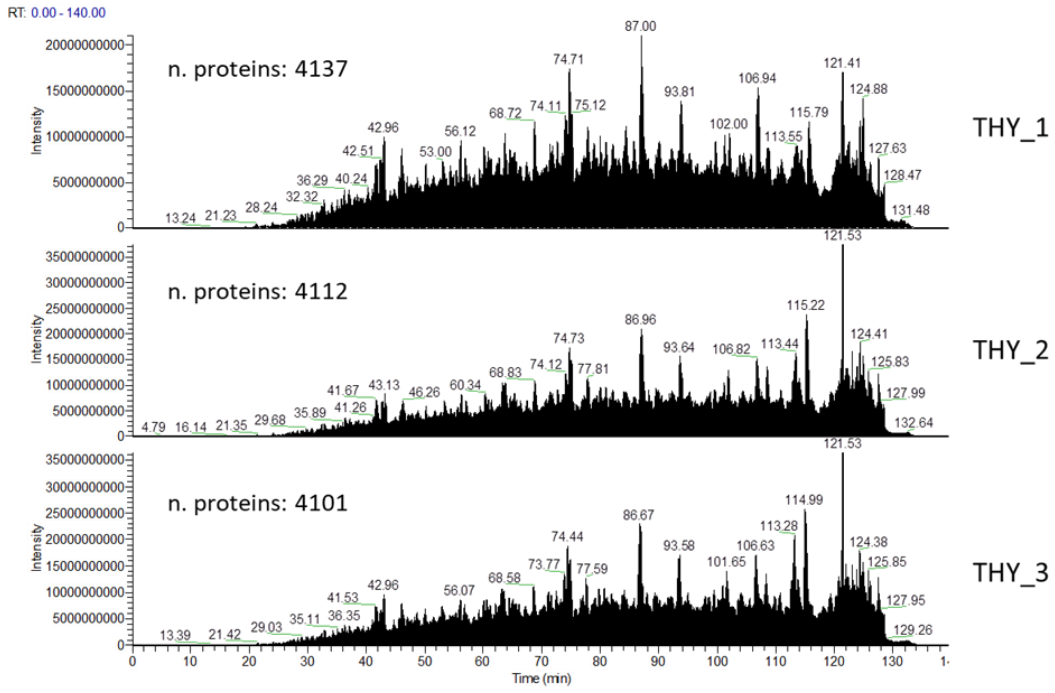

Figure 31. TICs of rat THY biological replicates. The total number of identified proteins are shown on the left of the chromatogram. Ionic intensity are shown in y-axis, minutes are shown in x-axis

Figure 32 shows the TICs of six rat TSC/P biological replicates. As for the THY biological replicates, conservative distribution of the chromatograms between TSC/P samples are shown, with slight differences in the replicates 1, 2 and 3.

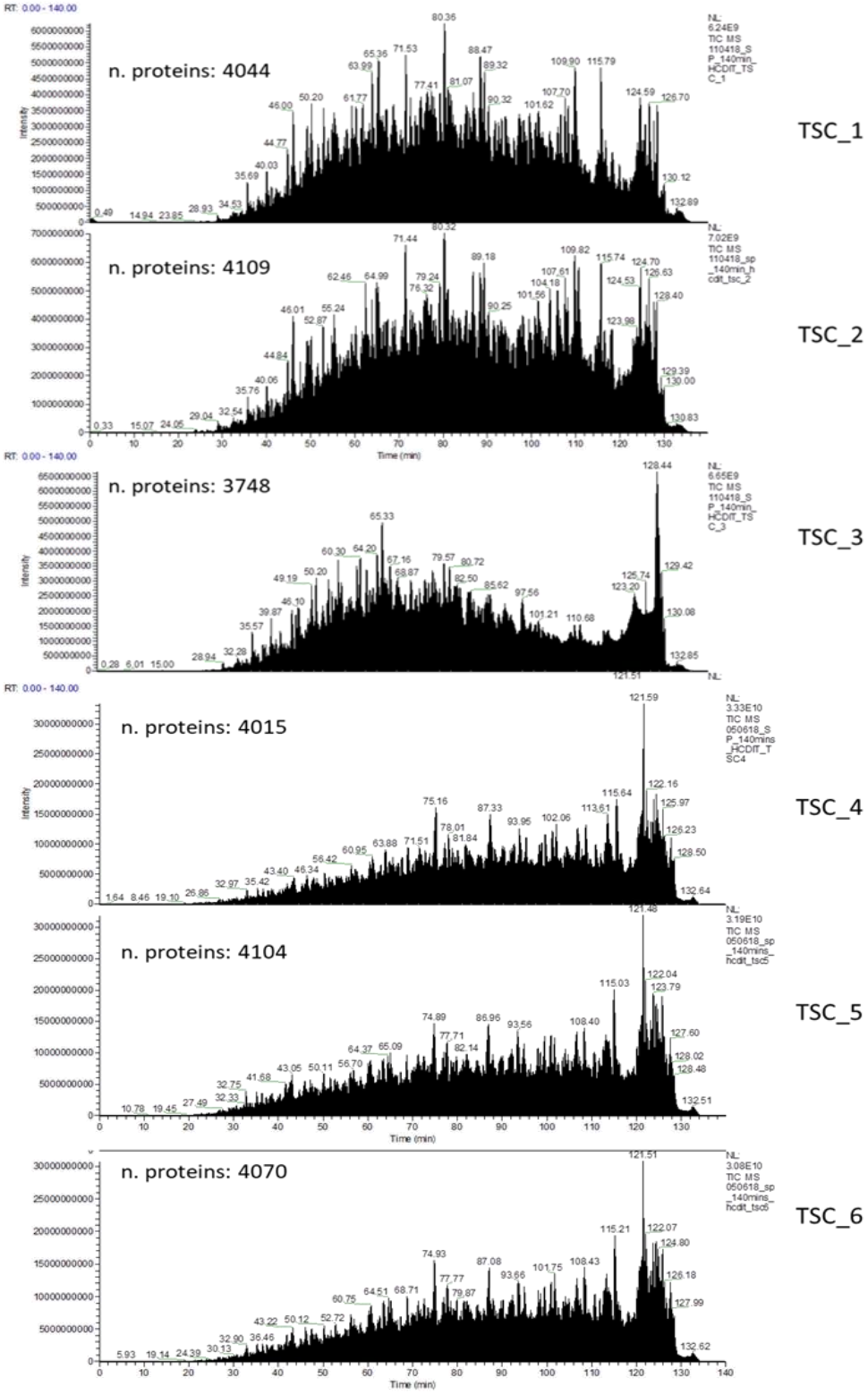

Figure 32. TICs of rat TSC/P biological replicates. The total number of identified proteins are shown on the left of the chromatogram. Ionic intensity are shown in y-axis, minutes are shown in x-axis

Figure 33 shows the overlap between the biological replicates of rat THY and TSC/P. In total, 4482 proteins has been identified in all samples. An high overlap (94.13%) has been observed between these two cell populations.

Figure 33. Venn diagram of total proteins identification and overlap between rat THY and TSC/P.

Figure 34 shows the overlap between biological replicates of THY and TSC/P. An overlap of 91.13% has been reached for rat THY, while an overlap of 75.22% has been observed for the six biological replicates on rat TSC/P, with 3312 common identified proteins in all six samples.

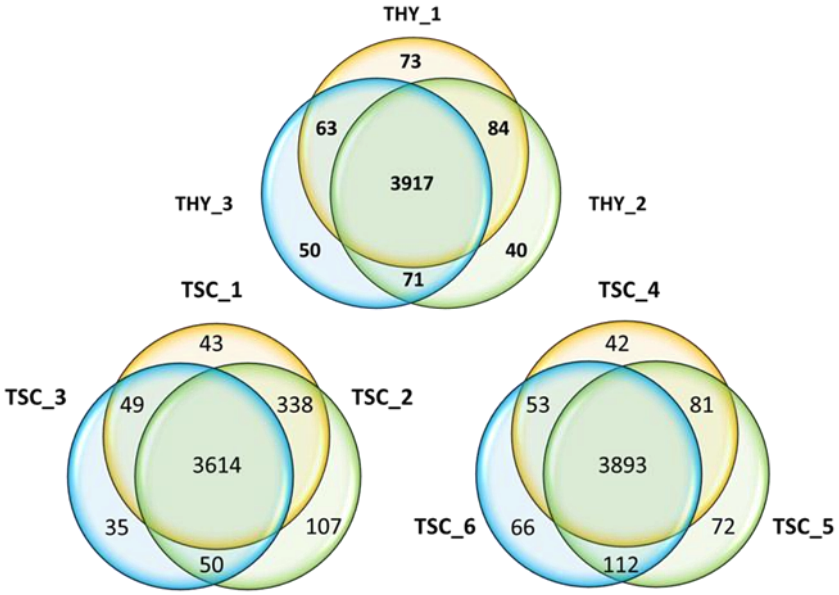

Figure 34. Overlap between biological replicates of rat THY and TSC/P.

Figure 35 shows the Pearson correlation at the quantification level. The total average correlation in all samples was 0.93. The correlations between THY and TSC/P biological replicates were 0.97 and 0.96, respectively.

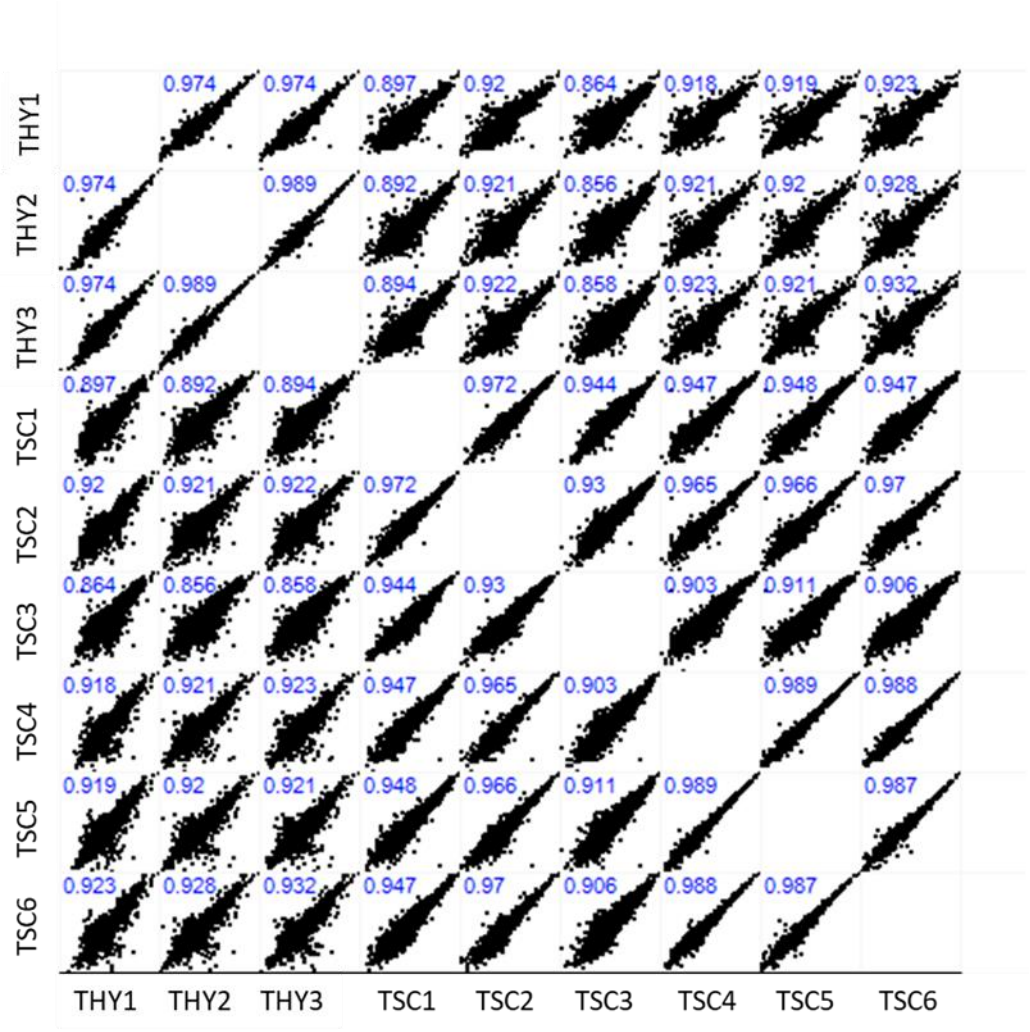

Figure 35. Multi scatter plot and Pearson correlation of all analysed samples.

Figure 36 shows the principal component analysis (PCA) enlightening separation between samples based on proteins expression. Biological replicates of THY and TSC/P were grouped together, with larger differences inside the latter cell populations as a possible consequence of higher variability in protein expression in the TSC/P biological replicates.

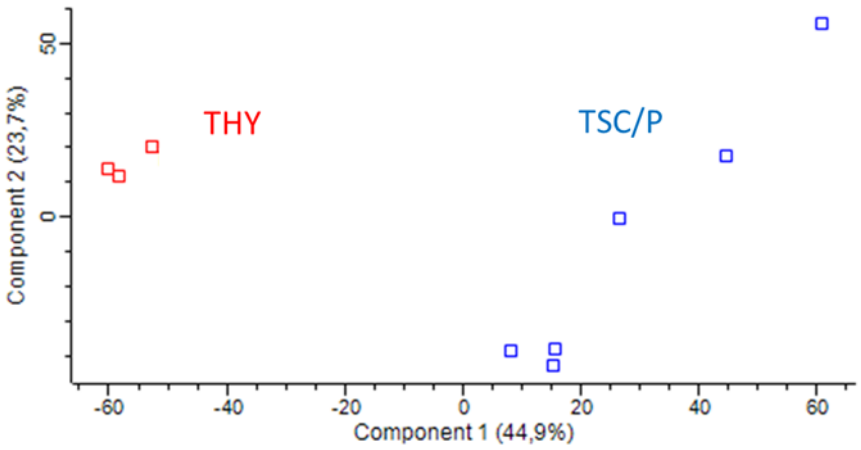

Figure 36. Principal component analysis of rat THY and TSC/P showed similarities and differences between the biological replicates and the two cell populations.

As showed in Figure 37, membrane proteins represent 63.8% of the total Gene Ontology Cellular Compartment (GOCC) annotations, meaning more than 2800 proteins. Because membrane annotation could also include proteins belonging to intracellular membranes such as mitochondria or other organelles, further manual research has been made for PM proteins (anchored-, intrisic-, extrinsic- and integral to PM).

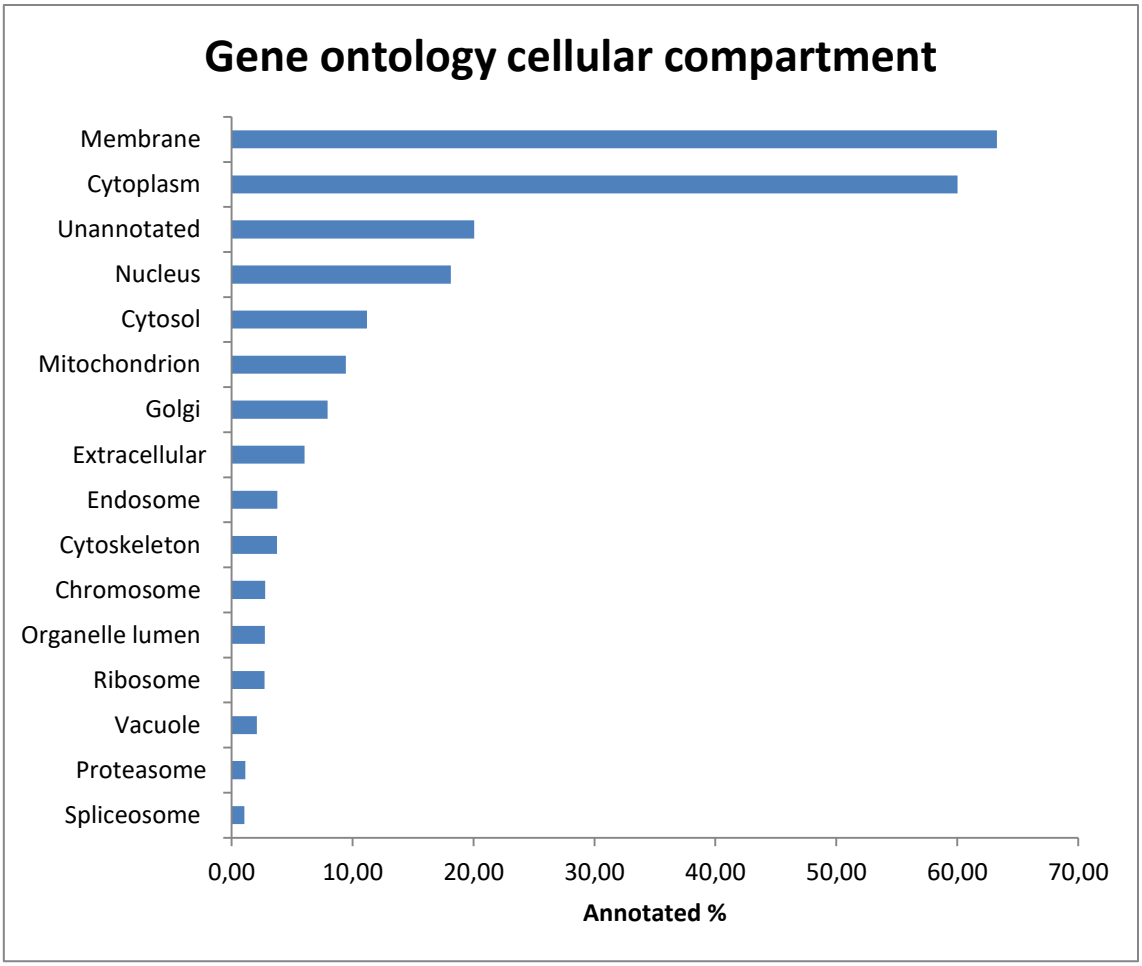

Figure 37. GOCC of whole cell lysates of rat THY and TSC/P.

3.2 STATISTICAL ANALYSIS AND BIOLOGICAL INTERPRETATION OF THE DATA

Figure 38 shows the hierarchical clustering of the 721 proteins whose expression is statistically different between rat TSC/P and THY, as evidenced by the two samples Student t-test. Of those 721 differently expressed proteins (corresponding to the 16% of the total proteins identified in this analysis), 375 were up-regulated in TSC/P while 346 were down-regulated.

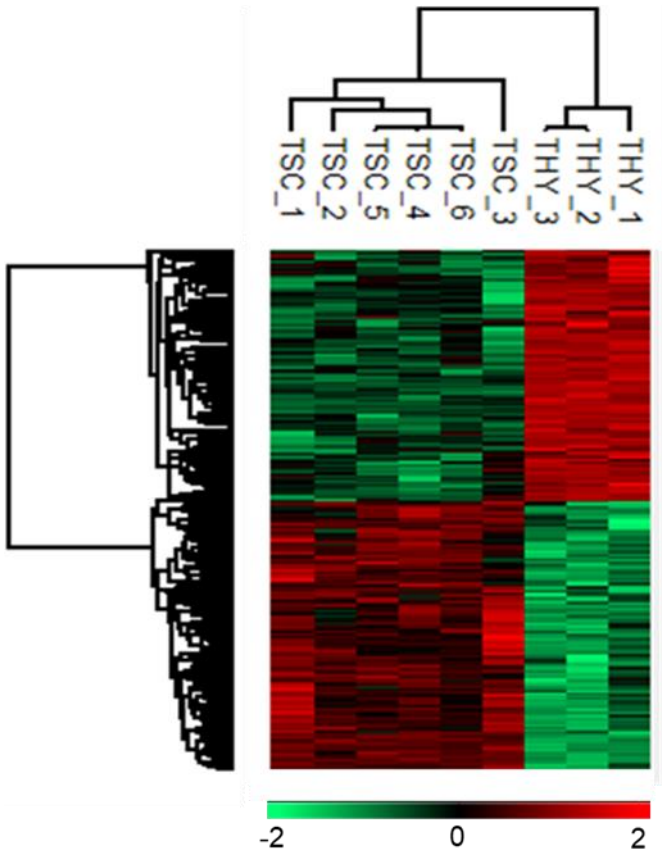

Figure 38. The heat map of 721 proteins differentially expressed based on clustering. Each column represents a different sample, plotted as a three biological replicates for THY and six for TSC. Red color indicates proteins that were up-regulated and green color indicates proteins that were down-regulated. Black spot evidence proteins whose expression unchanged between samples.

Table 13 highlight that regulation of metabolism, cell cycle, and DNA replication are the main up-regulated processes in TSC/P.

Table 13. Up-regulated Gene Ontology biological process (GOBP) and KEGG (Kyoto Encyclopedia of Genes and Genomes) pathways in rat TSC/P according to Perseus GO annotations and STRING analysis.

GOBP names	GO-IDs
Organic substance metabolic process	GO:0071704
Nitrogen compound metabolic process	GO:0006807
Response to chemical	GO:0042221
Organonitrogen compound metabolic process	GO:1901564
Organic acid metabolic process	GO:0006082
Carboxylic acid metabolic process	GO:0019752
Cellular amide metabolic process	GO:0043603
Peptide metabolic process	GO:0006518
Amide biosynthetic process	GO:0043604

KEGG pathway names	IDs
Ribosome	03011
Cell cycle	04110
DNA replication	03032

Table 14 shows the biological processes down-regulated in the TSC/P according to the annotations of Perseus and STRING. These processes are related to the regulation of cell death, cell-substrate interaction and cytoskeleton modification.

Table 14, Down-regulated biological process in TSC/P according to Perseus GOBP annotation and STRING analysis.

GOBP names	GO-IDs
Regulation of cellular component organization	GO:0051128
Response to endogenous stimulus	GO:0009719
Regulation of cell death	GO:0010941
Regulation of apoptotic process	GO:0042981
Regulation of cell migration	GO:0030334
Actin cytoskeleton organization	GO:0030036
Cell-substrate adhesion	GO:0031589
Extracellular matrix organization	GO:0030198

Table 15 shows the top 10 up-regulated proteins in the TSC/P proteome. The molecular processes of these proteins are consistent with the biological pathways in table 13, which are referred to the 375 up-regulated proteins clustered together in the heat map. Most of the up-regulated proteins belongs to enzymes family, and are involved in metabolism, DNA transcription, and duplication. Two ECM proteins (*Lama5* and *Col18a1*) and the integrin alpha 6 (*Itga6*) are included among the top 10, up-regulated proteins.

Table 15. Top 10 up-regulated proteins in TSC/P. Protein ID, protein name, gene name, log2 fold change, p-value and description are listed for each protein. Description of each protein come from the Uniprot database.

Protein IDs	Protein names	Gene names	Log2 fold change TSC/THY	t-Test p-value	Description
F1MAN8	Laminin subunit alpha 5	Lama5	7.87	1.76E-07	ECM and basement membrane protein
A0A0G2JT33	Telomerase protein component 1	Tep1	7.06	1.21E-06	Essential for the replication of chromosome termini
P15429	Beta-enolase	Eno3	7.04	4.29E-07	Involved in the glycolysis
G3V667	Integrin subunit alpha 6 (CD49f)	Itga6	6.91	1.04E-04	Cell-matrix interaction proteins and stem cell marker
D4A3X3	ISG15 ubiquitin-like modifier	Isg15	6.32	3.03E-05	Ubiquitin-like molecule
F1LR02	Collagen type XVIII alpha 1 chain	Col18a1	6.30	2.57E-07	ECM protein
D3ZHZ3	Oxysterol-binding protein	Osbpl3	5.73	1.91E-05	Involved in the lipid transport
Q5M939	Histone acetyltransferase type B	Hat1	5.20	1.01E-05	Involved in nucleosome assembly during DNA replication
P11883	Aldehyde dehydrogenase	Aldh3a1	4.78	2.82E-05	Involved in the metabolism of corticosteroids, amines, neurotransmitters, and lipid peroxidation
A0A0G2JWH3	Condensin complex subunit 1	Ncapd2	4.72	0.0002	Involved in the mitotic chromosome condensation

Table 16 shows that the top 10, down-regulated proteins are involved in the negative regulation of cell growth (*Tes* and *Cnn1*), intercellular adhesion, and enzymatic activities.

Table 16. Top 10 down-regulated proteins in TSC/P. Protein ID, protein name, gene name, log2 fold change, p-value and description are listed for each protein. Description of each protein come from the Uniprot database.

Protein IDs	Protein names	Gene names	Log2 fold change TSC/THY	t-Test p-value	Description
A0A0G2KAJ7	Collagen type XII alpha 1 chain	Col12a1	-11.11	5.21E-07	ECM protein
Q2LAP6	Testin	Tes	-9.13	3.61E-05	Negative regulation of cell proliferation and motility
Q08290	Calponin-1	Cnn1	-8.53	5.89E-06	Binding to cytoskeleton protein and negative regulation of cell proliferation
Q62745	CD81 antigen	Cd81	-7.86	7.90E-05	Involved in the transmission of extracellular stimuli to intracellular signaling pathways like cytoskeleton modification and negative regulation of cell proliferation
Q64122	Myosin regulatory light polypeptide 9	Myl9	-7.77	5.68E-06	Implicated in cytokinesis, receptor capping, and cell locomotion
Q63639	Retinal dehydrogenase 2	Aldh1a2	-7.72	3.56E-07	Involved in the pathway of retinol metabolism
F1LRJ9	Selenium-binding protein 1	Selenbp1	-7.71	2.83E-05	Involved in the sensing of reactive xenobiotics in the cytoplasm and intra-Golgi protein transport
Q6IN11	Connective tissue growth factor	Ctgf	-7.69	5.87E-08	Role in cell adhesion, migration, proliferation, angiogenesis, skeletal development
Q4G075	Leukocyte elastase inhibitor A	Serpinb1a	-7.35	1.02E-05	Regulation of protein catabolic process
P29534	Vascular cell adhesion protein 1	Vcam1	-7.19	9.07E-05	Important in cell-cell recognition and mediate the adhesion to vascular endothelium

3.3 PLASMA MEMBRANE MOLECULAR SIGNATURE OF RAT THYROID STEM CELL/PROGENITORS

Figure 39 shows the 67 PM proteins found to be up-regulated in TSC/P. Analysis of GOBP showed that 77% of these proteins are involved in the response to external stimuli, 62% in metabolic processes, 47% in cell development, 41% in membrane transport, 22% in cell communication and differentation, and 14% in cell proliferation. Between PM proteins, we have identified 9 up-regulated cluster of differentiation (CD) proteins including: *Itga6*, *Itga3*, *Itgb3*, *Sirpa*, *Tfrc*, *PVR*, *Ptgfrn*, *Igf2r*, *Mrc2*.

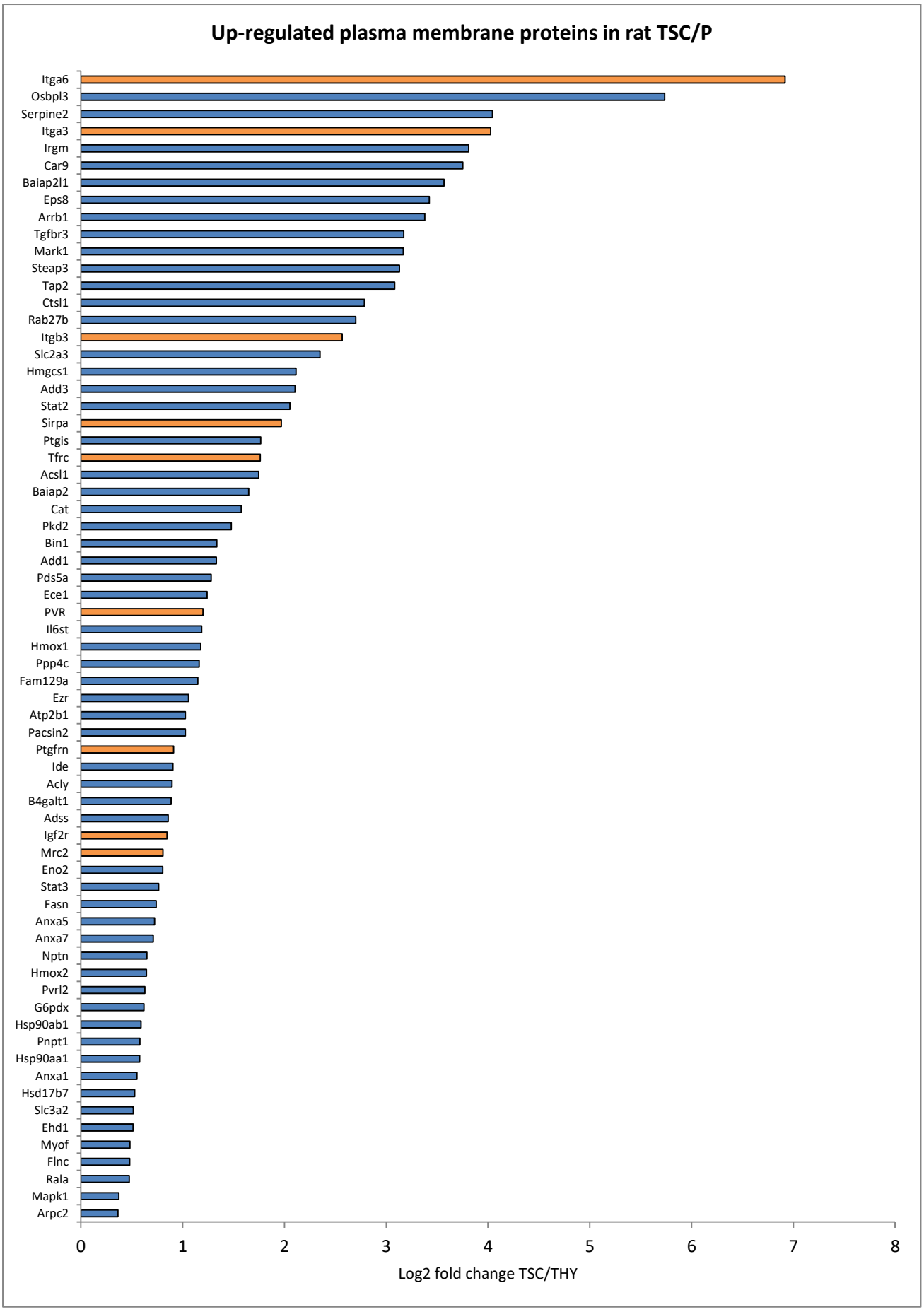

Figure 39. Up regulated plasma membrane proteins in rat TSC/P according to the Log2 fold change TSC/THY. In orange are highlighted proteins that are CD markers.

Table 17 shows the CD proteins identified on the PM of rat TSC/P and THY whose expression does not statistically change between these two thyroid cell populations.

Table 17. CD proteins found to be non-statistically significant expressed between rat TSC/P and THY. Protein ID, protein name and gene name are listed for each protein.

Protein IDs	Protein names	Gene names
P40241	Cd9 antigen	Cd9
P07861	Neprilysin (CD10)	Mme
P15684	Aminopeptidase N (CD13)	Anpep
P14740	Dipeptidyl peptidase 4 (CD26)	Dpp4
P49134	Integrin beta 1 (CD29)	Itgb1
B1PLB1	Cd34 antigen	Cd34
Q64244	ADP-ribosyl cyclase 1 (CD38)	Cd38
P26051	Cd44 antigen	Cd44
P97829	Cd47	Cd47
P10252	Cd48 antigen	Cd48
A0A0G2JVZ6	Integrin alpha V (CD51)	Itgav
Q00238	Intercellular adhesion molecule 1 (CD54)	Icam1
P13596	Neural cell adhesion molecule 1 (CD56)	Ncam1
P28648	Cd63 antigen	Cd63
P21588	5-nucleotidase (CD73)	Nt5e
O70352	Cd82 antigen	Cd82
G3V928	LDL receptor-related protein 1 (CD91)	Lrp1
A0A0G2K0P8	Choline transporter-like protein 1 (CD92)	Slc44a1
Q63199	Tumor necrosis factor receptor superfamily member 6 (CD95)	Fas
Q63016	Large neutral amino acids transporter small subunit 1 (CD98)	Slc7a5
B4F7A5	Cd99 antigen	Cd99
M0RBA8	Endoglin (CD105)	Eng
P14562	Lysosome-associated membrane glycoprotein 1 (CD107a)	Lamp1
P17046	Lysosome-associated membrane glycoprotein 2 (CD107b)	Lamp2
P20786	Platelet derived growth factor receptor alpha (CD140a)	Pdgfra
Q05030	Platelet derived growth factor receptor beta (CD140b)	Pdgfrb
P26453	Basigin (CD147)	Bsg
Q9QZA6	Cd151	Cd151
Q63072	ADP-ribosyl cyclase 2 (CD157)	Bst1
O35112	Cd166 antigen	Alcam
P97675	Ectonucleotide pyrophosphatase (CD203c)	Enpp3
P13852	Major prion protein (CD230)	Prnp
D3ZN06	Cd248 antigen	Cd248
Q63377	Sodium/potassium-transporting ATPase subunit beta-3 (CD298)	Atp1b3
F1LQ10	CD302 antigen	Cd302
G3V803	Cadherin-2 (CD325)	Cdh2

Table 18 shows the up-regulated, CD proteins in rat TSC/P. In these cells, a total of 9 proteins have been found up-regulated. The most expressed proteins were 3 different types of integrins (*Itga3*, *Itga6* and *Itgb3*) which share a Log2 fold change higher than 2.

Table 18. Up-regulated CD proteins in rat TSC/P. Protein ID, protein name, gene name, log2 fold change, and p-value are listed for each protein.

Protein IDs	Protein names	Gene names	Log2 fold change TSC/THY	t-Test p-value
D3ZQM3	Integrin alpha 3 (CD49c)	Itga3	4.02	0.0024
G3V667	Integrin alpha 6 (CD49f)	Itga6	6.91	0.0001
A0A0G2JWK0	Integrin beta 3 (CD61)	Itgb3	2.56	0.0006
Q99376	Transferrin receptor protein 1 (CD71)	Tfrc	1.76	0.0005
Q5U334	Poliovirus receptor (CD155)	PVR	1.20	0.0004
P97710	Signal regulatory protein alpha (CD172a)	Sirpa	1.96	0.0012
G3V824	Insulin-like growth factor 2 receptor (CD222)	Igf2r	0.84	0.0010
F1LMA7	C-type mannose receptor 2 (CD280)	Mrc2	0.80	0.0032
Q62786	Prostaglandin F2 receptor negative regulator (CD315)	Ptgfrn	0.91	0.0009

Table 19 shows CD proteins down-regulated in TSC/P. Interestingly, the most down-regulated protein is an integrin (*Itga1*) that contributes to the negative regulation of cell proliferation.

Table 19. CD proteins down-regulated in rat TSC/P. Protein ID, protein name, gene name, log2 fold change, and p-value are listed for each protein.

Protein IDs	Protein names	Gene names	Log2 fold change TSC/THY	t-Test p-value
P18614	Integrin alpha 1 (CD49a)	Itga1	-6.75	4.89E-05
Q62745	Cd81 antigen	Cd81 antigen	-7.86	7.90E-05
P01830	Thy-1 membrane glycoprotein (CD90)	Thy1	-1.89	0.0047
P29534	Vascular cell adhesion protein 1 (CD106)	Vcam1	-7.19	9.07E-05
P43245	Multidrug resistance protein 1 (CD243)	Abcb1	-0.63	0.0044

Table 20 shows that numerous proteins belonging to annexins family were found to be up-regulated in TSC/P.

Table 20. Expression of proteins belonging to annexins family on TSC/P. Protein ID, protein name, gene name, log2 fold change, p-value and a brief description are listed for each protein.

Protein IDs	Protein names	Gene names	Log2 fold change TSC/THY	t-Test p-value	Description
P07150	Annexin A1	Anxa1	0.54	0.0024	Involved in endo- and exocytosis, signal transduction, cytoskeletal rearrangements, regulation of metabolic enzymes, cell growth, differentiation, apoptosis, migration, hormone secretion, and inflammatory response [111].
Q07936	Annexin A2	Anxa2	no statistical difference		Implicated in cell proliferation, angiogenesis, foetal immune tolerance, ion-channel activation, cell-to-cell interactions and the bridging of membranes [112].
P14669	Annexin A3	Anxa3	-1.60	1.37E-05	Calcium binding protein with a variety of biological activities such as regulating ion channels, mediating inflammatory response and participating in membrane trafficking [113]. Expression of annexin A3 seems to negative regulate adipocyte differentiation [114].
P55260	Annexin A4	Anxa4	1.06	0.0070	Is highly expressed on apical membranes of epithelial cells in many tissues, where it might be involved in the regulation of chloride ion efflux [116].
P14668	Annexin A5	Anxa5	0.72	0.0007	Is expressed in most cells and tissues and its levels change with proliferation and differentiation. Is involved in Ca2+ signaling, cell cycle regulation, apoptosis, membrane trafficking and organization [111].
P48037	Annexin A6	Anxa6	no statistical difference		Involved in all biological processes regulating cell proliferation, survival, migration, differentiation, and inflammation [111].
Q6IRJ7	Annexin A7	Anxa7	0.70	4.43E-05	Involved in regulation of secretion, hormone release, cell survival, cell volume and inflammation [111, 115].
Q4FZU6	Annexin A8	Anxa8	no statistical difference		Membrane proteins that bind F-actin and is involved in the regulation of late endosome organization and function [116]
Q5XI77	Annexin A11	Anxa11			Involved in cell division, Ca2+ signaling, vesicle trafficking and apoptosis [117].

Table 21 shows proteins of the integrins family identified in the analysis.

Table 21. Panel of identified integrins in rat TSC/P and THY.

Protein IDs	Protein names	Gene names	Log2 fold change TSC/THY	t-Test p-value	Description
P18614	Integrin alpha 1 (CD49a)	Itga1	-6.75	4.89E-05	Heterodimerizes with the beta 1 subunit to form a cell-surface receptor for collagen and laminin [118].
D3ZQM3	Integrin alpha 3 (CD49c)	Itga3	4.02	0.0024	Involved in the interaction with many ECM proteins. It is a potential molecular marker for cells undergoing epithelial to mesenchyme transition (EMT) [119].
A0A0G2JVZ6	Integrin alpha V (CD51)	Itgav	no statistical difference		Involved in the adhesion to substrate proteins likes fibronectin and vitronectin [120].
G3V667	Integrin alpha 6 (CD49f)	Itga6	6.91	0.0001	One of the only biomarker commonly found in more than 30 different populations of stem cells, including some cancer stem cells. The expression of CD49f among stem cell populations indicates an important and conserved role in stem cell biology [121].
B5DEG1	Integrin subunit alpha 8	Itga8	Identified only in THY samples		Is expressed on mesenchymal cells, vascular smooth-muscle cells, fibroblasts and undifferentiated epithelial cells. After dimerization with theβ 1 integrin chain, it serves as a receptor for ECM proteins [122].
F1LUU1	Integrin subunit alpha 11	Itga11			Is a collagen receptor which is expressed in a subset of mesenchymally-derived tissues. Itga11-expressing cells mainly show an osteogenic differentiation profile with limited adipogenic differentiation [123].
P18614	Integrin beta 1 (CD29)	Itgb1	no statistical difference		MSC marker. Is the major adhesion receptor for various ECM components like collagen fibers, providing cell-substrate adhesion [124].
A0A0G2JWK0	Integrin beta 3 (CD61)	Itgb3	2.56	0.0005	Involved in the interaction with many ECM proteins [118].

MS analysis allows the investigation of specific phenotype markers expressed on cell surface and cytoplasm. Figure 40 shows that rat TSC/P tend to express more mesoderm/mesenchyme markers than endoderm/epithelial ones.

Protein IDs	Protein names	Gene names	Log2 fold change TSC/THY	t-Test p-value
P15429	Beta enolase	Eno3	7.04	4.29E-27
D3ZQM3	Integrin alpha 3 (CD49c)	Itga3	4.02	0.0024
A0A0G2JWK0	Integrin beta 3 (CD61)	Itgb3	2.56	0.0005
P97710	Signal regulatory protein alpha (CD172a)	Sirpa	1.96	0.0012
Q99376	Transferrin receptor protein 1 (CD71)	Tfrc	1.76	0.0006
P63014	Paired mesoderm homeobox protein 1	Prrx1	1.66	1.36E-06
Q8K3R4	Adiponectin	Adipoq	1.45	0.0001
Q62786	Prostaglandin F2 receptor negative regulator (CD315)	Ptgfrn	0.91	0.0009
G3V824	Insulin-like growth factor 2 receptor (CD222)	Igf2r	0.84	0.0010

t-Test p-value	Log2 fold change TSC/THY	Gene names	Protein names	Protein IDs
0.0007	1.06	Anxa4	Annexin A4	P55260
9.23E-06	1.05	Ezr	Ezrin	P31977
0.0076	0.67	Emb	Embigin	A0A0G2JU92

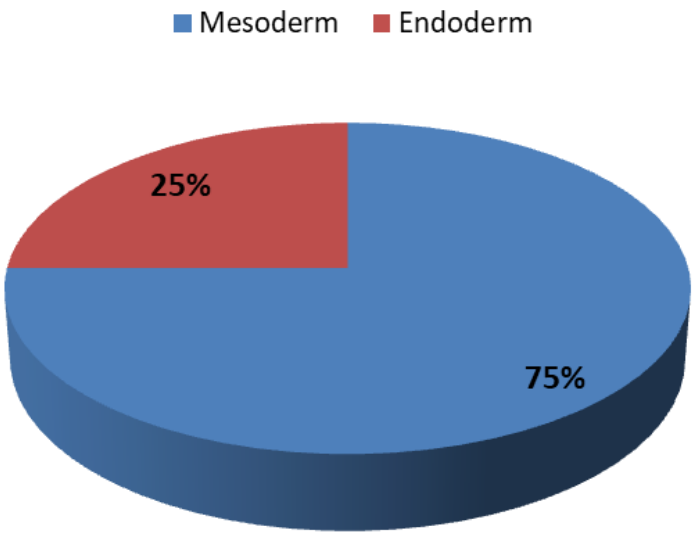

Figure 40. Proteins identified as markers of mesodermal and endodermal lineages. Proteins used as a markers of endoderm are highlighted in red , proteins used as a marker of mesoderm are highlighted in blue.

DISCUSSION

1. DECELLULARIZED RAT THYROID GLAND

Results from DNA content analysis using CyQuant® assay confirm that all three decellularization protocols guarantee the complete removal of cells and DNA from the thyroid matrix. However, HPLC-MS/MS SRM showed that the first decellularization protocols allows for retention of less protein material than the other two protocols, each keeping an amount of collagen residues higher than the first protocol. It is possible that different times of exposition to chemical/enzymatic agents impaired the stability and distribution of matrix proteins. In the first protocol, a higher concentration of trypsin and a long exposure to the detergent Triton X-100 partially solubilizing the extracellular proteins and may have negatively influenced the distribution of matrix protein. Moreover, trypsin is a protease that digest both cells and ECM proteins, and could change the mechanical properties of the matrix. For this reason, trypsin should be used with caution and for a limited time. Remarkably, the action of DNAase used in the third protocol does not affect the matrix proteins.

A good decellularization process represent a fundamental step in order to obtain a thyroid matrix that is free of potentially immunogenic cells, allowing the seeding of rat TSC/P. Since stem cells are influenced by several factors related to the substrate including its stiffness, 3D geometry, and composition knowledge of the composition of the ECM of the decellularized rat thyroid gland is advisable. For this reason, we have chosen two different MS approaches to obtain characterization of its composition.

In the literature, few works have applied proteomics to study the ECM composition. The most representative was made by Naba *et al*. in the 2017[125]. They used a reversed-phase HPLC couple to a QExactive mass spectrometer for study differences in ECM composition in breast cancer and adjacent mammary tissue, omental metastasis from high-grade serous ovarian cancer, and normal omentum. Compared to our work, they were able to identified a similar number of collagen types (from 20 to 25 types) and proteoglycans (up to 10), but significantly greater number of glycoproteins[125].

LTQ Orbitrap XL analysis allowed us to characterize the composition of each thyroid matrix obtained with different decellularization protocols. In particular, collagens I to VI and collagens XXVII are present in all decellularized thyroids, with a predominance of collagen type I. Collagen type XXII was maintained only after the first and the third protocols while collagen XXV after the first and the second. Collagen XVI was detected in the second and third protocols. Collagens VII, XIX and collagens VIII and IX were detected only after the second and third decellularization protocol, respectively.

Qualitative analysis shows that collagens I to IV and collagens VI are the most represented collagens into the thyroid matrix. The predominance of the α1 isoform of collagen I likely reflects the α1α1α2 heterotrimeric structure of the native protein. Collagen I is found in various connective tissues, including cartilage, bone and tendon, and is arranged into long, thin fibrils that cross-link to one another[126]. The presence of collagen III as second most abundant collagen in thyroid gland is a consistent finding. Together with collagens type I, II, V and XI, collagen type III is a fibril-forming collagen and one of the main component of the stroma. There is evidence that *in vivo* type I and type III collagens are present in the same fibril, which polymerize in the ECM with a characteristic 67 nm periodicity[127]. Of interest is the presence of collagen type IV after each decellularization protocols. Unlike most collagens, type IV collagen is an exclusive member of the BM, which in the rat thyroid is present around follicles and vessels[59], and through a complex

networks can influence cell adhesion, migration, and differentiation[128]. Laminin is another fundamental BM proteins and it is connected to collagen IV network through nidogen/entactin[56]. Based on MS results, only decellularization protocol 3 is able to retain laminin into the thyroid matrix, even though a positive immunoreaction for laminin was observed in our previous immunohistochemistry experiments (figure 8). The maintenance of type IV collagen and laminin is mandatory for a correct recellularization of the rat thyroid matrix as they may be able to influence cells polarization and follicles formation.

Several proteoglycans have been detected in our samples. However, decorin is the only one that is present in all samples. Decorin belongs to a family of structurally related proteins, grouped as the small leucine-rich proteoglycans (SLRPs) whose functional roles includes regulation of collagen fibrillogenesis, modulation of growth factor activity, and regulation of cellular growth[129]. Decorin structure consists of an arch shape with an inner concave surface that bind to collagen type I triple helix, leading to the correct arrangement of collagen molecules[130]. For this evidence, the detection of decorin as the most relevant non-collagenous proteins in all samples can be related to the high presence of collagen type I, which is the most abundant proteins in the rat thyroid ECM.

After the first decellularization protocol, the two proteoglycans lumican and versican have been detected in the thyroid matrix. ECM is composed of collagens and elastic fibres which are embedded in a viscoelastic gel that comprises proteoglycans and, within these, versican is one of the most widespread. Versican function comprise cell adhesion, proliferation and migration[131]. The same functions are exploited by lumican, together with its role in control collagen fibrillogenesis[132].

Although their importance in maintain the BM integrity, nidogens and SPARC were never detected in the male rat thyroid gland matrix. Nidogens (also called entactins) are ubiquitous components of all BMs and are present as two different isoforms[133], with nidogen 2 being predominant in vascular BMs. They are structural glycoproteins of 160

kDa that connect the network formed by laminins and collagen IV to each other[134]. Nidogens are essential for the stabilization of the BM during late embryogenesis, and for its proper function in adult tissues when mechanical stresses increase[135]. SPARC (secreted protein, acidic, cysteine-rich; also call osteonectin) is a calcium-binding matricellular glycoprotein that recognizes non-denatured triple helical collagen, and appears to regulate cell growth through interactions with ECM and cytokines[136]. It has been suggested that SPARC act as a chaperone for collagen type IV and it collagen-binding domain is highly conserved in all vertebrate and invertebrate[137].

The ECM is also a reservoir of GFs and bioactive molecules[138]. For this reason, in the Orbitrap results were included also receptors, enzymes and GFs that could favour or otherwise hinder a subsequent recellularization. Among the molecules that could interfere with future recellularization there were matrix metalloproteinsases, which were present after all decellularization protocols. Only in the first and third protocols, however, detectable fragments of the major histocompatibility complex were identified. Whether their presence could represent an obstacle to cell growth after recellularization is still to be determined. On the other hand, some GFs were preserved. Specifically, connective tissue growth factor was present in protocol 1 while epidermal growth factor and vascular endothelial growth factor were detected in protocol 2. Thyroglobulin, a precursor of the thyroid hormones, has been detected in protocol 3.

Surprisingly, fibronectin was never observed although previously detected by immunocytochemistry. Indeed, fibronectin is a widespread ECM glycoprotein[139] and it has been previously found in the intact thyroid gland[53]. Possibly, decellularization protocols could have influenced its availability in quantities detectable by our analysis.

The presence of the first five collagen types in all decellularized thyroid lead us to set up a micro-quantitative LC-MS/MS-SRM method for the quantification of these collagens into

the rat thyroid matrix. Results from the quantification analysis substantially confirm and validate data from the MS analysis, with the only exception of collagen type II that was never detected in the first decellularization protocol. The application of an HPLC-MS/MS-SRM methods for the investigation and quantitation of collagens types I-V in rat skin, tail tendon and aorta was previously used by Pataridis *et al*.[140]. They were able to quantify only collagen types I and III in their tissue samples, with detection limits restricted above the nanomolar range. Conversely, our methodology can quantify also collagen types II-IV and V, substantially increasing the analytical power of the technique. In conclusion, the MS workflow here applied could be improved for the quantitation of other important rat thyroid gland ECM proteins such as laminins and proteoglycans, and also be suitable for the quantitation of the principal ECM proteins of different organs of the same endodermal origin like the liver, lungs and pancreas.

2. 3D BIOPRITING OF COLLAGEN FROM RAT TAIL TENDONS

The fundamental concept behind the 3D bioprinting is to fabricate biocompatible scaffold that acts as a support for cells growth[66]. A typical approach is the layer by layer deposition of material in order to generate a simple 3D structure. However, the most complex printers are able to reproduce part of the body such as bone or soft tissues[141]. In our case, the porous 3D collagen scaffolds represents a good starting point for mimicking the decellularized thyroid's follicular structure, i.e. the morphological and functional unit composed by thyrocytes.

The success for obtaining a 3D collagen scaffold with FDM printing methods highly rely on two important factors: viscosity and temperature[142]. Viscosity is a fundamental rheological parameter to be verified; using too much viscous solutions would lead to difficulties in the homogeneous outflow of the biomaterial from the extrusion cannulae. In addition, solutions having a viscosity value under the acceptable range would have lower concentrations of biomaterial and therefore a greater percentage of water. This would lead to a greater dilatation of the extruded biomaterial once frozen on the printing surface. This effect not only causes a reduction in the mechanical strength of the biomaterial, but also a greater steric bulk that could interfere both with the passage inside the extruder needle and outside it, where it could cause breaking of the filament, and interruption of the printing process. The viscosity values obtained with the 2% w/v (tendons in water) solution, solubilized with 1M acetic acid, was within the range of acceptability of the instrument. This allowed us to extrude material that was able to maintain a structure adequate to give rise to the final morphology of the scaffold.

Temperature is another critical point of the printing process. Specifically, a stable temperature during the process and across each replicates is mandatory for the correct freezing of the scaffold, to maintain the desired structure and porosity.

We used the ATR-IR spectroscopy to investigate whether the printing process and the subsequent freeze-drying could lead to chemical modifications in the biomaterial. This spectroscopic technique is used for surface analysis of solid materials, and gives information on the chemical bonds through the analysis of peaks that can be divided into two categories: those related to the presence of functional groups (region in the spectrum from 4.000 to 1.300 cm-1) and those considered to be finger-prints that are specific for each material (1.300-400 cm-1)[143]. Our analysis showed that the printing methodology does not alter the functional groups of the sample. Similarly, the chitosan bioprinting process is also considered not to alter the chemical bonds of the biomaterial.

The composition of the collagen from rat tail tendons has been investigated with the high-resolution LTQ Orbitrap XL MS. Differently from thyroid gland, we choose the pepsin as a specific enzyme due to the lower pH of the collagen solution (pH 3), which represent an optimal environment for pepsin activity but not for trypsin. Based on Proteome Discoverer protein score value, MS qualitative results showed that type I collagen prevails over the other proteins, confirming the data available in the literature that classify collagen type I as the main component of tendon bundles, together with the elastic fibers[144]. Moreover, this biomaterial share several typical ECM proteins with the thyroid matrix such as collagen I to V, IX, XVI, XXII, XXV and XXVII. Compared to the three different types of decellularized thyroid, the score value of collagen type I in rat tail tendons was considerably higher (collagen Iα1: 201.90 ± 47.71 score value for thyroid matrices respect to 674.30 for collagen from rat tail tendons). This finding may be related to an higher absolute abundance of collagen type I in rat tendons respect to thyroid gland, but a detailed quantitative analysis awaits an eventual quantitative MS evaluation.

The porous surface of the 3D collagen scaffolds can mimic the decellularized thyroid follicular cavities, whereas the ECM composition of the rat tail tendons can partially reproduce the thyroid interfollicular stroma. Thus seeding of cells on the spaces provided by the bioprinted collagen could induce a cellular behaviour similar as that expected in the follicular cavities.

Both chitosan and collagen have been observed to favour adhesion of fibroblasts and maintenance of their elongated morphology, although it seems that these cells grew much better on collagen substrate than on chitosan. Whether these differences could be exploited for seeding of fibroblasts in the construction of a 3D bioartificial thyroid organoid remains to be studied.

Collagen coating on PLLA was performed to evaluate the combined effect of these two biomaterials on cell viability and morphology. PLLA is a biocompatible biomaterial widely used in tissue engineering, especially in bone regeneration[145]. In this preliminary study, we have chosen collagen as a coating material in order to promote greater cell growth on PLLA. The goal was to obtain a collagen concentration and thickness that allowed cells to be in contact and influenced by both biomaterials. The most suitable collagen coating for PLLA has been demonstrated to be the collagen concentration of 0.5% and 0.1%, which allowed to simultaneous maintain the microporous surface of PLLA and the collagen coating. The adhesion of collagen to PLLA can be explained due to the presence of weak bonds between the hydrophobic portions of the two compounds.

SEM analysis shows that rat TSC/P tend to strongly adhere to collagen substrate rather than to PLLA, even at the lowest coating concentrations. The presence of numerous microvilli and secretion vesicles on cell surface confirms their vitality and metabolic activity.

An innovative aspect of this research concerns the possibility to functionalize the PLLA with chitosan coating, making this thermoplastic biomaterial much more suitable for

growing of thyroid cells. Differently from collagen, chitosan would coat PLLA through positive charges on the amino groups of D-glucosamine, capable of generating electrostatic attraction with PLLA in aqueous solution such as the culture medium[146]. SEM analysis showed that chitosan has a marked and totally unexpected ability to induce formation of TSC/P aggregates with spheroidal morphology, similar to those identifiable in the mature thyroid follicles. This effect can be already observed in the first 24 hours of culture, and it can be hypothesize that the rapid formation of follicular-like spheroids is initially due to cell-chitosan interactions, and subsequently maintained by cell-cell interactions favoured by the biomaterial. This property is maintained even when chitosan was used as a coating for PLLA, suggesting its possible application as an alternative coating substrate for TSC/P seeded in bioreactor on PLLA organomorphic 3D scaffolds to give rise to a 3D thyroid organoid.

3. PROTEOMICS SIGNATURE OF ADULT, MALE RAT THYROID STEM CELL / PROGENITORS

To our knowledge, this work represent the first proteomic analysis of rat TSC/P and the first step for their *in vitro* isolation. Before this analysis, studies on this thyroid cell population were focused on few surface and intracellular / nuclear markers. Modern tribrid high resolution mass spectrometry has proved to be the best tool to obtain an exhaustive characterization of cellular proteome and the application of the FASP method allowed the use of strong detergent such as SDS, led to a deep coverage of membrane proteins.

Highly consistent distribution of TIC's, high amount of proteins identified in both cell populations and a Pearson correlation higher than 0.90 have shown that the applied method is reproducible, allowing to use statistical tests for a quantitative analysis of the results.

Statistical analysis revealed that 16% (721 proteins) of identified proteins in TSC/P and THY proteomes were differentely expressed. Of those, the 52% (375 proteins) were up-regulated in TSC/P, and the GOBP highlighted that these proteins belonged to the cellular pathways controlling cell proliferation. This evidence is consistent with the fact that TSC/P replicates at least three times faster than THY.

Orbitrap Fusion analysis allowed to obtain an exhaustive panel of CD molecules. Of 50 identified CD proteins, 36 appeared to be expressed without any statistical differences in the analyzed samples while 9 CD were up-regulated in TSC/P, and 5 were down-regulated. Remarkably, we identified eleven typical MSC markers (identified: CD13, CD29, CD44, CD49a, CD54, CD71, CD73, CD90, CD105, CD106, CD166)[147, 148] but only two of those were differently expressed in TSC/P (CD71 and CD90) with respect to THY. Specifically, CD90 was 1.89 times more expressed in THY than TSC/P. This finding is in

agreement with previous evidence with flow cytometry collected by the research group of Prof. Toni (data not shown).

In addition to CD markers, the analysis showed that TSC/P express different types of annexins and integrins that could represent a suitable candidates markers of these cells. Annexins are implicated in a number of biochemical processes, including cell proliferation, immune tolerance, ion-channel activation, cell-cell interactions and cell differentiation. Integrins are involved in many cellular functions ranging from cell-substrate adhesion, cytoskeleton organisation, cell motility and response to stimuli. In particular, four types of integrins are normally expressed in mesenchyme-derived cells (*Itga3, Itga8, Itga11 and Itgb1*) and another one (*Itga6*) was used as a marker of several progenitor cells.

The analysis of phenotypic markers showed that TSC/P tend to primarily express proteins of the mesodermal / mesenchymal lineage, while no ectodermal markers have been identified including *Wnt, chromogranin, Notch*, and Hox gene products (*Hoxc4, Hoxc5, Hoxc8, Hoxd3, Hoxd8*) nor endodermal markers such as *Gata4, Sox17, Pax8, Foxa1* and *Foxa2*. Based on this evidence, we can assume that adult male rat TSC/P mainly comprise a population of mesodermal / mesenchymal origin although blotting analysis and immunocytochemistry have previously shown that these cells also express markers of the endodermal lineage such as *Hnf4α*, *Gata-4*, and *Sca-1* (data not shown). At the moment, whether TSC/P undergo a partial epithelial to mesenchymal transition *in vitro* thus acquiring a mesenchymal phenotype is not clear.

All these data are consistent with previous evidence that adult male rat TSC/P can differentiate to the adipogenic, thyrogenic, and hepatogenic lineages[104]. However, differently from MSCs TSC/P do not respond to osteogenic differentiation[149, 150] and are able to maintain the differentiation capacity following several *in vitro* passages. Overall, TSC/P show characteristics compatible with both endodermal and mesodermal cells, suggesting the possibility that are a mixed population with two different cell types.

It is interesting to note that these results can be correlated with those observed by Suzuki in 2011 regarding human TSC/P[151]. In this paper, using immunohistochemical techniques and analysis of gene transcription (microarray), the author shows that human TSC/P express markers of mesenchymal origin and can be expanded *in vitro* for a long period (3-4 months). Furthermore, rat and human TSC/P largely share high expression of proteins related to the regulation of metabolism and low expression of those related to cytoskeleton organization[151].

Of interest is the expression of nestin (*Nes*) only in TSC/P samples. This protein is used as a marker for neural stem cells, and its expression is inversely correlated with cellular differentiation[152]. Recently, nestin expression has also been described in several MSCs, progenitor cells[153, 154] and cancer stem cells[155].

As summarized in table 22, analysis of CD molecules allowed the identification of 4 putative markers that could be used for TSC/P isolation: *Itga6* (CD49f), *Sirpa* (CD172a), *Tfrc* (CD71) and *Igf2r* (CD222). All these CD proteins have been previously used as a markers of stemness for MSCs and progenitor cells of different origins and represent the main candidates for the TSC/P molecular signature. Of particular interest is the high expression of CD49f, which has been extensively characterized as a marker of a wide range of stem and progenitor cells of both mesodermal and endodermal origin[121]. By forming heterodimers with integrin α1 (CD29) or integrin α4 (CD104, not detected in this analysis), integrin α6/CD49f functions as a receptor for laminins. The expression of CD49f has been identified in somatic stem cells and germ cells from early developmental stages through adulthood[126]. It has been proved that in MSCs, the pluripotency factors OCT4 and SOX2 were recruited to the putative promoter region of CD49f, supporting the finding that these two transcription factors play positive roles in the expression of CD49f[156]. Moreover, MSCs positive in CD49f possess high colony forming unit (CFU) formation ability and differentiation potential[157,158]. This latter characteristic may be relevant for this research,

because also TSC/P showed high ability to form CFU *in vitro*. *Sirpa*/CD172a was used to isolate and characterize cardiac precursor populations of the endothelial and myogenic lineages[159] and is expressed also in iPSC and ESC during fetal heart development[160]. *Tfrc*/CD71 is a well charcterized and typical marker of MSCs[161,162] and adipose derived stem cells (ADSC)[163], while *Igf2r*/CD222 is expressed in MSCs and also in endothelial progenitor cells[164, 165].

Table 22. Putative markers for TSC/P molecular signature.

Protein IDs	Protein names	Gene names	Log2 fold change TSC/THY	t-Test p-value
G3V667	Integrin alpha 6 (CD49f)	Itga6	6.91	0.0001
P97710	Signal regulatory protein alpha (CD172a)	Sirpa	1.96	0.0012
Q99376	Transferrin receptor protein 1 (CD71)	Tfrc	1.76	0.0006
G3V824	Insulin-like growth factor 2 receptor (CD222)	Igf2r	0.84	0.0016

CONCLUSIONS

The aim of this PhD thesis was to produce and characterize a laboratory model of rat thyroid gland. Relying on Edelman's topobiological theory and the well know benefit of the 3D environment for cell growth, we have obtained two different types of substrates, the decellularized rat thyroid gland and the 3D printed scaffold made of collagen from rat tail tendons. Results show that all decellularization protocols guarantee the complete removal of cells and DNA from the thyroid and have similar proteins composition, included the basement membrane protein collagen type IV. Differences were found on the relative abundance of collagen I and III, and on the presence of proteoglycans, in particular protocol 1 retain less collagen type I than protocol 2 and 3, but more proteoglycans. For this reason, matrix obtained with the first decellularization protocol could represent the most complete substrate for engineering a complete thyroid organoid .

In alternative to the thyroid decellularization, we develop and standardized a method that combined the high-throughput efficiency of the 3D printing with the use of collagen from rat tail tendons. The ECM proteins composition of this biomaterial shows high similarities with the ECM of the thyroid gland, with collagen type I as the most representative protein, followed by collagen II to VI. Moreover, the 3D microstructure of the collagen scaffold (i.e. the porosities) partially recapitulate the morphology of the decellularized thyroid follicle, possibly inducing a similar cells proliferation and distribution on the surface of these biomaterials. Further comparison between decellularized thyroid gland and 3D printed collagen scaffold will be necessary to understand which materials represent the optimal substrate to improve the growing and differentiation of rat TSC/P compared to the standard culture conditions.

Finally, in the final part of this project we focused on the proteomic characterization of multipotent TSC/P. Proteomic analysis provided insights into the protein composition of these cells, leading to a putative molecular signature. This analysis revealed prominent surface markers of stemness for mesenchyme-derived cells, offering clues for their immunophenotyping, and potential new approaches for their isolation.

REFERENCES

1) Salvatori M, Katari R, Patel T, Peloso A, Mugweru J, Owusu K, Orlando G. Extracellular Matrix Scaffold Technology for Bioartificial Pancreas Engineering: State of the Art and Future Challenges. J Diabetes Sci Technol. 2014 8:159-169.

2) Benders KE, van Weeren PR, Badylak SF, Saris DB, Dhert WJ, Malda J. Extracellular matrix scaffolds for cartilage and bone regeneration. Trends Biotechnol. 2013 31:169-176.

3) Michel G, Tonon T, Scornet D, Cock JM, Kloareg B. The cell wall polysaccharide metabolism of the brown alga Ectocarpus siliculosus. Insights into the evolution of extracellular matrix polysaccharides in Eukaryotes. New Phytol. 2010 188:82-97

4) Cai L, Heilshorn SC. Designing ECM-mimetic materials using protein engineering. Acta Biomater. 2014 10:1751-1760.

5) Stocum DL. Stem cells in regenerative biology and medicine. Wound Repair Regen. 2001 9:429-442.

6) Stocum DL. Regenerative biology and engineering: strategies for tissue restoration. Wound Repair Regen. 1998 6:276-290.

7) Badylak SF, Taylor D, Uygun K.. Whole-organ tissue engineering: decellularization and recellularization of three-dimensional matrix scaffolds. Annu Rev Biomed Eng. 2011 13:27-53.

8) Toni R, Bassi E, Zini N, Zamparelli A, Barbaro F, Dallatana D, Mosca S, Lippi G, Spaletta G, Bassoli E, Denti L, Gatto A, Parrilli A, Fini M, Giardino R, Sandri M, Sprio S, Tampieri A. Bioartificial endocrine glands: at the cutting edge of translational research in endocrinology. In: Sprio S. Tampieri A (Eds). Bio-inspired regenerative medicine: material, processes, and clinical applications. Pan Standford Publishing, Singapore, 2016 15:357- 387,

9) Toni R, Casa CD, Spaletta G, Marchetti G, Mazzoni P, Bodria M, Ravera S, Dallatana D, Castorina S, Riccioli V, Castorina EG, Antoci S, Campanile E, Raise G, Rossi R, Ugolotti G, Martorella A, Roti E, Sgallari F, Pinchera A. The bioartificial thyroid: a biotechnological perspective in endocrine organ engineering for transplantation replacement. Acta Biomed. 2007 78:129-155.

10) Edelman GM. Morphoregulation. Dev Dyn. 1992 193:2-10.

11) Schofield R. The relationship between the spleen colony-forming cell and the haemopoietic stem cell. Blood Cells. 1978 4:7-25.

12) Spradling A, Drummond-Barbosa D, Kai T. Stem cells find their niche. Nature. 2001 414:98-104.

13) Kruegel J, Miosge N. Basement membrane components are key players in specialized extracellular matrices. Cell Mol Life Sci. 2010 67:2879-2895.

14) Toni R, Tampieri A, Zini N, Strusi V, Sandri M, Dallatana D, Spaletta G, Bassoli E, Gatto A, Ferrari A, Martin I. Ex situ bioengineering of bioartificial endocrine glands: a new frontier in regenerative medicine of soft tissue organs. Ann Anat. 2011 193:381-394

15) Edelman GM. Topobiology: An Introduction to Molecular Embryology. New York: Basic Books 1988.

16) Edelman, GM. and Thiery JP. The cell in contact: adhesions and junctions as morphogenetic determinants. New York Wiley 1985.

17) Edelman GM, Jones FS. Cytotactin: a morphoregulatory molecule and a target for regulation by homeobox gene products. Trends Biochem Sci. 1992 17:228-232

18) Toni R, Casa CD, Bodria M, Spaletta G, Vella R, Castorina S, Gatto A, Teti G, Falconi M, Rago T, Vitti P, Sgallari F. A study on the relationship between intraglandular arterial distribution and thyroid lobe shape: implications for biotechnology of a bioartificial thyroid. Ann Anat. 2008 190:432-441

19) Baptista PM, Orlando G, Mirmalek-Sani SH, Siddiqui M, Atala A, Soker S. Whole organ decellularization. A tool for bioscaffold fabrication and organ bioengineering. 31st Annual International Conference of the IEEE EMBS Minneapolis, Minnesota, USA, September 2-6, 2009

20) Tapias LF, Ott HC. Decellularized scaffolds as a platform for bioengineered organs. Curr Opin Organ Transplant. 2014 19:145-152.

21) Park KM, Woo HM. Systemic decellularization for multi-organ scaffolds in rats. Transplant Proc. 2012 44:1151-1154.

22) Crapo PM, Gilbert TW, Badylak SF. An overview of tissue and whole organ decellularization processes. Biomaterials. 2011 32:3233-3243.

23) Hrebikova H, Diaz D, Mokry J. Chemical decellularization: a promising approach for preparation of extracellular matrix. Biomed Pap Med Fac Univ Palacky Olomouc Czech Repub. 2015 159:12-17.

24) Keane TJ, Londono R, Turner NJ, Badylak SF. Consequences of ineffective decellularization of biologic scaffolds on the host response. Biomaterials. 2012 33:1771-1781.

25) Tidball JG, Villalta SA. Regulatory interactions between muscle and the immune system during muscle regeneration. Am J Physiol Regul Integr Comp Physiol. 2010 298:1173-1187.

26) Valentin JE, Stewart-Akers AM, Gilbert TW, Badylak SF. Macrophage participation in the degradation and remodeling of extracellular matrix scaffolds. Tissue Eng Part A 2009 15:1687-1694

27) Bonvillain RW, Danchuk S, Sullivan DE, Betancourt AM, Semon JA, Eagle ME, Mayeux JP, Gregory AN, Wang G, Townley IK, Borg ZD, Weiss DJ, Bunnell BA. A nonhuman primate model of lung regeneration: detergent-mediated decellularization and initial in vitro recellularization with mesenchymal stem cells. Tissue Eng Part A. 2012 18:2437-2452.

28) Keane TJ, Swinehart IT, Badylak SF. Methods of tissue decellularization used for preparation of biologic scaffolds and in vivo relevance. Methods. 2015 84:25-34.

29) Grauss RW, Hazekamp MG, Oppenhuizen F, van Munsteren CJ, Gittenberger-de Groot AC, DeRuiter MC. Histological evaluation of decellularised porcine aortic valves: matrix changes due to different decellularisation methods. Eur J Cardiothorac Surg. 2005 27:566-571.

30) Gilbert TW, Wognum S, Joyce EM, Freytes DO, Sacks MS, Badylak SF.. Collagen fiber alignment and biaxial mechanical behavior of porcine urinary bladder derived extracellular matrix. Biomaterials. 2008 29:4775-4782.

31) Hodde JP, Hiles M. Virus safety of a porcine-derived medical device: evaluation of a viral inactivation method. Biotechnol Bioeng. 2002 79:211-216.

32) Prasertsung I, Kanokpanont S, Bunaprasert T, Thanakit V, Damrongsakkul S. Development of acellular dermis from porcine skin using periodic pressurized technique. J Biomed Mater Res B Appl Biomater. 2008 85:210-219.

33) Reing JE, Brown BN, Daly KA, Freund JM, Gilbert TW, Hsiong SX, Huber A, Kullas KE, Tottey S, Wolf MT, Badylak SF. The effects of processing methods upon mechanical and biologic properties of porcine dermal extracellular matrix scaffolds. Biomaterials. 2010 31:8626-8633.

34) Gorschewsky O, Puetz A, Riechert K, Klakow A, Becker R. Quantitative analysis of biochemical characteristics of bone-patellar tendon-bone allografts. Biomed Mater Eng. 2005 15:403-411.

35) Xu CC, Chan RW, Tirunagari N. A biodegradable, acellular xenogeneic scaffold for regeneration of the vocal fold lamina propria. Tissue Eng. 2007 13:551-566.

36) Meyer SR, Chiu B, Churchill TA, Zhu L, Lakey JR, Ross DB. Comparison of aortic valve allograft decellularization techniques in the rat. J Biomed Mater Res A. 2006 79:254-262.

37) Flynn LE. The use of decellularized adipose tissue to provide an inductive microenvironment for the adipogenic differentiation of human adipose- derived stem cells. Biomaterials. 2010 31:4715-4724.

38) Brown BN, Freund JM, Han L, Rubin JP, Reing JE, Jeffries EM, Wolf MT, Tottey S, Barnes CA, Ratner BD, Badylak SF. Comparison of three methods for the derivation of a biologic scaffold composed of adipose tissue extracellular matrix. Tissue Eng Part C Methods. 2011 17:411-421.

39) Elder BD, Kim DH, Athanasiou KA. Developing an articular cartilage decellularization process toward facet joint cartilage replacement. Neurosurgery. 2010 66:722-777

40) Cole MB Jr. Alteration of cartilage matrix morphology with histological processing. J Microsc. 1984 133:129-140.

41) Rawlings ND, Barrett AJ. Families of serine peptidases. Methods Enzymol. 1994 244:19-61.

42) Funamoto S, Nam K, Kimura T, Murakoshi A, Hashimoto Y, Niwaya K, et al. The use of high-hydrostatic pressure treatment to decellularize blood vessels. Biomaterials 2010 31:3590-3095

43) Grauss RW, Hazekamp MG, Oppenhuizen F, van Munsteren CJ, Gittenberger- de Groot AC, DeRuiter MC. Histological evaluation of decellularised porcine aortic valves: matrix changes due to different decellularisation methods. Eur J Cardiothorac Surg. 2005 27:566-571.

44) Yang M, Chen CZ, Wang XN, Zhu YB, Gu YJ. Favorable effects of the detergent and enzyme extraction method for preparing decellularized bovine pericardium scaffold for

tissue engineered heart valves. J Biomed Mater Res B Appl Biomater. 2009 91:354-361.

45) Lehr EJ, Rayat GR, Chiu B, Churchill T, McGann LE, Coe JY, Ross DB. Decellularization reduces immunogenicity of sheep pulmonary artery vascular patches. J Thorac Cardiovasc Surg. 2011 141:1056-1062.

46) Wadeleux P, Nusgens B, Foidart JM, Lapiere C, Winand R. Synthesis of basement membrane components by differentiated thyroid cells. Biochim Biophys Acta. 1985 846:257-264.

47) Li M, Carcangiu ML, Rosai J. Abnormal intracellular and extracellular distribution of basement membrane material in papillary carcinoma and hyalinizing trabecular tumors of the thyroid: implication for deregulation of secretory pathways. Hum Pathol. 1997 28:1366-1372.

48) Lu S, Huang M, Kobayashi Y, Komiyama A, Li X, Katoh R, Kawaoi A. Alterations of basement membrane in di-isopropanolnitrosamine-induced carcinogenesis of the rat thyroid gland: an immunohistochemical study. Virchows Arch. 2000 436:595-601.

49) Timpl R, Brown JC. Supramolecular assembly of basement membranes. Bioessays. 1996 18:123-132.

50) Pankov R, Yamada KM. Fibronectin at a glance. J Cell Sci. 2002 115:3861-3863.

51) Stoffels JM, Zhao C, Baron W. Fibronectin in tissue regeneration: timely disassembly of the scaffold is necessary to complete the build. Cell Mol Life Sci. 2013 70:4243-4253.

52) Mosher DF. Fibronectin. San Diego: Academic Press, Inc. 1989

53) Usenko VS, Lepekhin EA, Kornilovska IN, Lyzogubov VV, Apostolov EO, Ralets IS, Witt M. Immunohistochemical study of fibronectin and thyroglobulin in the thyroid gland of female rats after exposure to radioactive iodine. Anat Rec. 1998 252:600-607.

54) Bürgi-Saville ME, Reut B, Gerber H, Peter HJ, Paulsson M, Kaempf J, Simon F, Marti U, Gerber H, Bürgi U. Alginate gel culture allows the retention of extracellular matrix and follicular structure of rat thyroid tissue but does not lead to the formation of follicles by FRTL-5 cells. Thyroid. 1998 8:1147-1155.

55) Engel J, Odermatt E, Engel A, Madri JA, Furthmayr H, Rohde H, Timpl R. Shapes, domain organizations and flexibility of laminin and fibronectin, two multifunctional proteins of the extracellular matrix. J Mol Biol. 1981 150:97-120.

56) Hohenester E, Yurchenco PD. Laminins in basement membrane assembly. Cell Adh Migr. 2013 7:56-63.

57) Timpl R. Macromolecular organization of basement membranes. Curr Opin Cell Biol. 1996 8:618-624.

58) Beck K, Hunter I, Engel J. Structure and function of laminin: anatomy of a multidomain glycoprotein. FASEB J. 1990 4:148-160.

59) Aplin JD, Hughes RC. Complex carbohydrates of the extracellular matrix structures, interactions and biological roles. Biochim Biophys Acta. 1982 694:375-418.

60) Borza DB, Bondar O, Ninomiya Y, Sado Y, Naito I, Todd P, Hudson BG. The NC1 domain of collagen IV encodes a novel network composed of the alpha 1, alpha 2, alpha 5, and alpha 6 chains in smooth muscle basement membranes. J Biol Chem. 2001 276:28532-28540.

61) Kuo DS, Labelle-Dumais C, Gould DB. COL4A1 and COL4A2 mutations and disease: insights into pathogenic mechanisms and potential therapeutic targets. Hum Mol Genet. 2012 21:97-110.

62) Kirn-Safran C, Farach-Carson MC, Carson DD. Multifunctionality of extracellular and cell surface heparan sulfate proteoglycans. Cell Mol Life Sci. 2009 66:3421-3434.

63) Farach-Carson MC, Carson DD. Perlecan a multifunctional extracellular proteoglycan scaffold. Glycobiology 2007 17:897-905

64) Mishra M, Naik VV, Kale AD, Ankola AV, Pilli GS. Perlecan (basement membrane heparan sulfate proteoglycan) and its role in oral malignancies: an overview. Indian J Dent Res. 2011 22:823-826.

65) Katoh R, Muramatsu A, Kawaoi A, Komiyama A, Suzuki K, Hemmi A, Katayama S. Alteration of the basement membrane in human thyroid diseases: an immunohistochemical study of type IV collagen, laminin and heparan sulphate proteoglycan. Virchows Arch A Pathol Anat Histopathol. 1993 423:417-424.

66) Pati F, Jang J, Ha DH, Won Kim S, Rhie JW, Shim JH, Kim DH, Cho DW. Printing three-dimensional tissue analogues with decellularized extracellular matrix bioink. Nat Commun. 2014 5:3935.

67) Zein I, Hutmacher DW, Tan KC, Teoh SH. Fused deposition modeling of novel scaffold architectures for tissue engineering applications. Biomaterials. 2002 23:1169-1185.

68) Hutmacher DW. Scaffolds in tissue engineering bone and cartilage. Biomaterials. 2000 21:2529-2543.

69) Badylak SF. The extracellular matrix as a scaffold for tissue reconstruction. Semin Cell Dev Biol. 2002 13:377-383.

70) Liu CZ, Xia ZD, Han ZW, Hulley PA, Triffitt JT, Czernuszka JT. Novel 3D collagen scaffolds fabricated by indirect printing technique for tissue engineering. J Biomed Mater Res B Appl Biomater. 2008 85:519-528.

71) Włodarczyk-Biegun MK, Del Campo A. 3D bioprinting of structural proteins. Biomaterials. 2017 134:180-201.

72) Kannus P. Structure of the tendon connective tissue. Scand J Med Sci Sports. 2000 10:312-320

73) Lehmann WD. "All proteins all the time"- a comment on visions, claims, and wording in mass spectrometry-based proteomics. Anal Bioanal Chem. 2015 407:2659-2663.

74) Aebersold R, Mann M. Mass spectrometry-based proteomics. Nature. 2003 422:198-207.

75) Omenn GS. The strategy, organization, and progress of the HUPO Human Proteome Project. J Proteomics. 2014 100:3-7.

76) Mehmood S, Allison TM, Robinson CV. Mass spectrometry of protein complexes: from origins to applications. Annu Rev Phys Chem. 2015 66:453-474.

77) Zhang Y, Fonslow BR, Shan B, Baek MC, Yates JR 3rd. Protein analysis by shotgun/bottom-up proteomics. Chem Rev. 2013 113:2343-2394.

78) Aebersold R, Mann M. Mass-spectrometric exploration of proteome structure and function. Nature. 2016 537:347-355.

79) Sajic T, Liu Y, Aebersold R. Using data-independent, high-resolution mass spectrometry in protein biomarker research: perspectives and clinical applications. Proteomics Clin Appl. 2015 9:307-321.

80) Tyanova S, Temu T, Carlson A, Sinitcyn P, Mann M, Cox J. Visualization of LC-MS/MS proteomics data in MaxQuant. Proteomics. 2015 15:1453-1456.

81) Tyanova S, Temu T, Sinitcyn P, Carlson A, Hein MY, Geiger T, Mann M, Cox J. The Perseus computational platform for comprehensive analysis of (prote)omics data. Nat Methods. 2016 13:731-740.

82) Chen Y, Wang F, Xu F, Yang T. Mass Spectrometry-Based Protein Quantification. Adv Exp Med Biol. 2016 919:255-279.

83) Manes NP, Nita-Lazar A. Application of targeted mass spectrometry in bottom-up proteomics for systems biology research. J Proteomics. 2018 1874-3919:30057-5.

84) MacLean B, Tomazela DM, Shulman N, Chambers M, Finney GL, Frewen B, Kern R, Tabb DL, Liebler DC, MacCoss MJ. Skyline: an open source document editor for creating and analyzing targeted proteomics experiments. Bioinformatics. 2010 26:966-968.

85) Aebersold R, Bensimon A, Collins BC, Ludwig C, Sabido E. Applications and Developments in Targeted Proteomics: From SRM to DIA/SWATH. Proteomics. 2016 16:2065-2067.

86) Rosenberger G, Koh CC, Guo T, Röst HL, Kouvonen P, Collins BC, Heusel M, Liu Y, Caron E, Vichalkovski A, Faini M, Schubert OT, Faridi P, Ebhardt HA, Matondo M, Lam H, Bader SL, Campbell DS, Deutsch EW, Moritz RL, Tate S, Aebersold R. A

repository of assays to quantify 10,000 human proteins by SWATH-MS. Sci Data. 2014 1:140031.

87) Abazova N, Krijgsveld J. Advances in stem cell proteomics. Curr Opin Genet Dev. 2017 46:149-155.

88) Eliuk S, Makarov A. Evolution of Orbitrap mass spectrometry instrumentation. Annu Rev Anal Chem (Palo Alto Calif). 2015 8:61-80.

89) Oveland E, Muth T, Rapp E, Martens L, Berven FS, Barsnes H. Viewing the proteome: how to visualize proteomics data? Proteomics. 2015 15:1341-1355.

90) Mulvey CM, Schröter C, Gatto L, Dikicioglu D, Fidaner IB, Christoforou A, Deery M, Cho LT, Niakan KK, Martinez-Arias A, Lilley KS. Dynamic proteomic profiling of extra-embryonic endoderm differentiation in mouse embryonic stem cells. Stem Cells. 2015 33:2712-2725.

91) Benevento M, Munoz J. Role of mass spectrometry-based proteomics in the study of cellular reprogramming and induced pluripotent stem cells. Expert Rev Proteomics. 2012 9:379-399.

92) Santos J, Milthorpe BK, Herbert BR, Padula MP. Proteomic analysis of human adipose derived stem cells during small molecule chemical stimulated pre-neuronal differentiation. Int J Stem Cells. 2017 10:193-217.

93) Uzozie AC, Aebersold R. Advancing translational research and precision medicine with targeted proteomics. J Proteomics. 2018 S1874-3919:30076-9.

94) Larsen PR. Decade in review-thyroid disease: The endocrinology of thyroid disease from 2005 to 2015. Nat Rev Endocrinol. 2015 11:634-636.

95) Mohebati A, Shaha AR. Anatomy of thyroid and parathyroid glands and neurovascular relations. Clin Anat. 2012 25:19-31.

96) Coclet J, Foureau F, Ketelbant P, Galand P, Dumont JE. Cell population kinetics in dog and human adult thyroid. Clin Endocrinol (Oxf). 1989 3:655-665.

97) Johansen R, Gardner Re, Galante M, Marchi Ff, Ledwich Tw, Soley Mh, Scott Kg, Miller Ef, Mccorkle Hj. An experimental study of thyroid regeneration following subtotal thyroidectomy. Surg Gynecol Obstet. 1951 93:303-309

98) Fierabracci A, Puglisi MA, Giuliani L, Mattarocci S, Gallinella-Muzi M. Identification of an adult stem/progenitor cell-like population in the human thyroid. J Endocrinol. 2008 198:471-487

99) Hoshi N, Kusakabe T, Taylor BJ, Kimura S. Side population cells in the mouse thyroid exhibit stem/progenitor cell-like characteristics. Endocrinology. 2007 148:4251-4258

100) Thomas T, Nowka K, Lan L, Derwahl M. Expression of endoderm stem cell markers: evidence for the presence of adult stem cells in human thyroid glands. Thyroid. 2006 16:537-544.

101) Barbaro F, Zamparelli A, Zini N, Dallatana D, Bassi E, Mosca S, Parrilli A, Fini M, Giardino M, Toni R. Adult stem / progenitor cells of the rat thyroid: side population distribution, intermediate filament expression, and long-term in vitro expansion. It. J. Anat Embryol. 2013 118:19.

102) Davies TF, Latif R, Minsky NC, Ma R. Clinical review: The emerging cell biology of thyroid stem cells. J Clin Endocrinol Metab. 2011 96:2692-2702.

103) Bassi E, Barbaro F, Zamparelli A, Zini N, Cattini L, Dallatana D, Gnocchi C, Lippi G, Mosca S, Parrilli A, Fini M, Giardino R, Toni R. Thyrogenic, adipogenic, and osteogenic differentiation of adult rat, thyroid stem cells enriched by long-term adherent subculture. It. J. Anat Embryol. 2014 119:15

104) Bassi E, Barbaro F, Zamparelli A, Zini N, Spaletta G, Ricci F, Velati C, Dallatana D, Gnocchi C, Lippi G, Alfieri M, Mosca S, Della Casa C, Crafa P, Parrilli A, Fini M, Toni R. Multipotent adult rat, thyroid stem cells can be differentiated to follicular thyrocyte, and hepatocyte- like cells in 2D and 3D culture systems. It. J. Anat Embryol. 2015 120:87.

105) Lin RY. New insights into thyroid stem cells. Thyroid. 2007 17:1019-1023

106) Martínez-Aguilar J, Clifton-Bligh R, Molloy MP. Proteomics of thyroid tumours provides new insights into their molecular composition and changes associated with malignancy. Sci Rep. 2016 6:23660

107) Ucal Y, Eravci M, Tokat F, Duren M, Ince U, Ozpinar A. Proteomic analysis reveals differential protein expression in variants of papillary thyroid carcinoma. EuPA Open Proteom. 2017 17:1-6

108) Liu X, Guo Z, Sun H, Li W, Sun W. Comprehensive Map and Functional Annotation of Human Pituitary and Thyroid Proteome. J Proteome Res. 2017 16:2680-2691

109) Pietsch J, Riwaldt S, Bauer J, Sickmann A, Weber G, Grosse J, Infanger M, Eilles C, Grimm D. Interaction of proteins identified in human thyroid cells. Int J Mol Sci. 2013 14:1164-1178.

110) Zamparelli A, Zini N, Cattini L, Spaletta G, Dallatana D, Bassi E, Barbaro F, Iafisco M, Mosca S, Parrilli A, Fini M, Giardino R, Sandri M, Sprio S, Tampieri A, Maraldi NM, Toni R. Growth on poly(L-lactic acid) porous scaffold preserves CD73 and CD90 immunophenotype markers of rat bone marrow mesenchymal stromal cells. J Mater Sci Mater Med. 2014 25:2421-2436.

111) Hoque M, Rentero C, Cairns R, Tebar F, Enrich C, Grewal T. Annexins - scaffolds modulating PKC localization and signaling. Cell Signal. 2014 26:1213-1225.

112) Gilmore WS, Olwill S, McGlynn H, Alexander HD. Annexin A2 expression during cellular differentiation in myeloid cell lines. Biochem Soc Trans. 2004 32:1122-1123.

113) Zhai JM, Sun SJ, Wang W, Zeng C. Expression of annexin A3 in gastric cancer and its correlation with proliferation and apoptosis. Asian Pac. J. Cancer Prev. 2014 15:3001-3004.

114) Watanabe T, Ito Y, Sato A, Hosono T, Niimi S, Ariga T, Seki T. Annexin A3 as a negative regulator of adipocyte differentiation. J. Biochem. 2012 152:355-363.

115) Luo D, Fajol A, Umbach AT, Noegel AA, Laufer S, Lang F, Föller M. Influence of annexin A7 on insulin sensitivity of cellular glucose uptake. Pflugers Arch. 2015 467:641-649.

116) Goebeler V, Poeter M, Zeuschner D, Gerke V, Rescher U. Annexin A8 regulates late endosome organization and function. Mol. Biol. Cell. 2008 19:5267-5278.

117) Wang J, Guo C, Liu S, Qi H, Yin Y, Liang R, Sun MZ, Greenaway FT. Annexin A11 in disease. Clin Chim Acta. 2014 431:164-168.

118) De Franceschi N, Hamidi H, Alanko J, Sahgal P, Ivaska J. Integrin traffic - the update. J. Cell Sci. 2015 128:839-852

119) Shirakihara T, Kawasaki T, Fukagawa A, Semba K, Sakai R, Miyazono K, Miyazawa K, Saitoh M. Identification of integrin α3 as a molecular marker of cells undergoing epithelial-mesenchymal transition and of cancer cells with aggressive phenotypes. Cancer Sci. 2013 104:1189-1197.

120) Lobert VH, Brech A, Pedersen NM, Wesche J, Oppelt A, Malerød L, Stenmark H. Ubiquitination of alpha 5 beta 1 integrin controls fibroblast migration through lysosomal degradation of fibronectin-integrin complexes. Dev. Cell. 2010 19:148-159.

121) Krebsbach PH, Villa-Diaz LG. The Role of Integrin α6 (CD49f) in Stem Cells: More than a Conserved Biomarker. Stem Cells Dev. 2017 26:1090-1099.

122) Volkert G, Jahn A, Dinkel C, Fahlbusch F, Zürn C, Hilgers KF, Rascher W, Hartner A, Marek I. Contribution of the α8 integrin chain to the expression of extracellular matrix components. Cell Commun Adhes. 2014 21:89-98.

123) Kaltz N, Ringe J, Holzwarth C, Charbord P, Niemeyer M, Jacobs VR, Peschel C, Häupl T, Oostendorp RA. Novel markers of mesenchymal stem cells defined by genome-wide gene expression analysis of stromal cells from different sources. Exp. Cell Res. 2010 316:2609-2617.

124) Calloni R, Cordero EA, Henriques JA, Bonatto D. Reviewing and updating the major molecular markers for stem cells. Stem Cells Dev. 2013 22:1455-1476

125) Naba A, Pearce OMT, Del Rosario A, Ma D, Ding H, Rajeeve V, Cutillas PR2, Balkwill FR, Hynes RO. Characterization of the Extracellular Matrix of Normal and Diseased Tissues Using Proteomics. J Proteome Res. 2017 16:3083-3091.

126) Miles CA, Sims TJ, Camacho NP, Bailey AJ. The role of the alpha2 chain in the stabilization of the collagen type I heterotrimer: a study of the type I homotrimer in oim mouse tissues. J. Mol. Biol. 2002 321:797-805.

127) Fleischmajer R, Perlish JS, Burgeson RE, Shaikh-Bahai F, Timpl R. Type I and type III collagen interactions during fibrillogenesis. Ann. NY Acad. Sci. 1990 580:161-175.

128) Khoshnoodi J, Pedchenko V, Hudson BG. Mammalian collagen IV. Microsc. Res. Tech. 2008 71:357-370.

129) Weber IT, Harrison RW, Iozzo RV. Model structure of decorin and implications for collagen fibrillogenesis. J. Biol. Chem. 1996 271:31767-31770.

130) Orgel JP, Eid A, Antipova O, Bella J, Scott JE. Decorin core protein (decoron) shape complements collagen fibril surface structure and mediates its binding. PLoS One. 2009 4:7028.

131) Sotoodehnejadnematalahi F, Burke B. Structure, function and regulation of versican: the most abundant type of proteoglycan in the extracellular matrix. Acta Med. Iran. 2013 51:740-750.

132) Nikitovic D, Katonis P, Tsatsakis A, Karamanos NK, Tzanakakis GN. Lumican, a small leucine-rich proteoglycan. IUBMB Life. 2008 60:818-823.

133) Durkin ME, Chakravarti S, Bartos BB, Liu SH, Friedman RL, Chung AE. Amino acid sequence and domain structure of entactin. Homology with epidermal growth factor precursor and low density lipoprotein receptor. J Cell Biol. 1988 107:2749-2756.

134) Yurchenco PD, Patton BL. Developmental and pathogenic mechanisms of basement membrane assembly. Curr Pharm Des. 2009 15:1277-1294.

135) Glentis A, Gurchenkov V, Matic Vignjevic D. Assembly, heterogeneity, and breaching of the basement membranes. Cell Adh Migr. 2014 8:236-245

136) Lane TF, Sage EH. The biology of SPARC, a protein that modulates cell-matrix interactions. FASEB J. 1994 8:163-173.

137) Hohenester E, Sasaki T, Giudici C, Farndale RW, Bächinger HP. Structural basis of sequence-specific collagen recognition by SPARC. Proc Natl Acad Sci U S A. 2008 105:18273-18277.

138) Yue B. Biology of the extracellular matrix: an overview. J. Glaucoma. 2014 23:20-23.

139) Adams JC, Chiquet-Ehrismann R, Tucker RP. The evolution of tenascins and fibronectin. Cell Adh Migr. 2015 9:22-33.

140) Pataridis S, Eckhardt A, Mikulíková K, Sedláková P, Miksík I. Identification of collagen types in tissues using HPLC-MS/MS. J. Sep. Sci. 2008 31:3483-3488.

141) Murphy SV, Atala A. 3D bioprinting of tissues and organs. Nat. Biotechnol. 2014 32:773-785.

142) Elviri L, Foresti R, Bergonzi C, Zimetti F, Marchi C, Bianchera A, Bernini F, Silvestri M, Bettini R. Highly defined 3D printed chitosan scaffolds featuring improved cell growth. Biomed Mater. 2017 12:045009.

143) Barth A. The infrared absorption of amino acid side chains. Prog. Biophys. Mol. Biol. 2000 74:141-173.

144) Thomopoulos S, Williams GR, Soslowsky LJ. Tendon to bone healing: differences in biomechanical, structural, and compositional properties due to a range of activity levels. J. Biomech. Eng. 2003 125:106-113.

145) Deepthi S, Nivedhitha Sundaram M, Deepti Kadavan J, Jayakumar R. Layered chitosan-collagen hydrogel/aligned PLLA nanofiber construct for flexor tendon regeneration. Carbohydr. Polym. 2016 153:492-500.

146) Lee DW, Lim C, Israelachvili JN, Hwang DS. Strong adhesion and cohesion of chitosan in aqueous solutions. Langmuir. 2013 29:14222-14229.

147) Calloni R, Cordero EA, Henriques JA, Bonatto D. Reviewing and updating the major molecular markers for stem cells. Stem Cells Dev. 2013 22:1455-1476.

148) Lv FJ, Tuan RS, Cheung KM, Leung VY. Concise review: the surface markers and identity of human mesenchymal stem cells. Stem Cells. 2014 32:1408-1419.

149) Birmingham E, Niebur GL, McHugh PE, Shaw G, Barry FP, McNamara LM. Osteogenic differentiation of mesenchymal stem cells is regulated by osteocyte and osteoblast cells in a simplified bone niche. Eur. Cell Mater. 2012 23:13-27.

150) Yuan Z, Li Q, Luo S, Liu Z, Luo D, Zhang B, Zhang D, Rao P, Xiao J. PPARγ and Wnt Signaling in Adipogenic and Osteogenic Differentiation of Mesenchymal Stem Cells. Curr. Stem Cell Res. Ther. 2016 11:216-225.

151) Suzuki K, Mitsutake N, Saenko V, Suzuki M, Matsuse M, Ohtsuru A, Kumagai A, Uga T, Yano H, Nagayama Y, Yamashita S. Dedifferentiation of human primary thyrocytes into multilineage progenitor cells without gene introduction. PLoS One. 2011 6:19354

152) Zhang L, Hong TP, Hu J, Liu YN, Wu YH, Li LS. Nestin-positive progenitor cells isolated from human fetal pancreas have phenotypic markers identical to mesenchymal stem cells. World J. Gastroenterol. 2005 11:2906-2911.

153) Wong A, Ghassemi E, Yellowley CE. Nestin expression in mesenchymal stromal cells: regulation by hypoxia and osteogenesis. BMC Vet. Res. 2014 10:173.

154) Zulewski H, Abraham EJ, Gerlach MJ, Daniel PB, Moritz W, Müller B, Vallejo M, Thomas MK, Habener JF. Multipotential nestin-positive stem cells isolated from adult pancreatic islets differentiate ex vivo into pancreatic endocrine, exocrine, and hepatic phenotypes. Diabetes. 2001 50:521-533.

155) Neradil J, Veselska R. Nestin as a marker of cancer stem cells. Cancer Sci. 2015 106:803-811.

156) Haraguchi N, Utsunomiya T, Inoue H, Tanaka F, Mimori K, Barnard GF, Mori M. Characterization of a side population of cancer cells from human gastrointestinal system. Stem Cells. 2006 24:506-513.

157) Yu KR, Yang SR, Jung JW, Kim H, Ko K, Han DW, Park SB, Choi SW, Kang SK, Schöler H, Kang KS. CD49f enhances multipotency and maintains stemness through the direct regulation of OCT4 and SOX2. Stem Cells. 2012 30:876-887.

158) Yang Z, Dong P, Fu X, Li Q, Ma S, Wu D, Kang N, Liu X, Yan L, Xiao R. CD49f Acts as an inflammation sensor to regulate differentiation, adhesion, and migration of human mesenchymal stem cells. Stem Cells. 2015 33:2798-2810.

159) Skelton RJ, Costa M, Anderson DJ, Bruveris F, Finnin BW, Koutsis K, Arasaratnam D, White AJ, Rafii A, Ng ES, Elefanty AG, Stanley EG, Pouton CW, Haynes JM, Ardehali R, Davis RP, Mummery CL, Elliott DA. SIRPA, VCAM1 and CD34 identify discrete lineages during early human cardiovascular development. Stem Cell Res. 2014 13:172-179.

160) Dubois NC, Craft AM, Sharma P, Elliott DA, Stanley EG, Elefanty AG, Gramolini A, Keller G. SIRPA is a specific cell-surface marker for isolating cardiomyocytes derived from human pluripotent stem cells. Nat. Biotechnol. 2011 29:1011-1018.

161) Calloni R, Cordero EA, Henriques JA, Bonatto D. Reviewing and updating the major molecular markers for stem cells. Stem Cells Dev. 2013 22:1455-1476.

162) Schu S, Nosov M, O'Flynn L, Shaw G, Treacy O, Barry F, Murphy M, O'Brien T, Ritter T. Immunogenicity of allogeneic mesenchymal stem cells. J. Cell Mol. Med. 2012 16:2094-2103.

163) Taghi GM, Ghasem Kashani Maryam H, Taghi L, Leili H, Leyla M. Characterization of in vitro cultured bone marrow and adipose tissue-derived mesenchymal stem cells and their ability to express neurotrophic factors. Cell Biol. Int. 2012 36:1239-1249.

164) Menicanin D, Bartold PM, Zannettino AC, Gronthos S. Genomic profiling of mesenchymal stem cells. Stem Cell Rev. 2009 5:36-50.

165) Maeng YS, Choi HJ, Kwon JY, Park YW, Choi KS, Min JK, Kim YH, Suh PG, Kang KS, Won MH, Kim YM, Kwon YG. Endothelial progenitor cell homing: prominent role of the IGF2-IGF2R-PLCbeta2 axis. Blood. 2009 113:233-243.

ACKNOWLEDGMENTS

At the end of this PhD course, I would like to spend a few words to thank those who believed in me and allowed me to reach this important goal for my career.

First of all, I want to thank my family for the support they have shown throughout all my academic career, not only these last three years of PhD.

I am grateful to Chiara, whom I met at the beginning of this long journey. She supported me in my long months away from Italy and she still does every day with her love.

I wish to thank all my lab mates and guys/girls I met in my journey, starting from the ones who help me more since the beginning: “many thanks indeed Davide, Elena, Fulvio and Elia! I’m sure that we’ll stay in touch for a long time in the future!”

Last but not least I really wish to thank who have been my guides during these three years, whose followed all my steps in the laboratory with professionalism, helpfulness and cordiality. I am obliged to Prof. Roberto Toni, supervisor of this thesis. I am very grateful to my co-tutor Prof. Lisa Elviri and Prof. Stephen R. Pennington for teaching me the beautiful principles of analytical chemistry and, particularly, mass spectrometry world. I will treasure your precious teachings for the rest of my life.